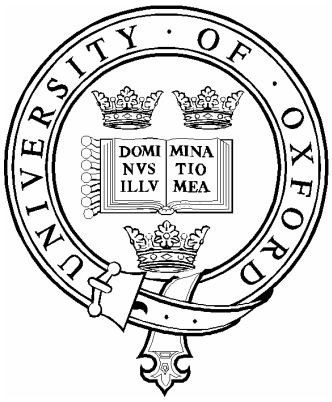

Analogy between equilibrium of structures and compatibility of mechanisms

by

András Lengyel

A thesis submitted for the degree of Doctor of Philosophy at the University of Oxford

St Edmund Hall, Oxford

Michaelmas Term, 2002

ABSTRACT

Planar bar-and-joint mechanisms with one degree-of-freedom are widely used in deployable structures and machines. Such mechanisms are designed to undergo a specific motion, which can be described mathematically by plotting out the compatibility conditions, resulting in a curve called the compatibility path. It has been observed that compatibility paths can develop singularities similar to that of equilibrium paths of elastic structures.

This dissertation studies singularities occurring in compatibility paths with the aid of knowledge in the theory of structural stability. An analogy is set up between the equilibrium path of elastic structures and the compatibility path of mechanisms with a single degree-of-freedom incorporating different types of bifurcation, effects of imperfections and detection of singularities. It is shown that the fundamentally distinct critical points such as limit points and bifurcation points can also appear in the compatibility path. Methods used to study singularities for compatibility conditions of mechanisms and equilibrium of structures are unified so that they can be used for both cases. A formulation of potential energy for mechanisms is also proposed in analogy with the potential energy function used in structural analysis.

Further analysis of the mechanisms is carried out to demonstrate that singularities of compatibility paths can also be dealt with by elementary catastrophe theory similar to stability theory. A relationship is established between the mathematical formulation of different compatibility bifurcations and the canonical forms of catastrophe types. Examples of mechanisms demonstrating the existence of cuspoids of the compatibility conditions are given. An overall classification of the compatibility paths is also proposed.

Keywords: bifurcation, catastrophe types, compatibility condition, compatibility path, elementary catastrophe theory, equilibrium path, imperfection, Jacobian matrix, mechanism with one degree-of-freedom, potential energy

CONTENTS

LIST OF FIGURES

LIST OF TABLES

1

INTRODUCTION

Contents

1.1 Mechanisms in engineering

The Oxford Advanced Learner's Dictionary (2000) defines the word *mechanism* as a set of moving parts in a machine or as a method or a system for achieving something. In engineering science, a *mechanism* is usually regarded as a physical system or a machine, which is an assemblage of working parts designed to produce some required effect (Hunt, 1978). Mechanisms are means of transmitting, controlling or constraining relative movements. In mechanical engineering other terms, such as linkage, etc. are also often used to refer to such machines.

However, this word is also used to indicate the mobilization of a device or an assembly of mechanical parts. It represents the action or a way a machine exerts its capability of motion. This interpretation of the word is used when the mobility of a structural assembly is considered.

Both technical aspects of the word are frequently used in engineering scientific publications, and, therefore in this dissertation we use the word in accordance with literature.

Mechanisms can exist in various structural forms; one group of them consists of rigid bodies and joints. A rigid body does not change its shape or size: the dimensions of the original shape remain invariable. This feature can be described as the distance of any two points and angles formed by any three points within the body remains unchanged. Consequently, the position of any point is determined once the position of the body is known. Though a completely rigid body does not exist, many engineering components are rigid to the extent that deformations are negligible in comparison with their relative movements. In general a rigid body may have an arbitrary two-dimensional or three-dimensional shape, but engineering applications can often be modelled by one-dimensional elements, e.g. bars.

Rigid bodies can be connected to each other by joints. A joint is usually formed by a simple contact. Though such a contact can be in the form of a flexible band, spring or other elastic components, the most elementary joint between two bodies is formed by

connecting them together at one point ensuring that the single point of contact is continuously maintained during relative movement. This joint enables relative rotation around it but no relative translation of the rigid bodies, and is called a pin joint.

This dissertation is concerned only with planar mechanisms consisting of completely rigid bars and frictionless pin joints. Such mechanisms are also commonly called linkages or, more specifically, bar-assemblies.

1.2 Rigidity and mobility of bar-assemblies

Bar-assemblies play an important role in engineering. Many problems in structural engineering are modelled by trusses, consisting of bars and frictionless pin joints, e.g. steel truss bridges, some roof structures, electrical pylons, etc. In trusses sufficient structural rigidity and strength are of prime concern as they are designed to meet the requirements of ultimate, serviceability and limit states. Consequently, bars are treated as deformable members, and stresses and strains are obtained due to the elastic deformations.

On the other hand, a bar-assembly as a mechanism is expected to perform some specified motions. The deformation of bars is far smaller than the displacements and therefore does not affect the motion. Thus it is appropriate to consider bars as rigid bodies while studying the mobility of a bar-assembly. The way how the rigid bodies are assembled is mathematically described by compatibility conditions.

A general bar-and-joint assembly is called rigid if it is not kinematically indeterminate. In structural engineering the so-called Maxwell's rule is a well-known necessary condition for kinematic determinacy (Maxwell, 1890; Calladine, 1978): a space truss having b straight bars and j frictionless pin joints is, in general, rigid if

$$b \geq 3j - 6 . \tag{1.1}$$

If

$$b < 3j - 6, \tag{1.2}$$

the structure is kinematically indeterminate. However, even though satisfying (1.1), a bar-assembly can be kinematically indeterminate by having a special geometry or topology.

A kinematically indeterminate structural assembly has mechanisms associated with it. They may be finite mechanisms, i.e. they extend into finite motions without deformations in the elements. But the lack of rigidity may refer to infinitesimal mechanisms, which allow only infinitesimal displacements without deformations.

However, the fulfilment of the Maxwell's rule does not correlate closely with kinematic determinacy as one can find structurally rigid bar-assemblies, infinitesimal and finite mechanisms complying with this condition while there are also examples of these types which are predicted as kinematically indeterminate by the condition.

1.3 Singularities

Another problem may arise about finite mechanisms which are known to have a single kinematic degree-of-freedom by the Maxwell's rule. In a general case a finite mechanism undergoes a specific motion. This motion can be mathematically prescribed by compatibility conditions and plotted, resulting in a curve called a compatibility path. However, the mobilization of some particular finite mechanisms may lead to special configurations where the degree of kinematic indeterminacy increases. The bar-assembly is then at a point of bifurcation (Tarnai, 1984, 1990). At such points the number of infinitesimal degrees-of-freedom increases, i.e. the possibility of motion in a number of different directions arises leading to branches in the compatibility path, though the structural assembly is a single-parameter finite mechanism.

It has been observed that, in a way, this phenomenon is similar to the buckling of elastic structures in stability theory. It is known that certain structures under a critical load lose their stability and can change equilibrium shape. At that position the relationship between the load and the displacement is not uniquely determined, hence the structure is at a point of bifurcation.

Bifurcations are parts of a large group of phenomena. The mathematical approach to natural phenomena usually requires governing equations. Generally they are nonlinear, contain variables, constants, time and space coordinates, derivatives of the variables, integral forms, etc. (Gilmore, 1981). In many physical problems they can be greatly simplified, resulting in a so-called dynamical system

$$F_i = \frac{d\psi_i}{dt} - f_i\left(\psi_j; c_l; t\right) = 0 \tag{1.3}$$

where ψ_i, c_l and t denote the variables, parameters and time, respectively. In a dynamical system only the first time derivatives remain. If functions f_i are independent of time, the problem is called an autonomous dynamical system. The study of dynamic bifurcation has made clear the mechanism of instability and chaos of dynamical systems (Ikeda and Murota, 2002). If the time derivatives are also neglected in (1.3), a static problem (or in a special case, a static bifurcation problem) is obtained. This formulation applies to the kinematics of mechanisms.

A special case occurs if functions f_i are obtained as the gradient of a potential function. This model applies to the stability theory of elastic structures with conservative forces.

Bifurcations of compatibility, equilibrium, etc. are singularities of ordinary smooth phenomena. The mathematical formulation of most phenomena in classical physics exhibits smooth behaviour, i.e. the governing equations react with small changes to small variations of the external factors. Hence these systems are described by differential equations, e.g. the motion of planets, vibrating strings, heat conduction, etc. However, this does not apply to several phenomena when a small pertubation of the

system causes sudden ‘jumps’. Such phenomena and the related functions were given the name ‘catastrophe’ by the French mathematican René Thom (Thom, 1972, 1975). Though he proposed his idea for biology, the theory is actually able to cover a much broader range of disciplines in science, engineering, economics. For instance, it proves an efficient tool in the stability theory as catastrophe theory provides a classification of singularities of the equilibrium paths.

1.4 Objectives and layout

Although a great deal of research has been conducted to understand and mathematically describe bifurcation phenomena in structural stability, little has been done in kinematics of mechanisms. The aim of this dissertation is to analyse the bifurcation of planar finite mechanisms, including the use of catastrophe theory. An analogy is to be created between kinematics of mechanisms and stability of structures based on the known bifurcation phenomena which are possible in both cases. The analogy enables the application of well-established methods in structural stability to kinematics of mechanisms. Several aspects of this analogy are examined and various techniques are presented, which are demonstrated throughout the dissertation by a set of mechanism examples: a kite-shaped four-bar linkage, a square-shaped four-bar linkage, a six-bar linkage, and a special A-shaped linkage. The outline of the dissertation is as follows.

Chapter 2 summarizes the previous studies that are relevant to the topic of this dissertation. They include bifurcation of compatibility paths of mechanisms, other bifurcation phenomena in kinematics of mechanisms and catastrophe theory. It also gives a brief review on stability theory with the illustration of the fundamental bifurcation modes of equilibrium paths of structures.

An analogy between bifurcation phenomena in stability theory and compatibility of mechanisms is established in Chapter 3. Following the fundamental modes of equilibrium bifurcations, the analogous phenomena for mechanisms are presented.

Bifurcations of compatibility paths of mechanisms are shown and imperfection-sensitivity curves are determined. The analogy is extended to cover all types of bifurcations and is demonstrated by examples of mechanisms. A classification of the compatibility paths is proposed. Moreover, Chapter 3 examines a new dimension of the analogy between kinematics of mechanisms and stability of structures: the concept of potential functions. Various possible counterparts to the potential energy function of elastic structures used in the stability theory are proposed for use in kinematics of mechanisms.

Chapter 4 extends the analogy further to the analysis of mechanisms. Various analytical approaches are presented for the identification of bifurcation points occurring on compatibility paths. The methods are based on the first- and second-order analysis of the constraint equations of the systems. Analogous behaviour for structures is shown in comparison with those of mechanisms. Mechanism examples are given to demonstrate the applicability of these methods and also their limitations. This is followed by numerical methods aimed to cope with the limitations, and to provide an alternative mathematical approach for the analysis of the singularities of compatibility paths. These methods are applied to the mechanisms introduced in the previous chapters. An algorithm is also presented to approximate numerically the graphs of compatibility paths.

Chapter 5 is dedicated to the application of catastrophe theory to the kinematics of mechanisms. It starts with a discussion of problems encountered in the previous chapters, followed by detailed examination of mechanisms in view of catastrophe theory. A formulation of the problem is proposed and discussed in detail with the aid of examples. The approach is based on the analogy between compatibility and equilibrium.

A study regarding the creation of mechanisms that exhibit higher-order types of catastrophe is also given. The possibility of the assembly of more complicated linkages is examined followed by the analysis of an infinitely degenerate case. Several questions related to the mathematical formulation of the problem are also discussed in this chapter.

Chapter 6 gives a summary of the achievements of this dissertation and a number of directions for future research, which concludes the dissertation.

2

LITERATURE REVIEW

Contents

2.1 The stability theory of structures

2.1.1 Equilibrium equations and equilibrium paths

It has been mentioned in Section 1.3 that bifurcations of compatibility paths of mechanisms can be compared to those of equilibrium paths of elastic structures (Tarnai, 1999). As our goal is to create a complete analogy between the two subjects, it is important to review the achievements in the theory of structural stability.

Unlike the kinematics of mechanisms, the theory of elastic stability has been very well developed. It is known in structural mechanics that structures may lose their stability under certain conditions. Euler's work (1744) on stability dates back to the mid 18th century and was later followed by others. A major contribution to this field was Koiter's (1945) dissertation on a nonlinear bifurcation theory for continuous elastic systems.

Many structural systems can be described by introducing generalized coordinates. A great deal of work has been done in general nonlinear theory of elastic stability in terms of generalized coordinates (Thompson, 1963). A good summary of elastic stability is given by Thompson and Hunt (1973, 1984). In general, the relationship between the generalized coordinates and the load parameters of a structure is represented by equilibrium equations, which can be plotted resulting in equilibrium paths. Stability theory focuses on the study of critical points of these paths. Figure 2.1 reproduces the

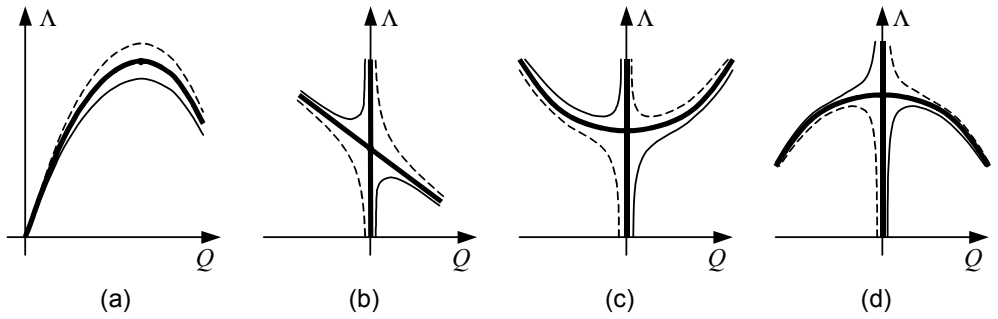

Figure 2.1: Equilibrium paths of structures with fundamental types of critical points (thick lines) and paths of the disturbed systems (thin lines). (a) Limit point. (b) Asymmetric bifurcation. (c) Stable symmetric bifurcation. (d) Unstable symmetric bifurcation.

four well-known modes of instability associated with distinct critical points in the coordinate system of a generalized coordinate (Q) and and a load parameter (Λ): the *limit point,* the *asymmetric bifurcation*, the *stable symmetric bifurcation,* and the *unstable symmetric bifurcation*. A comprehensive review article is given by Thompson (1969).

2.1.2 Potential energy of structures

In solid mechanics potential energy is defined as the work done by external and internal forces acting on a solid body on its displacements and deformations (Kaliszky, 1990). The external forces are assumed to be conservative. The potential energy is always given with respect to a reference position, frequently the undeformed state of a solid body. The external potential is the work done by the external forces on the corresponding displacement of the body. The internal potential is the amount of work to produce deformations due to stresses, which is also called the strain energy. Geometrically possible displacement-deformation systems of a linearly elastic body may correspond to different values of the potential energy. The actual system at which the body is in equilibrium is obtained when the total potential energy is stationary.

In the case of structural systems consisting of an elastic continuum under concentrated and distributed loads, in general they would have infinite degrees-of-freedom (Gáspár, 1999). However, assumptions are usually made concerning the geometry of the structure, the mechanical behaviour, the loads, etc., so that a finite number of generalized coordinates associated with predefined mode shapes are sufficient to describe deformations. At an equilibrium position

$$\mathbf{v} = \frac{\partial \Pi(\mathbf{Q}, \mathbf{p})}{\partial \mathbf{Q}} = \mathbf{0} \tag{2.1}$$

where Π denotes the potential energy function and $\mathbf{Q}$ and $\mathbf{p}$ are the vectors of the generalized coordinates and parameters, respectively. The stability of the equilibrium is assessed by the Hessian matrix:

$$\mathbf{H} = \frac{\partial^2 \Pi(\mathbf{Q}, \mathbf{p})}{\partial \mathbf{Q}^2}. \tag{2.2}$$

An equilibrium position is stable if **H** is positive definite, i.e. all eigenvalues are positive. The existence of negative eigenvalues implies that the equilibrium is unstable. When **H** is positive semidefinite, the equilibrium is critical and further analysis is required (Thompson and Hunt, 1984).

Some structures can be described by a single variable without any loss of generality. Accordingly, **v** in (2.1) has one element only. The second-order derivative, **H** has also one element. If it is positive, negative or zero, the equilibrium is stable, unstable or critical, respectively. In special cases neutral equilibrium points are possible but they will become stable or unstable when the system is disturbed. An example of neutral equilibrium is given in Section 2.2.4 where the load is constant, and therefore independent of the displacement.

The analysis presented in this section, which aims to determine the critical points of an equilibrium path, is called the *linear eigenvalue analysis* (Thompson and Hunt, 1984).

2.2 Bifurcations in the stability theory of structures

Three common bifurcation modes of equilibrium paths, shown in Figure 2.1(b)-(d), are discussed in more details in the following, as they represent one of the foundations of the analogy, and will be referred to frequently in this dissertation. Though the principle of the stability theory applies to elastic continuum systems as well, here we choose rigid-body models with finite generalized coordinates for simplicity (Koiter, 1945).

2.2.1 Stable symmetric bifurcation

Consider a simple structure consisting of a rigid bar in a vertical position supported by an elastic rotational spring shown in Figure 2.2(a). A vertical force P is applied at the

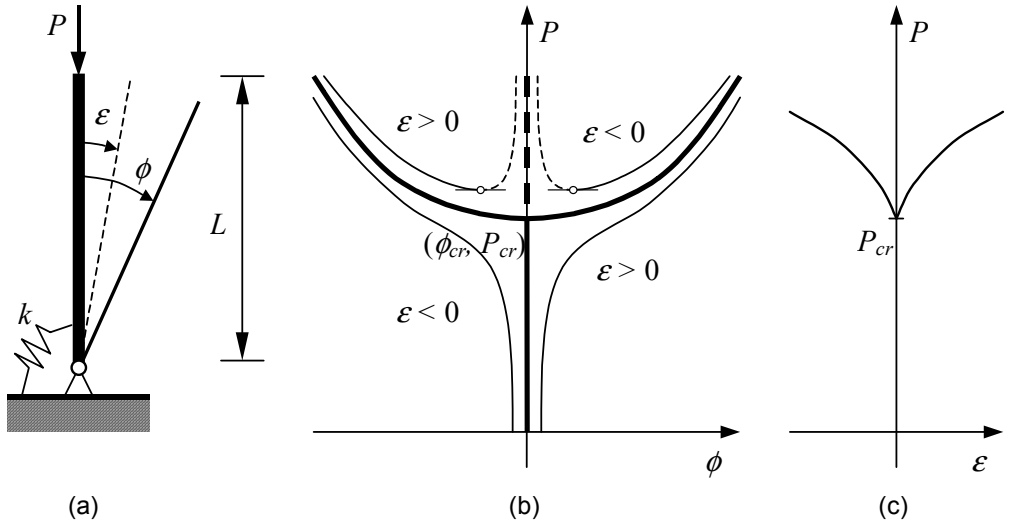

Figure 2.2: An example of the stable symmetric bifurcation. (a) A hinged cantilever bar supported by an elastic rotational spring under vertical load. (b) Equilibrium paths. (c) Imperfection-sensitivity.

tip of the bar. If the bar moves sideways by an angle ϕ, the equilibrium equation of the structure can be written as

$$-PL\sin\phi + k\phi = 0 \tag{2.3}$$

where L and k denotes the length of the bar and the stiffness of the spring, respectively.

When ϕ is zero, this relationship is shown by vertical straight thick lines in the diagram of equilibrium paths in Figure 2.2(b). The equilibrium is stable if the load is small but becomes unstable if the load exceeds a critical value:

$$P_{\text{cr}} = \frac{k}{L}. \tag{2.4}$$

This equilibrium path is denoted by the dashed line. The vertical path is called the *primary path*.

At the critical load a *secondary path* appears, as static equilibrium is possible with a non-zero ϕ. The new equilibrium positions are stable and are represented by a thick curved line in Figure 2.2(b). Note that this path has axis of symmetry and increasing deformations, i.e. ϕ, is associated with increased loading. Hence this bifurcation type is also called the *stable symmetric* bifurcation.

The equilibrium equation and the critical load could also have been derived from the potential energy of the structure. An analysis of the potential energy function is given later in Section 2.3.2.

Imperfections of the system can also be analysed. Suppose that the perfect geometry is disturbed as the unloaded bar has a small initial inclination ε due to the imperfection of the spring, as shown in Figure 2.2(a). Equation (2.3) then becomes

$$-PL\sin\phi + k(\phi - \varepsilon) = 0\,. \tag{2.5}$$

The imperfect equilibrium paths are denoted by thin lines in Figure 2.2(b), whereas continuous and dashed lines refer to stable and unstable equilibrium, respectively. Note that no bifurcation occurs and the new paths are located so that any one of the imperfect paths is in the neighbourhood of one of the original ones. Curves that belong to the same imperfection are located diagonally to the original bifurcation point, e.g. for $\varepsilon > 0$ they are in the lower right and the upper left quadrant of the graph. The former is entirely stable, referring to increasing deformations when P increases. On the other hand, the other path has a limit point where the stable state turns to an unstable one. Similar conclusions can be drawn for negative imperfections, i.e. to the left of the axis.

At the limit point of the equilibrium path $\partial P/\partial\phi = 0$, and the load has an extremum. From equation (2.5) an approximate formula for the deflected critical shape can be derived, which yields the relationship between the critical force and the imperfection:

$$P_{cr} \approx \frac{k}{L}\left(1 + \frac{1}{2}(3\varepsilon)^{2/3}\right). \tag{2.6}$$

This relationship is called the *imperfection-sensitivity* and is schematically plotted in Figure 2.2(c).

2.2.2 Unstable symmetric bifurcation

The unstable symmetric bifurcation can be illustrated with a simple rigid bar supported by an elastic horizontal spring shown in Figure 2.3(a). In a similar way to the previous

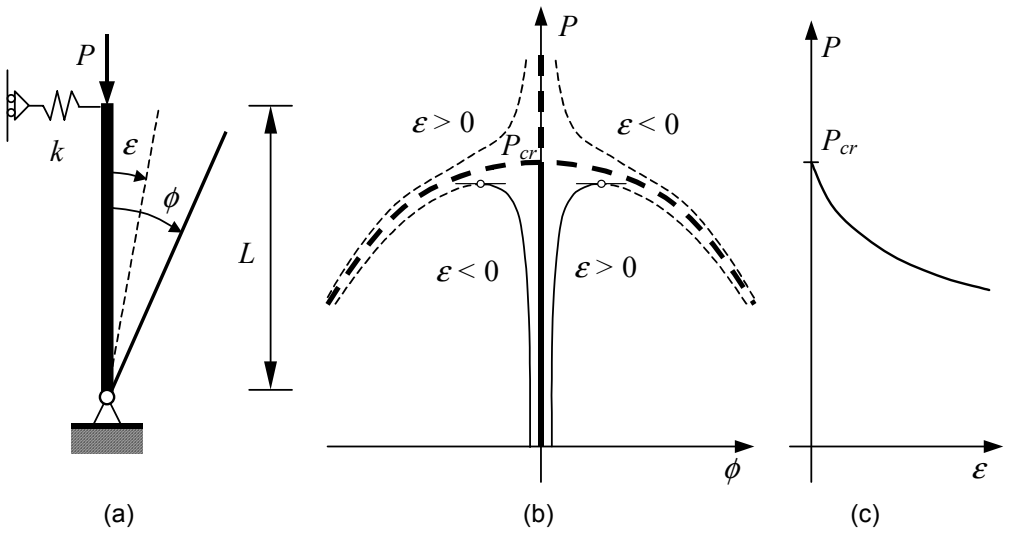

Figure 2.3: Unstable symmetric bifurcation. (a) Hinged cantilever bar supported by an elastic horizontal spring, under vertical load. (b) Equilibrium paths. (c) Imperfection-sensitivity.

example a vertical force P is applied on the top of the bar and ϕ denotes the angle between the inclined and the original position of the bar. Assume an initial imperfection ε can be applied. The equilibrium equation is formulated as

$$P\sin\phi - kL\cos\phi\left(\sin\phi - \sin\varepsilon\right) = 0 \tag{2.7}$$

where L and k denote the length of the bar and the stiffness of the spring, respectively. The primary and secondary equilibrium paths are obtained when $\varepsilon = 0$ and they are shown by thick lines in Figure 2.3(b). The primary equilibrium path is stable and turns unstable at the critical value of the load

$$P_{\text{cr}} = kL\,. \tag{2.8}$$

The secondary equilibrium path is again symmetric. The equilibrium is unstable as the postbuckling load-bearing capacity of the structure falls and thus this type of bifurcation is called the *unstable symmetric* bifurcation. The structure is sensitive to imperfections.

The equilibrium paths for $\varepsilon \neq 0$ are also plotted in Figure 2.3(b) with the same notation as in Figure 2.2. At the limit points the exact and the approximate value of the critical load is

$$P_{cr} = kL\left(1-\left(\sin\varepsilon\right)^{2/3}\right)^{3/2} \approx kL\left(1-\frac{3}{2}\varepsilon^{2/3}\right). \tag{2.9}$$

Thompson and Hunt (1973) used the sine of the actual and initial inclination angles as parameters. As $\sin\varepsilon$ is approximated linearly by ε for small ε, the approximate formula (2.9) is valid for both kinds of notations.

2.2.3 Asymmetric bifurcation

The third fundamental bifurcation mode is the *asymmetric* bifurcation. A simple example associated with this mode is shown in Figure 2.4(a), where the spring is at an inclined position with an angle $\pi/4$. Due to the geometry of the structure now the equilibrium equation is a more complicated formula:

$$-PL\sin\phi + P\varepsilon\cos\phi + kL^2\cos\phi - kL^2\frac{\cos\phi}{\sqrt{1+\sin\phi}} = 0\,. \tag{2.10}$$

The primary equilibrium path shows behaviour similar to the previous cases and the critical force is given as:

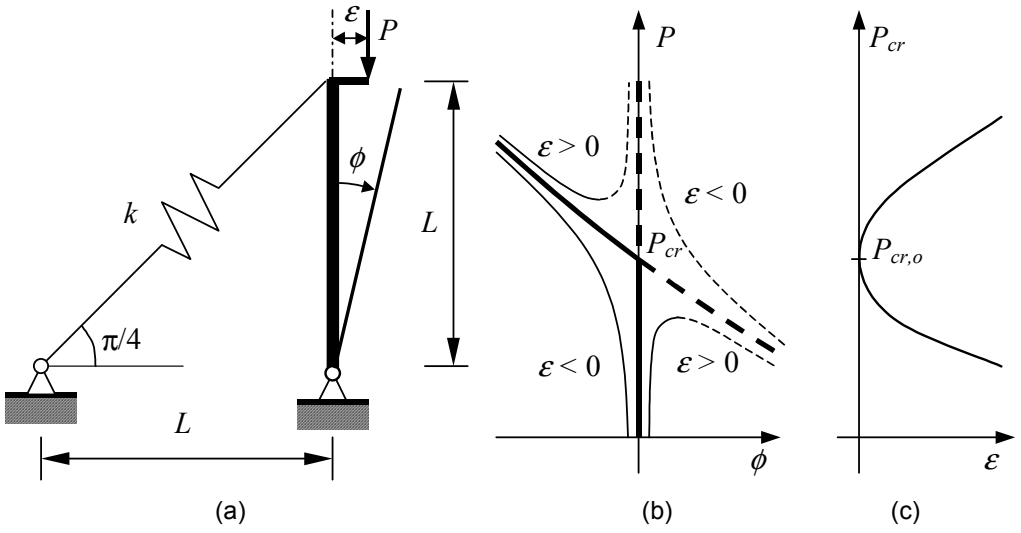

Figure 2.4: Asymmetric bifurcation. (a) Hinged cantilever bar supported by an inclined elastic spring, under vertical load. (b) Equilibrium paths. (c) Imperfection-sensitivity.

$$P_{\mathrm{cr}} = \frac{kL}{2} \tag{2.11}$$

where L is the length of the bar, as well as the distance between the two supported nodes, and k denotes the stiffness of the spring. The two branches of the secondary equilibrium path are now asymmetric in position, see Figure 2.4(b).

The imperfect equilibrium paths are shown in Figure 2.4(b) with the same notations as before. For positive ε the paths have limit points while for a negative one no stability problem occurs. The imperfection-sensitivity curve is plotted in Figure 2.4(c) and approximated as

$$P_{cr} \approx \frac{kL}{2}\left(1 \pm (3\varepsilon)^{1/2}\right). \tag{2.12}$$

2.2.4 Degenerate symmetric bifurcation

It is important to mention here that cases for an infinitely degenerate bifurcation were also found previously (Gáspár, 1984, 1999 and Tarnai, 2002) in addition to the three fundamental bifurcation modes. Consider a structure supported by a fixed hinge and two elastic springs of the same stiffness (Gáspár, 1984), as shown in Figure 2.5(a).

Figure 2.5(b) shows equilibrium paths. Solid, dashed and dotted heavy lines denote

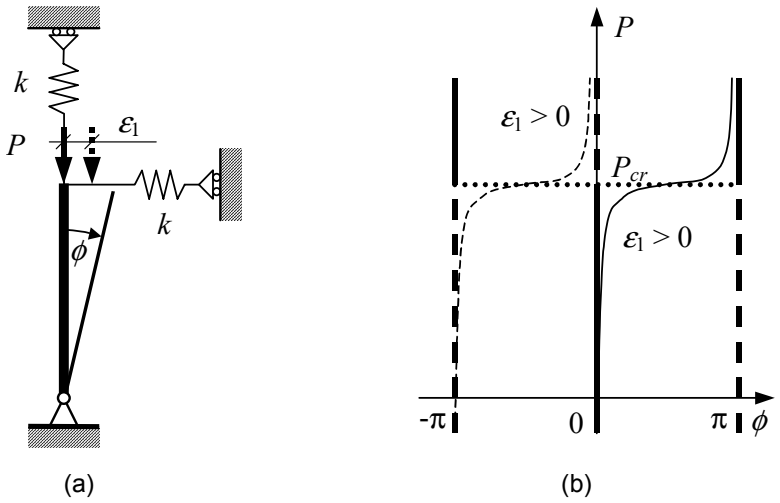

Figure 2.5: Infinitely degenerate symmetric bifurcation. (a) Hinged bar supported by two elastic springs, under vertical load. (b) Equilibrium paths.

stable, unstable and neutral equilibrium states, respectively. The primary equilibrium path, shown by thick vertical lines, corresponds to the undeformed original position. The secondary path, shown by thick dotted line, which intersects the other, is now a straight line parallel to axis ϕ at the critical force, i.e. the structure is in the equilibrium state at any arbitrary deformation under a constant load.

Introduce now an imperfection to the system. Assume that the load is offset by a small distance ε_1. If $\varepsilon_1 > 0$, the imperfect equilibrium paths are shown by thin lines in Figure 2.5(b). Note that none of the paths has limit points. In case of a negative ε, the equilibrium paths are mirror images of the positive ones to the axis *P*.

2.3 Catastrophe theory

The linear eigenvalue analysis determines the critical loads with the aid of the second variation of the potential function. It provides no information about the post-buckling behaviour of the structure, which is controlled by higher variations of the potential function about the critical state. Furthermore, it has been a general viewpoint in engineering to examine instabilities in terms of a single control parameter, usually the load, and hence obtain equilibrium paths in the space of the generalized coordinates and the load parameter. Secondary parameters, usually imperfections, are introduced afterwards, resulting in a perturbed set of equilibrium paths (Thompson and Hunt, 1984). Contrary to this *bifurcational view*, it has been realized that all parameters should be treated equally leading to equilibrium surfaces. This approach received further attention in the development of the catastrophe theory and hence it is usually called the *catastrophe theory view*. The difference between the two is illustrated in Figure 2.6 for the unstable symmetric point of bifurcation. Figure 2.6(a) shows the equilibrium paths in the coordinate system of the load parameter λ and the generalized coordinate *Q*. Imperfect paths are calculated in terms of an imperfection parameter ε. The catastrophe theory view, on the other hand, does not require the specific definition of the load

parameter and the imperfection but maintains the general orientation of the equilibrium surface in the parameter space (Λ_1, Λ_2), see Figure 2.6(b).

The study of elastic stability gained a new dimension by the development of a new mathematical tool, catastrophe theory in the 1970's. Catastrophe theory was introduced by the French mathematician René Thom who gave the name 'catastrophe' to phenomena that exhibit sudden changes due to small perturbations of the system. The techniques developed by him became known through his book *Stabilité Structurelle et Morphogénèse* (1972, 1975). In his book, Thom proposed a theorem, which classifies families of functions with up to five parameters. Mathematical proof was provided by Zeeman (Trotman and Zeeman, 1976; Zeeman, 1977) and Arnol'd (1972) gave the elementary catastrophe types their names and systematic codes as now known in the literature.

One of the various applications of catastrophe theory, which is important for our case, is in the stability theory of structures. The analysis is done with the help of the total potential energy function of the structure. Various catastrophe types have been identified and analysed (Hunt, 1981; Hansen and Hui, 1977; Hui and Hansen, 1980; Hunt and Williams, 1984ab; Thompson and Gáspár, 1977; Thompson and Supple,

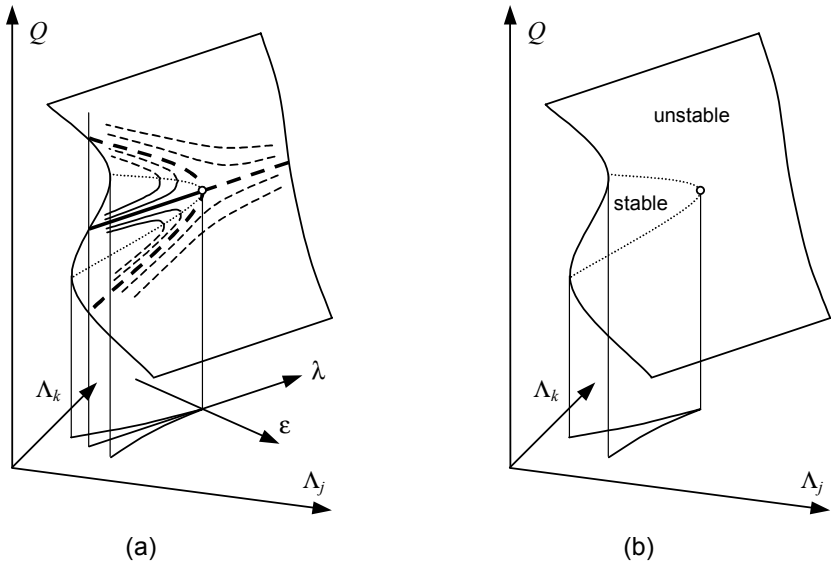

Figure 2.6: (a) The bifurcational view and (b) the catastrophe view of a cusp catastrophe at an unstable symmetric point of bifurcation.

1973; Gáspár, 1977). A good summarizing work on the subject is given by Gáspár (1999).

2.3.1 Thom's theorem

The term *catastrophe* in mathematics, unlike the usual meaning as 'disaster', means that smooth alterations in the controlling variables cause sudden changes in the phenomenon (Gáspár, 1999; Poston and Stewart, 1978). In mathematical terms it means that small changes in the parameters of a system causes a sudden change in the function that describes the phenomenon.

Natural phenomena are usually described by governing equations. Generally the equations are nonlinear, containing variables, constants, time and space coordinates, time and space derivatives of the variables, integral forms, etc. (Gilmore, 1981). In many cases they can be simplified by assuming that there are no integrals, and the problem is described by a set of partial nonlinear differential equations. Further assumptions can be made on the omission of the space coordinates and the space derivatives of the variables.

Another simplification step keeps only the first time derivatives and assumes a special form. This problem is called a *dynamical system* and the equations are written as

$$F_i = \frac{d\psi_i}{dt} - f_i\left(\psi_j; c_l; t\right) = 0 \tag{2.13}$$

where ψ_i, c_l and t denote the variables, parameters and time, respectively. If functions f_i are independent of time, the problem is called an *autonomous dynamical system*. If the time derivatives are also neglected in (2.13), a static bifurcation problem is obtained. This formulation applies to the compatibility of mechanisms:

$$F_i = -f_i\left(\psi_j; c_l\right) = 0 \tag{2.14}$$

A special case occurs if functions f_i are obtained as the gradient of a potential function V. This model applies to the stability theory of elastic structures with

conservative forces. Such systems are called the *equilibria of gradient systems,* which is the subject of *elementary catastrophe theory*:

$$\frac{\partial V(\psi_j, c_l)}{\partial \psi_i} = 0, \quad 1 \le i, j \le n; 1 \le l \le r \tag{2.15}$$

where the notations are the same as in (2.13).

Equation (2.15) states that the gradient of the *n*-variable, *r*-parameter function V equals zero. The stability properties of the equilibrium may be determined from the Hessian matrix V_{ij}. If the matrix is not singular, then after a suitable diffeomorphism, a locally reversible smooth map, the potential can be locally written in the Morse canonical form (Morse, 1931):

$$V \approx -y_1^2 - \ldots - y_i^2 + y_{i+1}^2 + \ldots + y_n^2 \tag{2.16}$$

where *y*'s are a new set of variables related to ψ's. If the Hessian is singular, then some of the eigenvalues vanish and the potential can be split to a Morse and a non-Morse part due to Thom Splitting Lemma (Gromoll and Meyer, 1969). However, it is still possible to find a canonical form for the non-Morse part of the potential.

Consider an *n*-variable single-value function $f(\underline{x})$. It has a *critical point* at $\underline{x}_0$ if the first-order derivatives of $f(\underline{x})$ are all zero. If the Hessian matrix in non-singular, the point is a *non-degenerate* critical point[1]. The function $f(\underline{x})$ is *structurally stable* if, for all sufficiently small smooth functions $p(\underline{x})$, f and $f + p$ have the same numbers and same types of critical points, or in other words, f and $f + p$ are equivalent after a suitable translation of the origin.

Smooth functions are typically structurally stable but critical points are more interesting to us. Thom's theorem classifies the typical singularities of families of *r*-parameter *n*-variable functions $f: \mathbb{R}^n \times \mathbb{R}^r \to \mathbb{R}$ with less then 6 parameters.

[1] The mathematical definition of a critical point refers to the vanishing of the first derivatives, which corresponds to equilibrium in engineering terms. Degenerate critical points in the literature of mathematics refers to critical points of equilibrium in engineering (Gilmore, 1981).

Thom's theorem: Typically an *r*-parameter family of smooth functions $\mathbb{R}^n \to \mathbb{R}$, for any n and for $r \le 5$, is structurally stable and is equivalent around any point to one of the forms given in Table 2.1.

The forms are all catastrophes except the first two, that are not catastrophe forms since they do not change with *t*'s. The second formula is the Morse form. The rest are canonical forms of catastrophes consisting of the *catastrophe germ* and the *universal*

Table 2.1: Classification of families of functions by Thom's theorem

No.	Canonical form	Name
1.	u_1	
2.	$u_1^2 + \ldots + u_i^2 - u_{i+1}^2 - \ldots - u_n^2 \quad (0 \le i \le n)$	
3.	$u_1^3 + t_1 u_1 + (M)$	the fold (A_2)
4.	$\pm(u_1^4 + t_2 u_1^2 + t_1 u_1) + (M)$	the cusp (A_3)
5.	$u_1^5 + t_3 u_1^3 + t_2 u_1^2 + t_1 u_1 + (M)$	the swallowtail (A_4)
6.	$\pm(u_1^6 + t_4 u_1^4 + t_3 u_1^3 + t_2 u_1^2 + t_1 u_1) + (M)$	the butterfly (A_5)
7.	$u_1^7 + t_5 u_1^5 + t_4 u_1^4 + t_3 u_1^3 + t_2 u_1^2 + t_1 u_1 + (M)$	the wigwam (A_6)
8.	$u_1^2 u_2 - u_2^3 + t_3 u_1^2 + t_2 u_2 + t_1 u_1 + (N)$	the elliptic umbilic (D_4^-)
9.	$u_1^2 u_2 + u_2^3 + t_3 u_1^2 + t_2 u_2 + t_1 u_1 + (N)$	the hyperbolic umbilic (D_4^+)
10.	$\pm(u_1^2 u_2 + u_2^4 + t_4 u_2^2 + t_3 u_1^2 + t_2 u_2 + t_1 u_1) + (N)$	the parabolic umbilic (D_5)
11.	$u_1^2 u_2 - u_2^5 + t_5 u_2^3 + t_4 u_2^2 + t_3 u_1^2 + t_2 u_2 + t_1 u_1 + (N)$	the second elliptic umbilic (D_6^-)
12.	$u_1^2 u_2 + u_2^5 + t_5 u_2^3 + t_4 u_2^2 + t_3 u_1^2 + t_2 u_2 + t_1 u_1 + (N)$	the second hyperbolic umbilic (D_6^+)
13.	$\pm(u_1^3 + u_2^4 + t_5 u_1 u_2^2 + t_4 u_2^2 + t_3 u_1 u_2 + t_2 u_2 + t_1 u_1) + (N)$	the symbolic umbilic (E_6)

where $(u_1, \ldots, u_n) \in \mathbb{R}^n$, $(t_1, \ldots, t_r) \in \mathbb{R}^r$ and

$(M) = u_2^2 + \ldots + u_i^2 - u_{i+1}^2 - \ldots - u_n^2 \quad (1 \le i \le n)$

$(N) = u_3^2 + \ldots + u_i^2 - u_{i+1}^2 - \ldots - u_n^2 \quad (2 \le i \le n).$

unfolding. They are either *cuspoid catastrophes* with one active variable u_1 (3 to 7) or *umbilic catastrophes* with two active variables u_1 and u_2 (8 to 13). They are usually referred to by the names and the symbols given in the last column of Table 2.1 (Arnol'd, 1972). Note that four of the forms in the list given by Thom, (4, 6, 10 and 13) have double signs. The positive sign corresponds to the standard form while the negative to the dual form.

It should be pointed out that in Table 2.1, the canonical form (regarding only the active part of the function) is a function with one or two variables: $f(u_1; t_1, \ldots)$ or $f(u_1, u_2; t_1, \ldots)$. At the critical point the gradient of f is zero: $\partial f / \partial u_i = 0$, which defines the equilibrium surface. The catastrophe occurs when the Hessian matrix $\left[\partial^2 f / \partial u_i \partial u_j\right]$ becomes singular. Eliminating the variable(s) from these two equations, the bifurcation set is obtained in terms of the parameters. The bifurcation set divides the parameter space to regions within which the same number and type of equilibria occur. Catastrophe occurs on the borders between the regions. Figure 2.7 illustrates three cuspoid types: the fold, the cusp and the swallowtail. The equilibrium of the fold and the cusp can be plotted in the coordinate systems (u_1, t_1) and (u_1, t_1, t_2), respectively. The equilibrium of the swallowtail requires a four-dimensional space though it is possible to plot the bifurcation set, which consists of surfaces in the coordinate system (t_1, t_2, t_3). A detailed study of this complicated type is shown in Chapter 5.

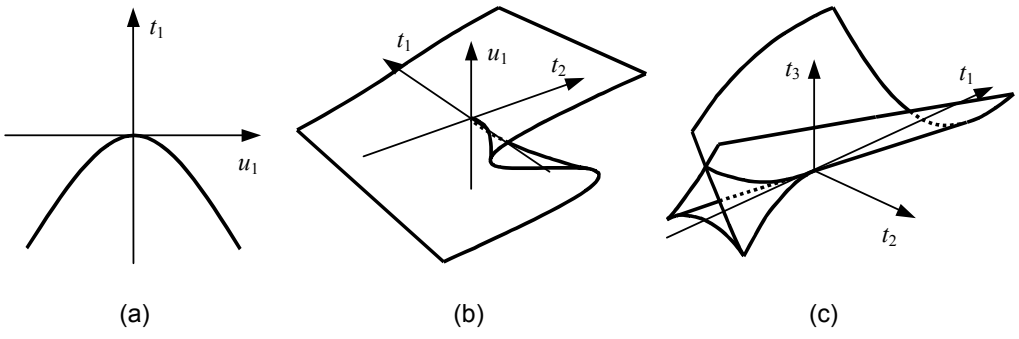

Figure 2.7: (a) Equilibrium of the fold. (b) Equilibrium of the cusp. (c) Bifurcation set of the swallowtail.

2.3.2 Application of elementary catastrophe theory in stability theory

Catastrophe theory provides a new approach to examine the behaviour of structures involved in stability problems. In order to apply the theory to a structure, several steps need to be taken (Gáspár, 1999):

1. In reality structures have infinite degrees-of-freedom but for our analysis a discrete model is required. The deformations are approximated by a linear combination of some basic functions resulting in a finite number of generalized coordinates.
2. The total potential energy function is formulated in terms of the generalized coordinates and the load parameter. In the critical state the gradient of the function becomes zero and the Hessian matrix is singular.
3. The potential energy function is extended by including imperfections. The Taylor series expansion is used at the critical point and local variables and parameters are introduced. It is sufficient to deal with the active part of the function, which is obtained by omitting the Morse part.
4. A suitable linear transformation is applied so that the potential energy function matches the canonical form of the corresponding catastrophe type.
5. Substituting this transformation into the equations of the catastrophe, gives the equilibrium surface, equilibrium path and the imperfection-sensitivity surface.

Now let us analyse the three examples shown in Section 2.2 in this way. All three structures are discrete models and the potential energy function and the critical state have already been determined previously (Step 1 and 2). Imperfections are introduced as the eccentricity of the location of the vertical force applied on the structure. It is regarded as positive if the force is shifted to right off the axis and negative if to left. The following steps are applied to the structures individually.

First let us examine the structure in Figure 2.2(a). The extended potential energy function now is:

$$\Pi(P,\phi,\varepsilon) = P(L\cos\phi - \varepsilon\sin\phi) + \frac{1}{2}k\phi^2 \tag{2.17}$$

where ε denotes the imperfection. The expression in the brackets defines the position of the load if the hinge is taken as a datum line. The second term gives the strain energy of the spring. At the critical state the deformation is $\phi_{cr} = 0$ and the critical load is given in Equation (2.4). The Taylor series expansion in a local system gives:

$$V = \frac{1}{24}ku^4 - \frac{1}{2}L\lambda u^2 - \frac{k}{L}\varepsilon u \tag{2.18}$$

where

$$u = \phi - \phi_{cr},\ \lambda = P - P_{cr} \text{ and } V = \Pi - \Pi_{cr}. \tag{2.19}$$

Note that only terms of order up to four and the least order mixed terms are included since they are the characteristic ones. Equation (2.18) is clearly equivalent to the *cusp*.

Now let us examine the second structure shown in Figure 2.3(a). In a similar way to the first case we include imperfections into the potential energy function:

$$\Pi(P,\phi,\varepsilon) = P(L\cos\phi - \varepsilon\sin\phi) + \frac{1}{2}k(L\sin\phi)^2 \tag{2.20}$$

whose Taylor series expansion gives:

$$V = -\frac{1}{8}kL^2u^4 - \frac{1}{2}L\lambda u^2 - kL\varepsilon u, \tag{2.21}$$

which is the canonical form of the dual *cusp* catastrophe.

And finally the third example shown in Figure 2.4(a) is to be analysed. Again the potential energy function is:

$$\Pi(P,\phi) = P(L\cos\phi - \varepsilon\sin\phi) + kL^2\left(\sqrt{1+\sin\phi} - 1\right)^2. \tag{2.22}$$

The Taylor series expansion gives

$$V = -\frac{1}{8}kL^2u^3 - \frac{1}{2}L\lambda u^2 - \frac{1}{2}kL\varepsilon u. \tag{2.23}$$

A linear transformation $u = \bar{u} - 4\lambda/3kL$ eliminates the second order term in the Taylor series. The new form in terms of the new variable $\bar{u}$ is now equivalent to the third form in Thom's theorem and thus the structure has the *fold* catastrophe.

2.4 Bifurcations of compatibility paths of mechanisms

2.4.1 Definitions

Maxwell's rule in structural engineering, as in (1.1) is a fundamental tool to assess the kinematic indeterminacy of a bar-assembly, but it is only a necessary condition for the rigidity of an assembly. There are special assemblies that are kinematically indeterminate due to their special topology though they are expected to be rigid by Maxwell's rule. Moreover, researchers discovered that the kinematic indeterminacy of a bar-and-joint assembly is affected by not only the topology but the metric properties of the assembly as well. A discussion on this topic can be found in more recent literature (Szabó and Roller, 1978; Tarnai, 1984, 1990). If a special geometry with unchanged topology makes the bar-assembly kinematically indeterminate, then that geometry is called the critical form. A simple example is a three-hinged two-bar structure supported at both ends as shown in Figure 2.8(a). In the original configuration the assembly is a load-bearing structure. In the special case of reducing the height of the structure to zero, see Figure 2.8(b), the bar-assembly loses its structural stiffness and becomes an infinitesimal mechanism.

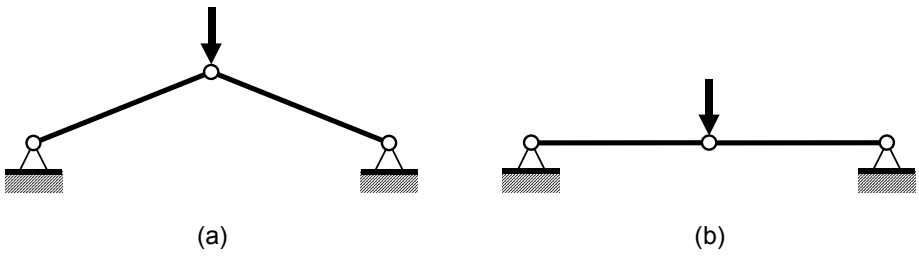

Figure 2.8: Three-hinged two-bar structure. (a) Non-collinear joints result in a statically determinate, load-bearing structure. (b) Collinear joints lead to an infinitesimal mechanism.

Infinitesimal mechanisms can undergo displacements with only infinitesimal elongations of bars. The order of a mechanism is determined by the highest possible order of elongations due to a suitable displacement system. Based on this, we can say that the two-bar linkage shown in Figure 2.8(b) is a first-order infinitesimal mechanism as the vertical displacement of the middle node does not cause first-order elongations but only second-order ones. The mobility of infinitesimal mechanisms was studied in the past by many researchers including Pellegrino and Calladine (1978), Kuznetsov (1989) as well as Tarnai and Szabó (2002).

A kinematically indeterminate bar-assembly can be a *finite mechanism*, which carries out finite motions while its elements remain inextensional. Maxwell's rule may help to determine the number of *kinematic degrees-of-freedom* at a general position of the mechanism. However, a finite mechanism may also have a *critical form* where the number of kinematic degrees-of-freedom increases. At the point of bifurcation the mechanism can change its configuration and hence continue its motion along different kinematic paths. Litvin (1980) has given a mechanism that produces such behaviour. In addition to the regular parallelogram shape, this four-bar linkage can also have a second configuration, which can be called anti-parallelogram shape, see Figure 2.9. Another example, a kite-shaped four-bar linkage has been shown by Tarnai (1999), which also has two configurations, see Figure 2.10.

Mechanisms require a certain number of kinematic state variables to determine the position of the elements. Placing the mechanism into a suitable coordinate system, an obvious choice of variables are the coordinates of the nodes. Since the nodes are connected by bars according to the topology of the mechanism, constraint equations should be formulated. Such an equation is called the *compatibility condition*. It can be in the form of the distance between the two nodes, which is equal to a given value: one compatibility condition is required for each bar.

Alternatively, an angle between a bar and a reference direction (in practice a coordinate axis) can be used. Assuming that particular bar to be rigid, the length of the bar and the angle replace the two coordinates of the end node. Consequently, the

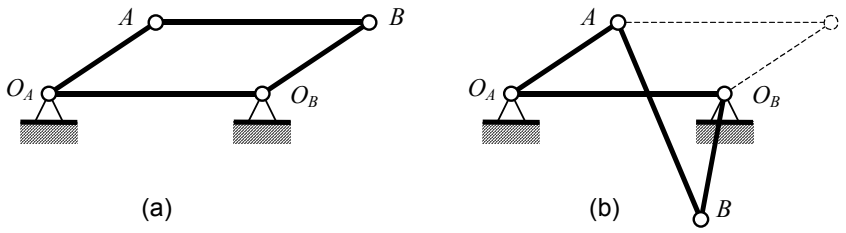

Figure 2.9: Two configurations of the parallelogram-shaped mechanism. (a) Parallelogram shape. (b) Anti-parallelogram shape.

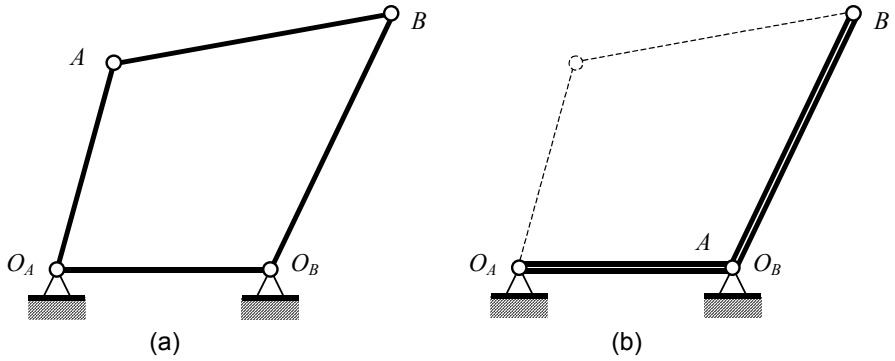

Figure 2.10: (a) Kite-shaped four-bar mechanism in which the neighbouring bars have the same length in pairs. (b) A configuration with adjoining bars.

compatibility condition for that bar is automatically fulfilled, e.g. two angles can describe the position of nodes *A* and *B* in Figures 2.9 and 2.10. A single compatibility condition is formulated for bar *AB*. Hunt (1978) has studied the input-output curves of a general four-bar linkage.

Values of the kinematic state variables which satisfy the compatibility conditions form *compatibility paths* (in the general case *compatibility manifolds*) in the variable space. A general configuration of a mechanism corresponds to a point on the compatibility path. A point where branches of compatibility paths intersect one another is called a *bifurcation point*. Here the mechanism is in *critical form* since in this position it can change its form and move along a different path.

2.4.2 Asymmetric kinematic bifurcation

The mechanism Tarnai has shown produces a bifurcation similar to the asymmetric equilibrium bifurcation. Tarnai (1999) pointed out that the kinematic bifurcation is

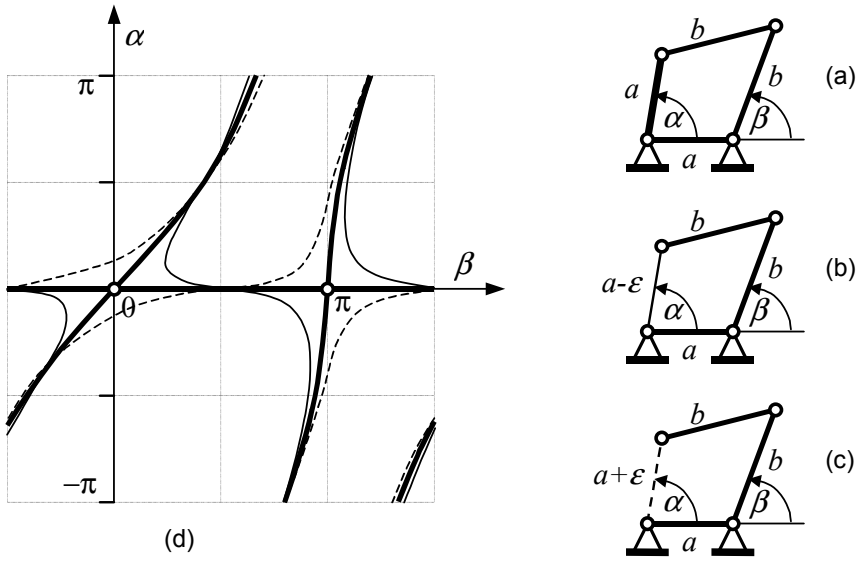

Figure 2.11: Kite-shaped four-bar linkage. (a)-(c) Perfect and imperfect geometries. Imperfection of the bar on the left side is considered. (d) Compatibility paths.

analogous to the well-known equilibrium bifurcations in stability theory. He suggested further study of kinematic bifurcations with respect to the similarities and differences between the two subjects. A numerical method for the simulation of kinematic bifurcations of deployable structures was proposed by Kumar and Pellegrino (2000).

The compatibility of the kite-shaped mechanism can be written for angles α and β as indicated in Figure 2.11(a). Points that correspond to compatible configurations of the mechanism, denoted by thick continuous lines, are plotted in Figure 2.11(d). The $\alpha = 0$ path, i.e. the horizontal line corresponds to the configuration shown in Figure 2.10(b). It has singular positions at $\beta = 0$ and $\beta = \pi$ where all bars are aligned with the line of the supports. At these points the mechanism can change its shape and move along a different path. The path crossing the origin of the coordinate system, also denoted by a thick line, corresponds to the configuration shown in Figure 2.10(a).

Tarnai also studied the behaviour of the imperfect mechanism. If a small error in length is introduced to the left bar, different compatible positions are obtained, see Figures 2.11(b) and (c). Graphs of imperfections with positive and negative sign are plotted in Figure 2.11(a) as solid and dashed thin lines, respectively.

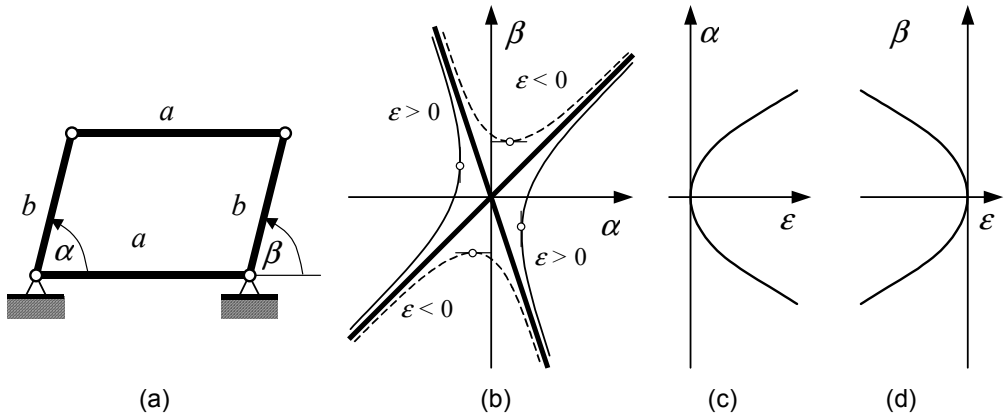

Figure 2.12: Parallelogram-like four-bar mechanism. (a) Basic structure. (b) Compatibility path. Thick lines denote the perfect system, thin continuous and dashed lines refer to positive and negative imperfections, respectively. (c)-(d) Imperfection-sensitivity.

Prior to Tarnai, Litvin (1980) showed a parallelogram-shaped four-bar linkage, which has an asymmetric bifurcation, see Figure 2.12(a). Two parameters, α and β are used to describe the system and the compatibility paths are shown by thick continuous lines in Figure 2.12(b). One path, defined by a straight line from the top right to bottom left, corresponds to the parallelogram shape while the other to the anti-parallelogram shape, see Figure 2.9.

Consider now a small ε manufacturing error in the length of the side bar on the left. The singularity of the mechanism is disturbed and the compatibility paths change. Paths corresponding to positive and negative imperfections are denoted by thin continuous and dashed lines in Figure 2.12(b), respectively. The paths have limit points now: if the imperfection is positive or negative, extrema are obtained for α or β, respectively. Tarnai (1999) has established the imperfection-sensitivity relationship for the particular case of $a = 2$ and $b = 1$. However, it is possible to derive the formulae in general:

$$\alpha_{extr} \approx \pm\sqrt{\frac{2(a-b)}{ab}}\,\varepsilon^{1/2}, \quad \varepsilon > 0 \tag{2.24}$$

and

$$\beta_{extr} \approx \pm\sqrt{\frac{2(a+b)}{ab}}(-\varepsilon)^{1/2}, \quad \varepsilon < 0\,. \tag{2.25}$$

The imperfection-sensitivity diagrams are shown in Figures 2.12(c) and (d).

2.4.3 Matrix analysis: the Jacobian and the Hessian

Tarnai (1990) has also proposed a method for the analysis of mechanisms. Given a suitable coordinate system, the Cartesian coordinates of the nodes of the mechanism are chosen to describe the configuration. The vector **Q** contains *n* kinematic state variables:

$$\mathbf{Q} = [Q_1 \dots Q_n]^{\mathrm{T}} = [\dots x_i \; y_i \dots]^{\mathrm{T}}. \tag{2.26}$$

where x_i and y_i represent coordinates. Compatible configurations are represented by the compatibility conditions in terms of the parameters:

$$F_k = \frac{1}{2}\left[(x_j - x_i)^2 + (y_j - y_i)^2 - l_k^2\right] = 0, \quad k = 1,\dots,m. \tag{2.27}$$

The Jacobian matrix of the compatibility condition system can be written as

$$\mathbf{J}(Q_1 \dots Q_n) = \left[\frac{\partial F_k}{\partial Q_i}\right]. \tag{2.28}$$

Denote $\mathbf{Q^0}$ as the kinematic parameters at a particular compatible configuration of the mechanism and calculate the rank of the Jacobian matrix at that configuration. Two possibilities may exist.

If $\rho(\mathbf{J})\big|_0 = m$, i.e., the rank of **J** at $\mathbf{Q^0}$ does not decrease, the equations of (2.27) are linearly independent, and therefore the system is a finite mechanism.

If $\rho(\mathbf{J})\big|_0 < m$, i.e., the rank of **J** at $\mathbf{Q^0}$ decreases, then the system is in a critical form and the equations in (2.27) are not linearly independent. Because of the linear dependency there exist $c_k \; (k = 1, \dots, m)$ constants so that function

$$\Phi = \sum_{k=1}^{m} c_k F_k \tag{2.29}$$

does not contain linear terms in its Taylor-series. At that point function □ has an extremum if the first-order derivatives are zero:

$$\frac{\partial \Phi}{\partial Q_i} = \sum_{k=1}^{m} c_k \left. \frac{\partial F_k}{\partial Q_i} \right|_0 = 0 \qquad i = 1, \ldots, n \,. \tag{2.30}$$

The equation system (2.30) can be written as

$$\mathbf{J}^{\mathrm{T}} \Big|_0 \mathbf{c} = \mathbf{0} \,, \tag{2.31}$$

which holds because of the definition of Φ. Now we define the Hessian matrix of function Φ:

$$\mathbf{H} = \sum_{k=1}^{m} c_k \mathbf{H}_k \tag{2.32}$$

where

$$\mathbf{H}_k = \left[\frac{\partial^2 F_k}{\partial Q_i \partial Q_j} \right], \qquad k = 1, \ldots, m \,. \tag{2.33}$$

If the Hessian matrix is *definite*, the system is an infinitesimal mechanism. If it has positive and negative eigenvalues, i.e. *indefinite*, the system is a finite mechanism, and if it is *semidefinite*, further examinations are required.

The compatibility path of the mechanism has a bifurcation at point $\mathbf{Q^0}$ if the mechanism is in a critical form there and preserves its mobility, i.e. the Hessian matrix is indefinite.

The method proposed in this section is discussed in detail in Chapter 4 and tested out with the aid of examples.

2.5 Other bifurcation phenomena in kinematics

Bifurcation phenomena occur in other fields of kinematics. Much work has been done on trajectory singularities of planar and spatial motions (Gibson and Hobbs, 1993, 1995, 1996; Donelan et al, 1999). Mechanism examples are also shown (Gibson et al, 1994, 1996, 1998). Xiang's thesis (1995) deals with planar mechanisms with one and two

degrees-of-freedom to demonstrate the singularities of trajectories of mechanisms. While compatibility paths define the relationship between the kinematic variables of a linkage in a multi-dimensional coordinate system, trajectories are two- or three-dimensional curves that chosen points of the linkage follow when the mechanism is activated.

3

ANALOGY BETWEEN EQUILIBRIUM PATHS OF STRUCTURES AND COMPATIBILITY PATHS OF MECHANISMS

Contents

It has been shown in the previous chapters that bifurcation phenomena have been found in kinematics of mechanisms that shows similar appearance to the well-known bifurcations of equilibrium paths in stability theory. In this chapter we extend the analogy along this line and show bifurcation modes other than the asymmetric one occurring for mechanisms, too. Kinematic counterparts of the equilibrium terms (e.g. variables, path, etc.) and the analogous behaviour are also discussed. A classification of the compatibility paths is proposed.

3.1 Bifurcation of compatibility paths

3.1.1 Extended analogy

The review given in Chapter 2 has shown great similarities between equilibrium paths of structures and compatibility paths of mechanisms. These similarities are listed in Table 3.1. The missing links are indicated by question marks.

Structures are expected to carry design loads, and consequently, their analysis requires both displacements and load parameters. Imperfections can be introduced, such as length errors of bars, initial inclination angles, and possibly imperfect position of load, etc. On the other hand, mechanisms are designed to transmit some specific motion and loads often are not included in the mathematical formulation. Thus, only kinematic state variables are used, such as Cartesian coordinates or angles. Accordingly, imperfections are taken into consideration only as geometric inaccuracies of elements, e.g. length errors of bars, etc.

As reviewed in Chapter 2, in both cases constraint conditions define the relationship between the variables, referring to feasible states of the system. For structures the constraints express static equilibrium, which is represented by equilibrium paths. Similarly, compatibility conditions are formulated for mechanisms, which define geometrically feasible configurations. They are represented by compatibility paths.

Table 3.1: Analogy between structures and mechanisms

	Stability	**Kinematics**
Object	Structure	Mechanism
Variables	Displacements Load	Coordinates, angles
Imperfections	Geometric Position of load	Geometric
Constraint condition	Equilibrium	Compatibility
Graph of constraint condition	Equilibrium path	Compatibility path
Bifurcation	Asymmetric Stable symmetric Unstable symmetric Degenerate symmetric	Asymmetric ? ? ?
Imperfect behaviour	Disturbed equilibrium paths may avoid bifurcation point (in the cases shown in Chapter 2)	Disturbed compatibility paths may avoid bifurcation point (in the cases shown in Chapter 2)
Classification of equilibrium / compatibility	Stable, unstable, neutral, critical	?

Three well-known common modes of bifurcation have been introduced in Section 2.2: the asymmetric, the stable symmetric (increasing load) and the unstable symmetric bifurcation (decreasing load). A degenerate symmetric bifurcation has been found later. On the other hand, the two examples of mechanisms, which have been analysed only have asymmetric bifurcations.

The imperfect behaviour of the asymmetric bifurcation has also been shown for both equilibrium paths and compatibility paths. All the structures and mechanisms discussed

above show that in the case of imperfections the new paths avoid the original bifurcation point. However, this may not always be the case.

In the following part of this chapter examples of mechanisms are presented which will extend the analogy and complete the missing parts in Table 3.1.

3.1.2 Symmetric bifurcation: a six-bar mechanism

Consider a six-bar mechanism shown in Figure 3.1(a). Bars O_AA and O_BB have unit length while all the others are $\sqrt{2}$. The two supported nodes are located at $O_A(-1, 0)$ and $O_B(1, 0)$. Node D is also supported by a roller allowing it to move along axis y only. As the mechanism has $j = 6$ nodes, $b = 6$ bars and $k = 5$ supported degrees-of-freedom, Maxwell's rule indicates that it has one kinematic degree-of-freedom. It can be represented by the motion of node D in the basic configuration.

A sufficient number of kinematic state variables and compatibility conditions are required to describe the mechanism in a most general way. Assuming that length of bars O_AA, O_BB and AC are given, four independent variables are necessary to define the positions of A, B, C and D. We choose ϕ_1, ϕ_2, ϕ_3 and ϕ_4 in Figure 3.1(b). Compatibility conditions can be formulated for the remaining bars, ①, ②, and ③:

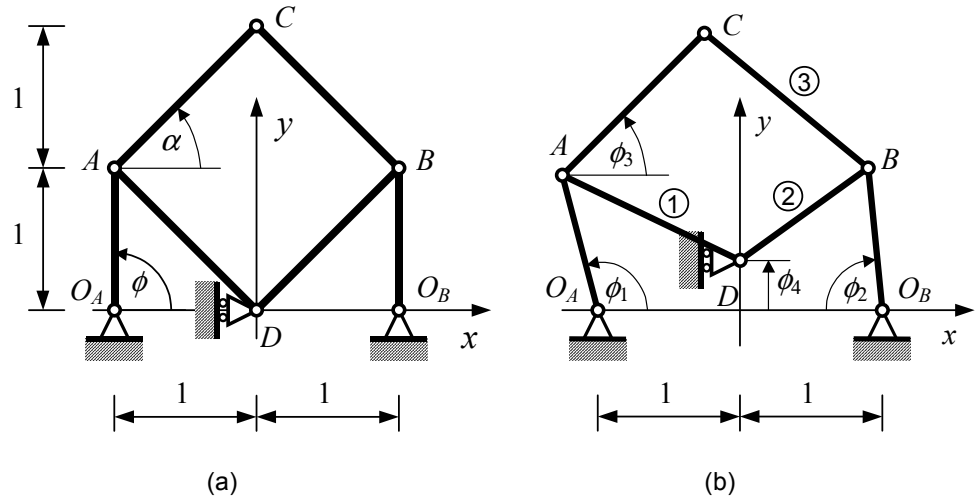

Figure 3.1: A six-bar mechanism. (a) Basic structure. (b) Kinematic variables. For bars ③, ①, and ① compatibility conditions are established.

$$F_1 = d_{AD}(\phi_1, \phi_4) - \sqrt{2} = 0,$$

$$F_2 = d_{BD}(\phi_2, \phi_4) - \sqrt{2} = 0, \qquad (3.1)$$

$$F_3 = d_{BC}(\phi_1, \phi_2, \phi_3) - \sqrt{2} = 0$$

where d_{AD}, d_{BD} and d_{BC} denote the distance between the nodes indicated in terms of the angles. (A detailed study of compatibility is given in Chapter 4.)

Sets of values of the variables that satisfy the compatibility conditions (3.1) form the compatibility paths in the four-dimensional space of $(\phi_1, \phi_2, \phi_3, \phi_4)$. Planar projections of the paths are plotted in Figure 3.2. Characteristic points of the paths are marked by numbers and the corresponding configurations are shown in Figure 3.3. Bars *AC* and *BC* may have two different positions: they are drawn by dashed and dotted lines, also coloured red and green, respectively. The two configurations are referred to by single and double quotes following the number, respectively: 2′, 2″, 3′, 3″, 4′, 4″, 6′, 6″, 7′, 7″, 8′, 8″, 10′, 10″, 11′ and 11″. The chain *ACB* has only one position at points 1, 5, 9 and 12.

Figure 3.2 shows that the compatibility paths consist of four closed loops and two straight lines. Curve *A* connects points 1, 2′, 3′, 12, 11′, 7′ and 1, curve *B* connects 1, 2″, 3″, 12, 11″, 7″ and 1, curve *C* connects 5, 4″, 3″, 10″, 9, 8″, 7″, 6″ and 5, and finally curve *D* connects 5, 4′, 3′, 10′, 9, 8′, 7′, 6′ and 5. Paths *A* and *B* correspond to symmetric configurations while the other two to asymmetric ones. The straight line E_1 connects points 2′ and 2″, and E_2 connects 11′ and 11″.

The two lines are projected to a single point in the plane (ϕ_1, ϕ_2). The projections of curves *A* and *B* coalesce as well as curves *C* and *D*. The two lines coalesce in the plane (ϕ_2, ϕ_3). One loop is the projection of curves *A*, *B* and *D*, while the other loop refers to curve *C* only. The straight lines are separated in plane (ϕ_3, ϕ_4) while the curves coalesce in pairs: *A* with *D*, and *B* with *C*. Finally, the lines are projected to one point each and the curves all coalesce in plane (ϕ_1, ϕ_4).

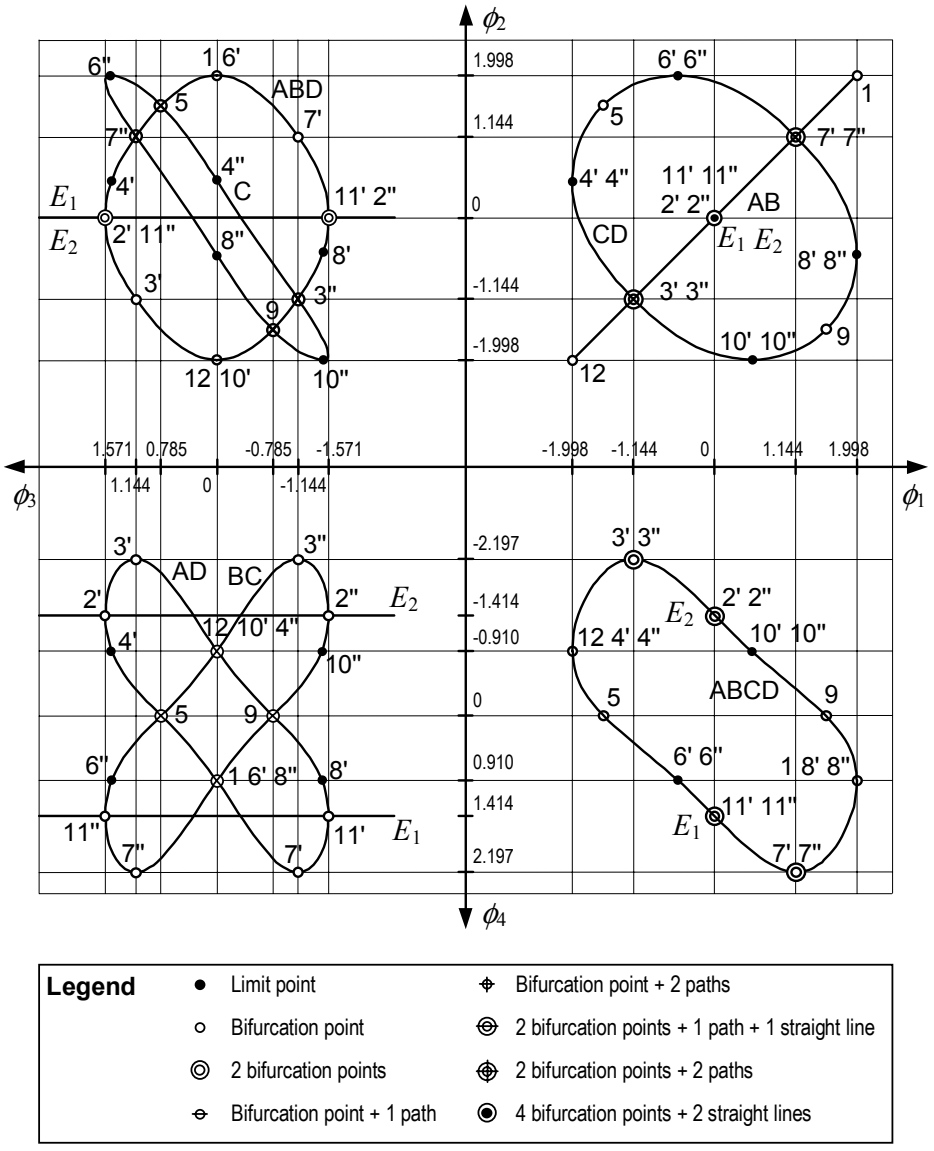

Figure 3.2: Planar projections of the compatibility paths of the six-bar mechanism. Numbers mark characteristic configurations, followed by ′ and ″ if node *C* have two different positions. Closed compatibility paths are marked as *A*, *B*, *C* and *D*. Straight lines are marked as E_1 and E_2. Crossing paths without marking imply no intersecting of the paths.

In the projections of the compatibility paths the curves may coalesce, intersect each other with bifurcation or cross without bifurcation. It is easy to tell that the paths bifurcate in the configurations 1, 2′, 2″, 3′, 3″, 5, 7′, 7″, 9, 11′, 11″ and 12. The points of the four-dimensional paths produce special coincidences in the two-dimensional projections, resulting in a large variety of different points. Therefore various notations are introduced as shown in Figure 3.2. It is important to mention a multiple coincidence

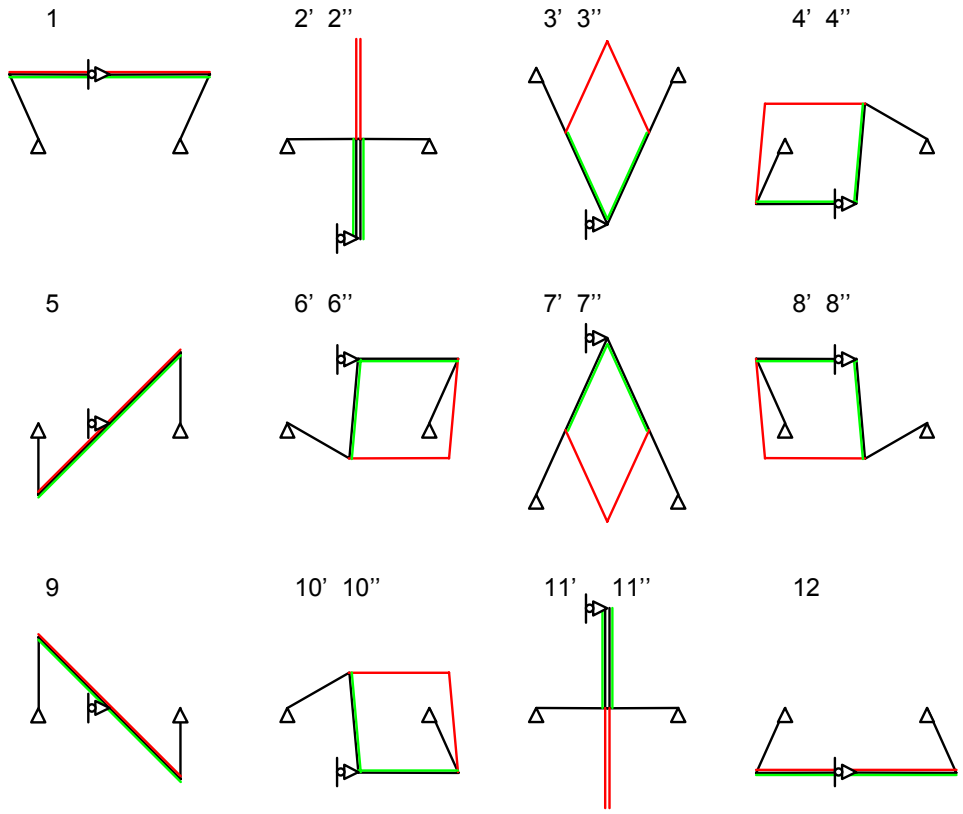

Figure 3.3: Characteristic configurations of the six-bar mechanism. Numbers correspond to those of positions in Figure 3.2. Black lines denote chain $O_A ADBO_B$. Red and green lines denote two possible positions of chain ACB.

where four bifurcation points and the two straight lines are projected to the single point $(0, 0)$ in plane (ϕ_1, ϕ_2). Crossing paths without marking correspond to non-intersecting compatibility paths.

Let us study three most representative characteristic points in detail. First consider point 1. The corresponding configuration of the mechanism is shown in the first diagram in Figure 3.3 and is reproduced in Figure 3.4(a). Here all the longer bars are horizontal. The coordinates of this configuration are $\phi_{1,0} = \phi_{2,0} = \arccos\left(1 - \sqrt{2}\right)$, $\phi_{3,0} = 0$ and $\phi_{4,0} = \sqrt{2\sqrt{2} - 2}$. The compatibility paths are best viewed in the projection (ϕ_3, ϕ_4). Here curves A and B intersect creating a bifurcation point. In this projection point 1 coalesces with points $6'$ and $8''$, which belong to curves D and C, respectively. Omitting these independent compatibility paths, the relevant section is plotted in thick solid lines in the local coordinate system (ϕ_3, ϕ_4') centred at the bifurcation point as

shown in Figure 3.4(b) where $\phi_4' = \phi_4 - \phi_{4,0}$. The two paths are locally symmetric to axis ϕ_3 and they have an inclined tangent to axis ϕ_4. They correspond to node *C* moving up or down when node *D* is actuated by changing ϕ_4.

Consider an imperfection of the mechanism: bar *AC* is made longer or shorter by a small amount ε with respect to the original size. The bifurcation is disturbed and the

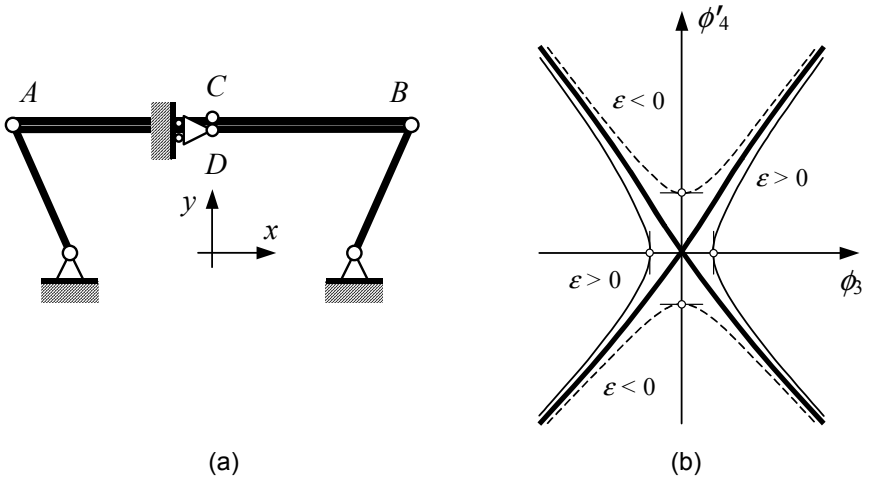

Figure 3.4: Bifurcation point 1 of the six-bar mechanism. (a) Configuration. (b) Compatibility paths. Thick lines correspond to perfect geometry. Thin continuous and dashed lines denote paths with positive and negative ε, respectively, which is imperfection of bar *AC*.

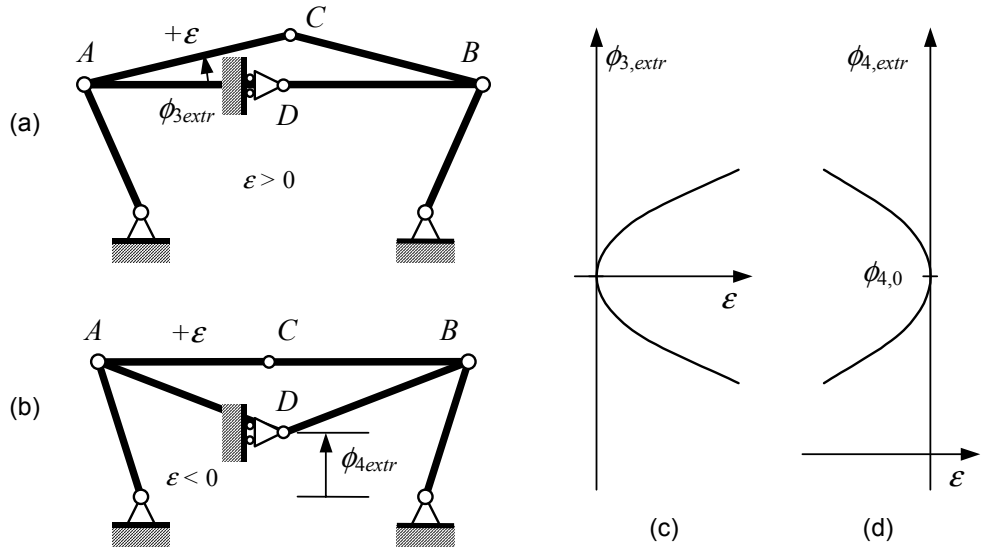

Figure 3.5: Imperfection-sensitivity of the six-bar mechanism near bifurcation point 1. (a) Extreme configuration at positive imperfection of bar *AC*. (b) Extreme configuration at negative imperfection. (c)-(d) Imperfection-sensitivity diagrams for positive and negative imperfections, respectively.

compatibility paths change. The new paths are plotted in thin continuous and dashed lines in Figure 3.4(b).

Note that all curves have limit points near the bifurcation point of the path for the perfect mechanism. In the case of a positive imperfection, parameter ϕ_3 has extrema, a maximum on one of the paths and a minimum on the other. The corresponding configuration of the mechanism can be determined by geometric considerations. As line *AB* is parallel to axis *x*, ϕ_3 in triangle *ABC* is minimized (or maximized) when the distance *AB* is maximized. This occurs when *A*, *D* and *B* are collinear. The configuration corresponding to the minimum position is shown in Figure 3.5(a). Denote $\phi_{3,extr}$ as the extremum of ϕ_3. Now the cosine of $\phi_{3,extr}$ can be calculated in triangle *ABC*, from which the exact and approximate formula for the angle is obtained:

$$\phi_{3,extr} = \arccos\left(\frac{8+2\sqrt{2}\varepsilon+\varepsilon^2}{4\sqrt{2}\left(\sqrt{2}+\varepsilon\right)}\right) \approx \pm 2^{-1/4}\varepsilon^{1/2}. \tag{3.2}$$

This relationship is shown in Figure 3.5(c).

If a negative imperfection is considered, parameter ϕ_4 can have extremum points. In Figure 3.5(b) a position is shown at which ϕ_4 is maximized in the lower curve. In a similar way to the previous case, $\phi_{4,extr}$, which is the extremum of ϕ_4, can be calculated in triangle *ABC*:

$$\phi_{4,extr} = \phi_{4,0} \pm \sqrt{-\sqrt{2}\varepsilon - \frac{\varepsilon^2}{4}} \approx \phi_{4,0} \pm 2^{1/4}\left(-\varepsilon\right)^{1/2}. \tag{3.3}$$

This relationship is shown in Figure 3.5(d).

Consider now bifurcation point 2′, which is one of the intersection points between paths *A* and E_1. The coordinates of the point are $\phi_1 = \phi_2 = 0$, $\phi_3 = \pi/2$ and $\phi_4 = -\sqrt{2}$ and the configuration is shown in Figure 3.6(a). The two bars with unit length are aligned along axis *x* so that nodes *A* and *B* coalesce at the origin of the coordinate system. Bars *AD* and *BD* are adjoined as well as bars *AC* and *BC* and node *C* is on axis *y*.

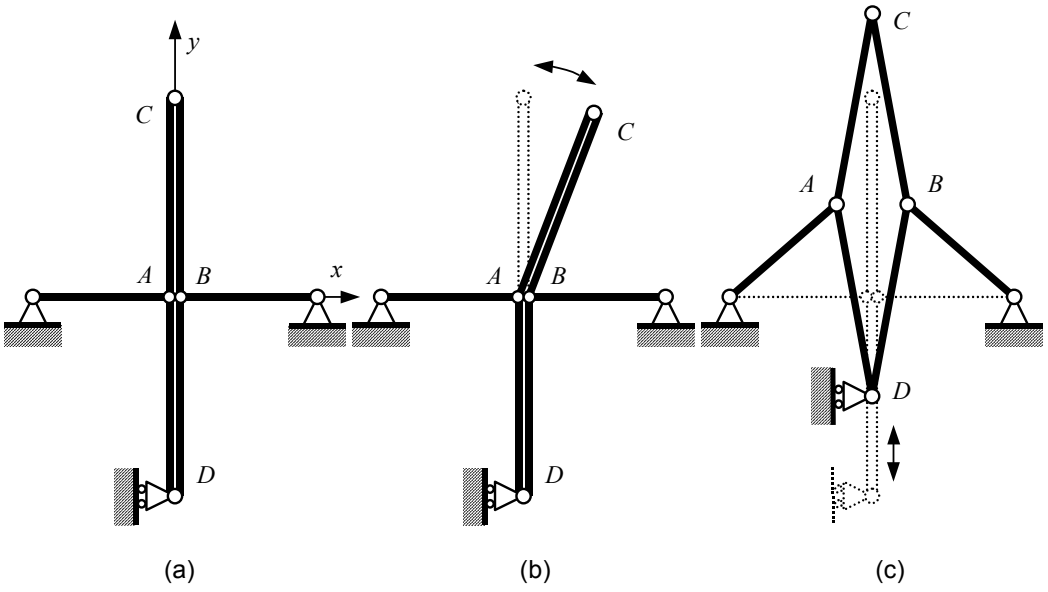

Figure 3.6: Bifurcation point 2′ of the six-bar mechanism. (a) Configuration at the bifurcation point. (b, c) Configurations corresponding to paths A and E_1.

Moving from that position, the mechanism may have two different configurations as shown in Figure 3.6(b) and (c). The first configuration involves the movement of node C only while the rest of the mechanism is motionless. Parameter ϕ_2 is constant zero and ϕ_3 changes as bars AC and BC are simultaneously rotating around the common centre. The corresponding path is a straight line denoted by E_1 in Figure 3.2.

The other configuration involves the motion of the entire mechanism. As ϕ_2 changes linkage $ABCD$ opens up to make a diamond shape, see Figure 3.6(c). This motion corresponds to the curved path denoted by A in Figure 3.2. As nodes A and B are moving apart during the motion, ϕ_3 is decreasing regardless of the sign of ϕ_2. Furthermore, the symmetry of the mechanism also ensures the symmetry of the compatibility path.

Paths A and E_1 have another intersection at point 2″. At this point the coordinates are the same with the exception of $\phi_3 = -\pi/2$. Hence the configuration is very similar to 2′ but node C is pointing down coalescing with D. It is easy to show that a similar behaviour occurs at this bifurcation point. The compatibility path is now a mirror image with the opposite sign of ϕ_3.

The behaviour of the mechanism at points 2′ and 2″ is best viewed in the projection (ϕ_2, ϕ_3). The compatibility paths are shown in Figure 3.7(a) by thick solid curves. At point 2′, the bifurcation is a symmetric decreasing one, similar to an unstable symmetric equilibrium bifurcation in structural stability theory, while the bifurcation at point 2″ is a symmetric increasing one close to the same named stable symmetric equilibrium bifurcation in the structural stability theory.

Imperfection is again taken into consideration as the inaccuracy ε of the length of bar *AC*. Compatibility paths of positive and negative imperfections are denoted by thin continuous and dashed thin lines, respectively, in Figure 3.7(a). Bifurcation again does not occur and the graph is separated into several branches. Paths that correspond to positive imperfections have limit points and the others do not. Similarly, some of the imperfect equilibrium paths in Figures 2.2(b) and 2.3(b) have limit points while others

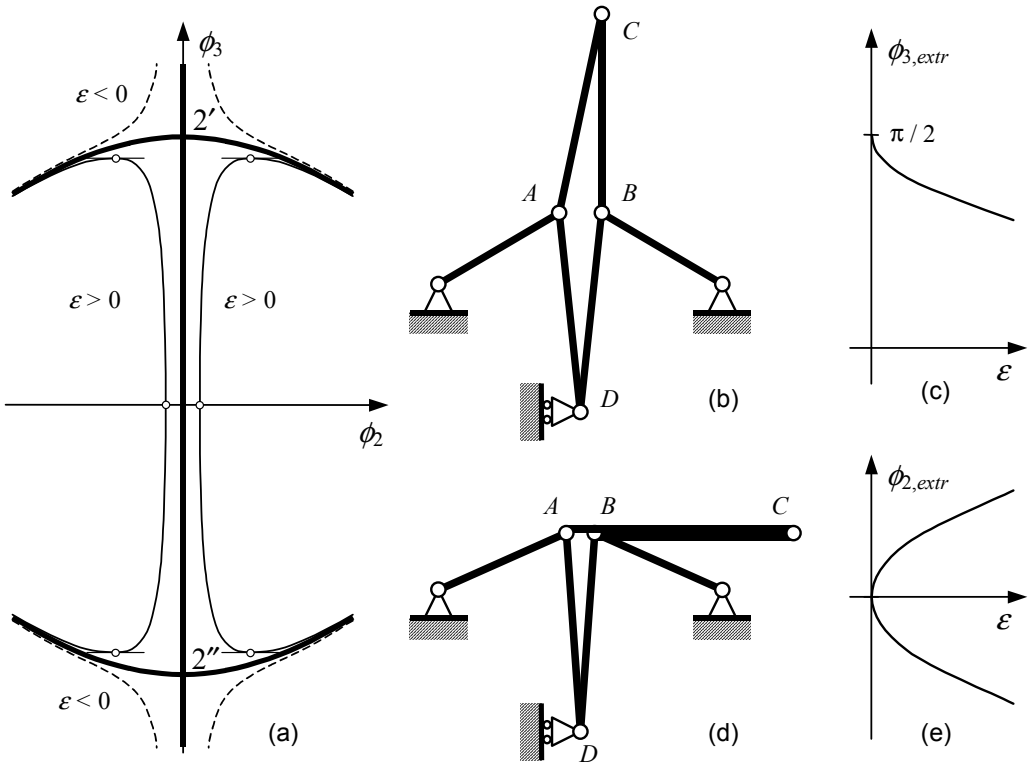

Figure 3.7: Bifurcation points 2′ and 2″ of the six-bar mechanism. (a) Compatibility paths. Thick lines denote perfect structure, thin continuous and dashed lines denote positive and negative imperfection of bar *AC*, respectively. (b) Extremum of ϕ_3 at $\varepsilon > 0$. (c) Extremum of ϕ_2 at $\varepsilon > 0$. (d)-(e) Imperfection-sensitivity diagrams for cases *b* and *c*, respectively.

do not. But contrary to the equilibrium case, compatibility paths corresponding to the same imperfection are now symmetric in position as they are in adjacent sections of the graph on the two sides of axis ϕ_3. (In the equilibrium case they are in opposite quadrants of the graph.)

The negative paths are on the upper and lower part and have no limit points. The positive paths are between the perfect curved paths and have two limit points each. This means that during the motion ϕ_3 cannot exceed a particular value which depends on the magnitude of the imperfection. The corresponding configuration of one of the limit points ($\phi_2 > 0$, $\phi_3 > 0$) is shown in Figure 3.7(b). Here ϕ_3 reaches a maximum which can be determined by geometric considerations. As *AB* is parallel to axis *x*, ϕ_3 is equal to the angle at node *A* in the triangle *ABC*. Angle ϕ_3 is maximized if its sine is maximized. As the latter quantity is proportional to the distance between node *C* and line *AB*, the extremum is obtained if bar *BC* is perpendicular to line *AB*. Now ϕ_3 is calculated in triangle *ABC*:

$$\phi_{3,extr} = \arcsin\left(\frac{\sqrt{2}}{\sqrt{2}+\varepsilon}\right) \approx \frac{\pi}{2} - 2^{1/4}\varepsilon^{1/2}. \tag{3.4}$$

The imperfection-sensitivity diagram is shown in Figure 3.7(c).

The compatibility path in Figure 3.7(a) also shows that ϕ_2 reaches its extrema. The corresponding configuration is shown in Figure 3.7(d) which is again determined by simple geometric considerations. Since bar *AC* is by an amount ε longer then *BC*, the distance between nodes *A* and *B* cannot be smaller than ε. The extremum of ϕ_2 is reached when this distance equals ε. In this position nodes *A*, *B* and *C* are aligned parallel to axis *x*. As the distance of *A* and *B* is given in terms of ϕ_2, the following relationship is obtained:

$$\phi_{2,extr} = \arccos\left(1 - \frac{\varepsilon}{2}\right) \approx \pm\varepsilon^{1/2}. \tag{3.5}$$

The imperfection-sensitivity diagram is shown in Figure 3.7(e).

The implication of imperfections is that the mobility of the mechanism is significantly reduced. If the mechanism is actuated by bar O_AA, i.e. the actuator drives angle ϕ_2, it will halt as ϕ_2 reaches its minimum. Also at the limit point in Figure 3.7(a) maximum of ϕ_3 is less than the value at the original bifurcation point. Now bar AC cannot rotate freely and it cannot even rise to the vertical position.

3.1.3 Degenerate bifurcation: a square-shaped linkage

Consider now a special four-bar linkage shown in Figure 3.8(a). It is a special case of either the parallelogram-shaped mechanism or the kite-shaped one as all four bars are now of the same length. Two kinematic state variables are used again, angles α and β determine the position of nodes A and B, respectively. The compatibility condition can be written for bar AB, and the compatibility paths are plotted in Figure 3.8(b) by thick continuous lines.

The graph shows similarity to that of the kite-shaped mechanism previously shown in Figure 2.9(d). The straight branches at axis β are identical in both cases and the curved ones are now straight and in a similar position. Bifurcation occurs at three points

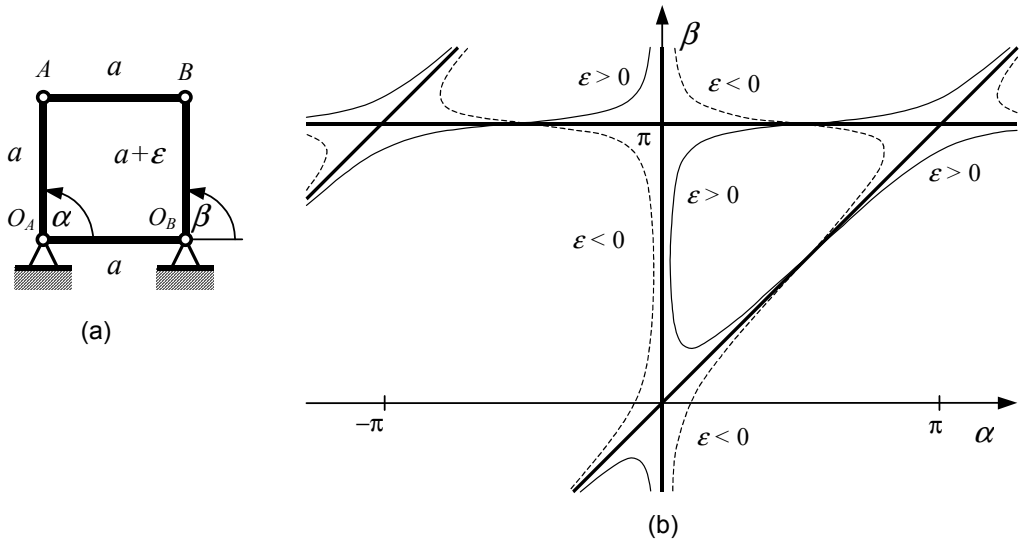

Figure 3.8: Square-shaped four-bar mechanism. (a) Basic structure, imperfection of bar O_BB is considered. (b) Compatibility paths. Thick lines denote perfect structure, while thin continuous and dashed lines refer to positive and negative imperfections, respectively.

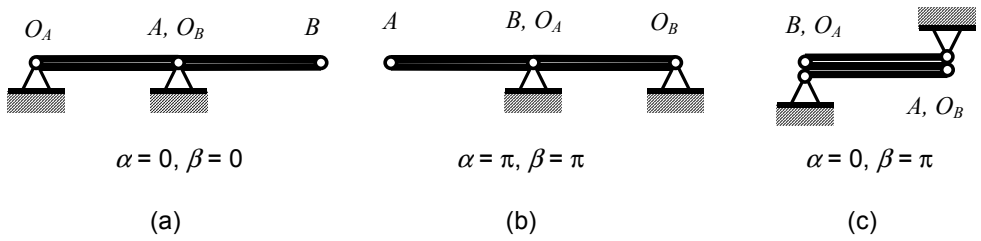

Figure 3.9: Bifurcation points of the square-shaped mechanism. (a) $\alpha = 0$, $\beta = 0$ (b) $\alpha = \pi$, $\beta = \pi$ (c) $\alpha = 0$, $\beta = \pi$

Figure 3.10: Configurations corresponding to the compatibility paths of the square-shaped four-bar mechanism at bifurcation point ($\alpha = 0$, $\beta = \pi$). (a) $\beta = \pi$ and α is varying. (b) $\alpha = 0$ and β is varying.

in the graph: $(\alpha = 0, \beta = 0)$, $(\alpha = \pi, \beta = \pi)$ and $(\alpha = 0, \beta = \pi)$. The first and the second are asymmetric bifurcations while the third is different. Since the two branches are straight lines that intersect at a right angle, this bifurcation is symmetric but at the same time it is neither increasing nor decreasing. It can be regarded as an infinitely degenerate case of the symmetric bifurcations shown above and be paralleled to the equilibrium bifurcation of the special structure shown in Section 2.2.4, see Figure 2.5.

Special configurations of the mechanism corresponding to bifurcation points are shown in Figure 3.9. In all cases the bars are aligned with axis *x*. At the first bifurcation point the mechanism can either move to the basic configuration in Figure 3.8(a) or bars *AB* and O_BB rotate simultaneously in a similar way to the kite-shaped mechanism. The second bifurcation point is similar with the difference of bars *AB* and O_AA rotating simultaneously. The third bifurcation point combines both of the previous ones as the mechanism is 'doubly-folded' and all bars occupy the same position. Note that in Figure 3.9(c) it is shown distorted for better visualization and bar O_AO_B is also omitted. At this position the mechanism can follow two compatibility paths. One of them corresponds to the simultaneous rotation of bars O_AA and *AB* around O_A and now α is

varying while β remains π. The situation is similar for the other compatibility path where bars AB and O_BB are rotating. Here α is constant zero and β is varying. The configurations are shown in Figure 3.10. The graphs are again distorted for better visualization and bar O_AO_B is omitted.

Imperfect behaviour is taken into consideration as the geometric error ε of bar O_BB. Compatibility paths of positive and negative values of ε are denoted by thin continuous and dashed lines, respectively, in Figure 3.9(b). Again the imperfect mechanism does not have bifurcations. The compatibility paths near the first and the second bifurcation points are similar to those of the kite-shaped four-bar mechanism shown in Figure 2.9(d). At each bifurcation point two paths have limit points and the other two do not. Imperfection-sensitivity diagrams can be drawn similar to those presented for the parallelogram-shaped four-bar mechanism.

At the third point the behaviour is different because both perfect paths are straight lines. Comparing the imperfect paths in Figure 3.8(b) with those in Figure 2.5(b) one can see that the compatibility and equilibrium paths have similar shape and position in the neighbourhood of the bifurcation point.

3.2 Classification of compatibility paths

The imperfect configuration of the six-bar mechanism demonstrates that irregular behaviour can occur not only at points where branches of compatibility paths meet but along the entire compatibility paths, too. Such irregular behaviour demands a classification which covers all points of the paths.

In stability theory points of equilibrium paths are typically stable or unstable depending on whether the potential energy at the equilibrium position has a local minimum or maximum. Entire sections of equilibrium paths are stable or unstable between points where the stability changes. These are the critical points, including limit points and bifurcation points. A curious exception is given by the state of neutral

equilibrium, which occurs for example on the secondary path of the degenerate structure shown in Figure 2.5.

No equivalent terms have been defined for the stability of a configuration of mechanisms for we have not considered the local minimum or maximum of a potential function but applied the compatibility conditions in the analysis directly. However, distinction should be made between *regular* and *irregular* behaviour of compatibility positions.

The irregularity can be in a way captured by applying perturbations to a perfect system. Consider again the six-bar mechanism and its compatibility paths shown in Figure 3.7(a). Thin lines denote the compatibility paths in the case where the length of bar AC is changed by ε. Regardless of the sign of the imperfection each of the curved compatibility paths has one imperfect path in its vicinity. If the imperfection is positive or negative, the imperfect paths are on the 'inner' or 'outer' sides of the bifurcation points, respectively, which, however, represent completely different behaviour. If the imperfection is positive, there are *two* imperfect lines along the section between the bifurcation points and *none* outside. With a negative imperfection the situation is the other way round. We can conclude that entire sections of the compatibility paths can either split into two or vanish. Note that in this case the bifurcation points have vanished, just as happens with the four-bar linkages.

It is also possible to introduce imperfections so that the bifurcation points do not vanish but themselves split. Bifurcation points of the six-bar mechanism occur when the two sidebars are aligned and nodes A and B coalesce. This special configuration is possible due to the equality of the distance between the two fixed supports and the total length of the two bars.

Consider a perturbation of the configuration by introducing an imperfection to the fixed supports: they are made either closer to or farther from each other by a small amount δ while the bar lengths remain unchanged, see Figure 3.11(a). Positive δ refers to the distance becoming larger. In this case no bifurcation occurs as nodes A and B cannot coalesce. Moreover, the entire straight path vanishes because the simultaneous

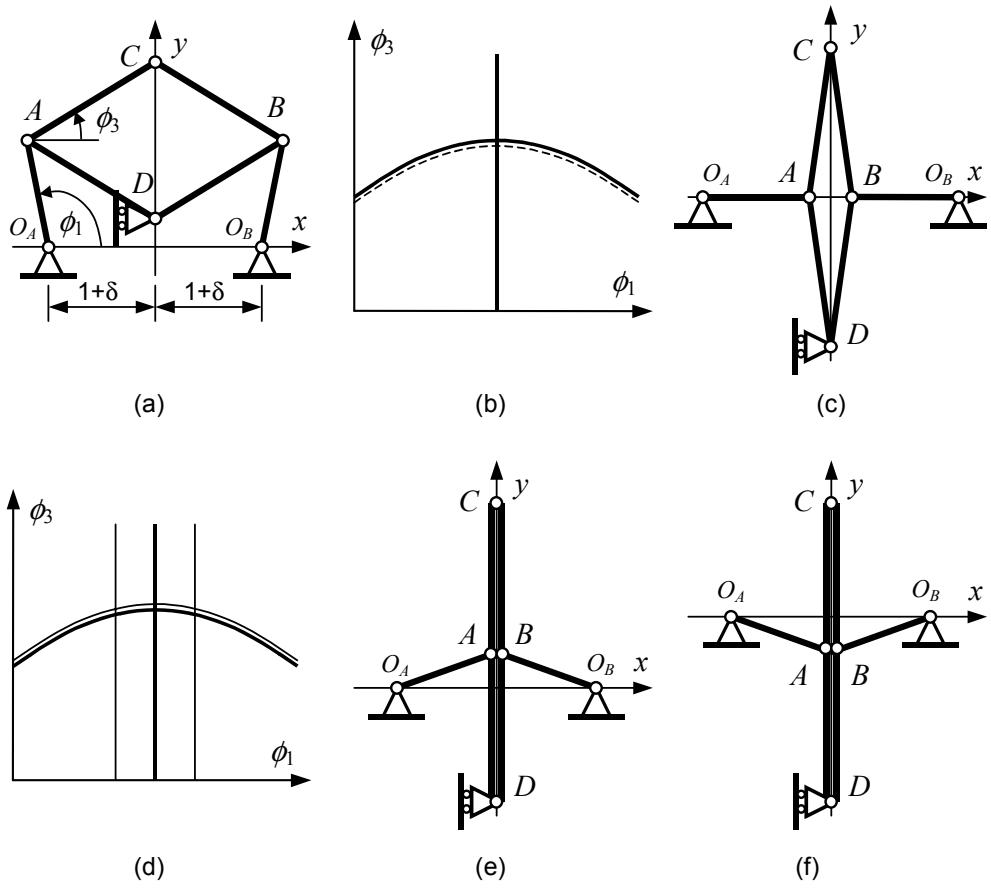

Figure 3.11: Split-vanish compatibility path of the six-bar mechanism. (a) Basic structure with imperfection δ. (b) Perfect compatibility paths (heavy lines) and imperfect compatibility paths for $\delta > 0$ (thin dashed line). (c) Configuration for the extremum of the imperfect curved path. (d) Perfect compatibility paths (heavy lines) and imperfect compatibility paths for $\delta < 0$ (thin continuous lines). (e)-(f) Bifurcation configurations of the imperfect mechanism.

(or near simultaneous) rotation of bars AC and BC is not possible, as shown in Figure 3.11(b). Note that the curved path is perturbed but exists. Figure 3.11(c) shows the configuration of the mechanism where the imperfect curved path reaches its extremum.

If the imperfection is negative, i.e. the fixed points are shifted towards each other, nodes A and B can coalesce before they reach the origin of the coordinate system. It happens in two positions on either sides of axis x. The simultaneous rotation is possible in both cases. Consequently, the entire straight path splits into two as shown in Figure 3.11(d). Note again that the perturbed curved paths exist and form new bifurcation points with the straight paths, i.e. the bifurcation points have also split, see

Figures 3.11(e) and (f). Due to the symmetry of the compatibility paths, Figures 3.11(b) and (d) show the vicinity of one bifurcation point only.

Considering the various kinds of behaviour, a classification of compatibility positions is clearly needed. We group points on compatibility paths into five types as follows:

(a) *Regular point*: a point on a compatibility path which cannot be made to split or vanish.

(b) *Regular bifurcation point*: points where two or more regular compatibility paths meet.

(c) *Limit point*: distinct point of a compatibility path where one of the state variables is maximized or minimized in terms of the others.

(d) *Split-vanish point*: a point that can either split or vanish by applying a suitable perturbation to the system. No bifurcation exists at the point.

(e) *Split-vanish bifurcation point*: a bifurcation point which can either split into two bifurcation points or vanish with a suitable perturbation applied to the system.

Most of the compatible positions of mechanisms are regular such as general points of the kite-shaped or the parallelogram-shaped mechanisms, etc. Note that straight compatibility paths can also be regular.

A compatibility path consisting of only regular points, limit points and/or regular bifurcation points is defined as a regular compatibility path. A compatibility path which has split-vanish points and/or split-vanish bifurcation points is defined as an irregular compatibility path.

3.3 Compatibility condition revisited

Compatibility conditions have been set up previously for the six-bar linkage and the parallelogram-shaped linkage in order to obtain compatibility paths. Here we revisit these equations and examine their general form and alternatives.

Compatibility conditions are defined as equations that determine values of the kinematic state variables corresponding to compatible configurations of a mechanism. The equation yields zero if and only if the condition is satisfied. Its analogue in structural mechanics is the equilibrium equation, which expresses the static equilibrium of a structure.

In both cases, in principle, the constraint equations can be formulated arbitrarily in terms of variables q_i if and only if the related system is in equilibrium or compatible, respectively:

$$F(\ldots q_i \ldots) = 0\,. \tag{3.6}$$

In structural stability, real equilibrium equations are used. Furthermore, they are derived from the potential energy of the structure, as shown in Section 2.1.

On the other hand, the situation is not obvious for mechanisms and various formulations of the compatibility conditions are possible. Tarnai (1990) used Cartesian coordinates of the nodes and created one compatibility condition for each bar of the linkage:

$$F_k = \frac{1}{2}\left[(x_j - x_i)^2 + (y_j - y_i)^2 - l_k^2\right] = 0 \tag{3.7}$$

where l_k is the length of bar k which connects nodes i and j. This formulation states that the square of the distance between the nodes is equal to the square of the length of the bar. A formally more complicated expression is obtained if the distances and the lengths are used:

$$F_k = \sqrt{(x_j - x_i)^2 + (y_j - y_i)^2} - l_k = 0\,. \tag{3.8}$$

Alternatively, the number of variables can be reduced by introducing angles instead of translational coordinates. All the mechanisms in Section 2.4 were described by two angles, which implicitly satisfied some of the compatibility conditions. In the remaining

single equation the coordinates of the nodes are all in terms of the angles. Two formulations are possible again:

$$F(\xi,\eta)=\frac{1}{2}\left\{\left[x_j(\xi,\eta)-x_i(\xi,\eta)\right]^2+\left[y_j(\xi,\eta)-y_i(\xi,\eta)\right]^2-l_k^2\right\}=0\,, \tag{3.9}$$

$$F(\xi,\eta)=\sqrt{\left[x_j(\xi,\eta)-x_i(\xi,\eta)\right]^2+\left[y_j(\xi,\eta)-y_i(\xi,\eta)\right]^2}-l_k=0 \tag{3.10}$$

where ξ and η denote the kinematic state variables.

The equations with square root forms in (3.8) and (3.10) express the difference between the length of the bar and the distance of the nodes. The other two equations deal with the square of these terms but have the advantage of easy applicability to mathematical calculus, as they are simple to differentiate. It should be mentioned that other formulations may also be considered.

3.4 Energy formulations

3.4.1 Potential energy function for mechanisms

It has been shown that the kinematic counterpart of equilibrium is the compatibility equation. Since the former is derived from the potential energy function of the structure, one may try to create a similar function for mechanisms.

Tarnai (1990) proposed a potential energy function for a system described by *n* generalized coordinates and *m* constraint equations:

$$\Pi=-\sum_{i=1}^{n}P_i\left(Q_i-\overline{Q}_i\right)+\sum_{k=1}^{m}\Lambda_k F_k \tag{3.11}$$

where the notations are as follows:

P_i, $i=1,\ldots,n$ external load components,

Q_i, $i=1,\ldots,n$ generalized coordinates,

$\overline{Q}_i$, $i=1,\ldots,n$ reference coordinates,

F_k, $k = 1,\ldots,m$ kinematic constraints or compatibility equations,

Λ_k, $k = 1,\ldots,m$ Lagrange-multipliers.

The kinematic constraints are derived by differentiating (3.11) with respect to the appropriate Lagrange-multiplier:

$$\frac{\partial V}{\partial \Lambda_k} = F_k = 0, \quad k = 1,\ldots,m\,. \tag{3.12}$$

Another function was proposed by Géradin (1999) for three-dimensional rigid bodies.

$$\Pi = -\int_{V_0} \mathbf{x}^{\mathrm{T}} \mathbf{b}\, dV - \int_{S_0} \mathbf{x}^{\mathrm{T}} \mathbf{t}\, dS \tag{3.13}$$

where the first term is the integral of the potential of body forces **b** over the volume V_0 and the second term is the integral of the potential of the surface tractions **t** over the surface S_0. **x** denotes points in the three-dimensional space. For a planar bar-assembly (3.13) reduces to the first term of (3.11) with the coordinate system as the reference.

The first term of (3.11) does not produce compatibility conditions, thus it cannot be used for our investigation. Though the second term incorporates compatibility equations, their coefficients are unknown Lagrange-multipliers and hence the potential energy is not uniquely defined. The compatibility conditions are obtained by derivation with respect to these unknown Lagrange-multipliers.

3.4.2 A complementary formulation

However, function (3.13) can lead to a formulation of compatibility conditions if restrictions are made on the linkage. Thus we propose a complementary formulation for the potential energy function for linkages comprising of bars:

$$\Pi = \sum_{i=1}^{N} \mathbf{F}_i \mathbf{r}_i \tag{3.14}$$

where N is the total number of nodes (including foundations). $\mathbf{F}_i$ and $\mathbf{r}_i$ denote the load component and the corresponding coordinates of node i, respectively. The reference positions for the coordinates are the coordinate axes. Equation (3.14) is an equivalent term of (3.13) if the forces are concentrated on the nodes of the bar-assembly.

The equilibrium equation and the potential energy function of elastic structures shown earlier are formulated assuming that the structure is compatible, i.e. the displacement of the structure is equal to the elongation of the spring. As a complementary formulation we assume that the external loads and forces S_{ij} of bar ij form an equilibrium system. Thus, for node i we can write:

$$\mathbf{F}_i = \sum_{j<i} S_{ij}\mathbf{e}_{ji} - \sum_{j>i} S_{ij}\mathbf{e}_{ij} \tag{3.15}$$

where $\mathbf{e}_{ij}$ denotes unit vectors of bar ij and the summation includes only bars connected to node i. Now (3.14) yields

$$\Pi = \sum_{i=1}^{N} \left[\left(\sum_{j<i} S_{ij}\mathbf{e}_{ji} - \sum_{j>i} S_{ij}\mathbf{e}_{ij} \right) \mathbf{r}_i \right]. \tag{3.16}$$

When differentiating (3.14) with respect to bar force S_{ij} $(i<j)$ only $\mathbf{F}_i$ and $\mathbf{F}_j$ are affected. Due to equilibrium of bar ij, $\mathbf{F}_i$ in (3.15) has term $-S_{ij}\mathbf{e}_{ij}$ while $\mathbf{F}_j$ has $+S_{ij}\mathbf{e}_{ij}$. The relevant terms in (3.16) then become:

$$\Pi = \mathbf{F}_i\mathbf{r}_i + \mathbf{F}_j\mathbf{r}_j + \ldots = -S_{ij}\mathbf{e}_{ij}\mathbf{r}_i + S_{ij}\mathbf{e}_{ij}\mathbf{r}_j + \ldots. \tag{3.17}$$

Since by definition,

$$\mathbf{e}_{ij} = \frac{\mathbf{r}_j - \mathbf{r}_i}{\left|\mathbf{r}_j - \mathbf{r}_i\right|}, \tag{3.18}$$

we easily obtain

$$\frac{\partial \Pi}{\partial S_{ij}} = \left|\mathbf{r}_j - \mathbf{r}_i\right|. \tag{3.19}$$

which represents the length of bar *ij*. The compatibility conditions now can be formulated as

$$\frac{\partial \Pi}{\partial S_{ij}} = l_{ij} . \tag{3.20}$$

This formulation is also valid for both Cartesian coordinates and angles as variables.

The advantage of the formulation of the potential energy function shown above is that it applies to various sets of kinematic state variables keeping the same external load components since they are eliminated through the equilibrium equations. In (3.11) different coordinates correspond to different load components, i.e. using angles would require only moments instead of forces.

In addition our formulation implicitly incorporates equilibrium equations and its derivative expresses compatibility condition. In this sense it is a counterpart of the potential energy function of structures that automatically satisfies compatibility and its derivative expresses equilibrium. However, at the same time it is disadvantageous as it is complicated to involve the equilibrium equations implicitly in the formulation of (3.14).

3.4.3 A formulation based on complementary potential

The second formulation for the potential energy function is proposed here.

Consider a linear elastic bar-assembly consisting of *N* members in which member *i* has an internal force S_i and the corresponding elongation is e_i. The potential energy can therefore be defined as strain energy because there are no conservative forces considered in the system:

$$\Pi = \sum_{i=1}^{N} a_i S_i e_i . \tag{3.21}$$

where a_i is constant. (3.21) is essentially a formula for complementary potential energy. Because elongation is the difference between the current length and the initial one, i.e.

$$e_i = L_i - L_i^0, \qquad i = 1, 2, \ldots, N \tag{3.22}$$

and

$$S_i = b_i e_i, \qquad i = 1, 2, \ldots, N \tag{3.23}$$

there is

$$\Pi = \sum_{i=1}^{N} \frac{a_i}{b_i} S_i^2 . \tag{3.24}$$

Differential of the potential energy function with respect to S_i gives

$$\frac{\partial \Pi}{\partial S_i} = \frac{2a_i}{b_i} S_i = 0 . \tag{3.25}$$

Due to (3.22) and (3.23),

$$L_i = L_i^0, \qquad i = 1, 2, \ldots, N \tag{3.26}$$

which gives the compatibility conditions for constant bar lengths. The differentiation of the complementary energy with respect to independent forces yields displacements.

This formulation is also valid for angles instead of Cartesian coordinates as state variables: the coordinates appear as functions of those angles and the compatibility is formulated only for the appropriate bars.

Now write (3.21) in a slightly different form. Instead of the elongations, let us eliminate the forces from the energy. Due to (3.23) now we obtain:

$$\Pi = \sum_{i=1}^{N} a_i b_i e_i^2 . \tag{3.27}$$

This formula is essentially the potential (strain) energy of the system. The length of the deformed bar in (3.22) is a function of the kinematic parameters q_j that describe the system. Differentiation gives:

$$\frac{\partial \Pi}{\partial q_j} = \frac{\partial}{\partial q_j} \sum_{i=1}^{N} a_i b_i \left(L_i - L_i^0\right)^2 = \sum_{i=1}^{N} 2\, a_i b_i \left(L_i - L_i^0\right) \frac{\partial L_i}{\partial q_j} . \tag{3.28}$$

At compatible configurations (3.28) is equal to zero because all terms become zero due to the expression in the brackets.

3.4.4 A formulation based on analogy

Both potential energy functions shown above deal with kinematic and load variables similarly to their structural analogue. However, the compatibility conditions of mechanisms do not contain load parameters but only kinematic state variables. Therefore, we present here a new approach, which attempts to create a function only in terms of angles and displacements, etc.

The basis of the function is the analogous role of the equilibrium and compatibility equations. As we have seen demonstrated by the simple structural examples in Section 2.2, the equilibrium equation defines a relationship between a displacement variable (a generalized coordinate) and the load parameter. In structural mechanics the relationship is typically unique, i.e. the displacement ϕ is uniquely determined by the given load P through a function: $\phi = f(P)$. It should be pointed out that in some cases more than one different displacements are possible, e.g. in examples shown in Figures 2.2(a), 2.3(a) and 2.4(a), equilibrium is achieved with more than one different displacement systems under a given load. However, between two equilibrium positions the potential energy is not stationary. Hence the displacement-force relationship is typically unique in the neighbourhood of the position in question. Stability theory deals with the singularities of equilibrium. At bifurcation points more equilibrium positions become possible under the critical value of the load and the structure can follow any of the equilibrium paths.

Consider a general four-bar linkage where bar lengths are randomly chosen. Let us select the positions of the side links as two state variables α and β. The relationship between the two state variables is given by the compatibility condition. It is usually a unique function. One state variable, called output, can be calculated in terms of the other, called input: $\alpha = f(\beta)$. Occasionally one input may be linked to two outputs

because the position of one side-link may result in two possible positions for the other two bars. In a similar way to the structures, the linkage cannot switch between the two configurations without straining the bars and hence the extra solution can be easily omitted. Only when singularities appear is one state variable is not enough to describe all the possible configurations. The implicit compatibility condition should be used. The possible configurations are obtained as the solutions of the condition.

Note that one can choose a larger number of state variables together with appropriate conditions to describe a mechanism with one degree-of-freedom, e.g. all Cartesian coordinates can be state variables and compatibility conditions are formulated for each bar as suggested by Tarnai (1990). However, if the mechanism is not at a singular position, it is possible to describe the entire configuration in terms of one suitably chosen parameter.

Now the input and output variables can be paralleled to the load parameter and the displacement of the structural system, respectively. It is important to draw the attention to the difference between the two systems. While the role of the variable and the load parameter of a structure are well defined, the choice of input and output seems to be arbitrary. However, a distinction can be made based on the actuation of the mechanism. As usually designed to perform some motion, a mechanism can be driven by one of its elements, e.g. a side link of the four-bar linkage. The state variable associated with the position of the bar is then taken as an input or control parameter.

Now it is possible to proceed with the comparison. We have seen that the equilibrium equation is derived from the potential energy function by differentiating with respect to its variable. One might try to create a function for mechanisms that has a similar relationship with the compatibility condition.

Consider that the compatibility can be formulated as in (3.9) or (3.10):

$$F(\xi,\eta)=0\,. \tag{3.29}$$

If ξ is taken as a variable and η as a parameter, the *potential energy function* will have the form of

$$\Pi(\xi,\eta) = \int F(\xi,\eta)\, d\xi + G(\eta) \tag{3.30}$$

where $G(\eta)$ is a function only in terms of η.

The actual form of (3.30) depends on the way the compatibility condition is formulated. If the square-root form (3.10) is used, the integration yields an enormous expression even for a simple linkage such as the parallelogram-shaped mechanism. If the square form (3.9) is used, (3.30) has a simpler expression.

Consider now a different singular behaviour. We have seen that the motion of the mechanism can be given in terms of one parameter at regular positions but two state variables and a compatibility condition is necessary at singularities. It is also possible to create a mechanism that requires more than two state variables at certain configurations. Figure 3.12 shows a mechanism which is a compound of two parallelogram-shaped four-bar linkages. The most general description of the system requires six Cartesian coordinates and five compatibility conditions. A more convenient choice of variables defines the three supported bars by angles α, β and γ and two compatibility conditions have to be written for the coupler bars.

$$F_1(\alpha, \beta) = l_{AB} - l_{AB,0} = \sqrt{(a + b\cos\beta - b\cos\alpha)^2 + (b\sin\beta - b\sin\alpha)^2} - a = 0\,, \tag{3.31}$$

$$F_2(\beta, \gamma) = l_{BC} - l_{BC,0} = \sqrt{(a + b\cos\gamma - b\cos\beta)^2 + (b\sin\gamma - b\sin\beta)^2} - a = 0\,. \tag{3.32}$$

The configurations can be given by one parameter typically but a singularity occurs at $\alpha = \beta = \gamma = 0$ where all the bars are aligned similarly to the original four-bar

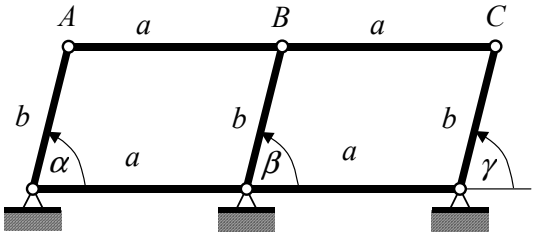

Figure 3.12: Parallelogram-shaped seven-bar mechanism compiled of two four-bar units. Bifurcation occurs when all bars are aligned.

linkage. At this position all three state variables have independent infinitesimal degrees-of-freedom; consequently all of them are required.

Note that (3.31) is independent of γ as well as (3.32) is independent of α. Due to this it is possible to formulate a function similar to (3.30):

$$\Pi(\alpha, \gamma; \beta) = \int F_1(\alpha, \beta)\, d\alpha + \int F_2(\beta, \gamma)\, d\gamma + G(\beta) \tag{3.33}$$

where β is assigned the parameter and the others are the variables. *G* is a function in terms of the parameter only. Now the compatibility conditions express that the gradient of (3.33) is zero:

$$F_1(\alpha, \beta) = \frac{\partial \Pi(\alpha, \gamma; \beta)}{\partial \alpha} = 0\,, \tag{3.34}$$

$$F_2(\beta, \gamma) = \frac{\partial \Pi(\alpha, \gamma; \beta)}{\partial \gamma} = 0\,. \tag{3.35}$$

An obvious drawback of the potential proposed here is the lack of physical meaning for Π. Furthermore, it is not always possible analytically to obtain integrals.

4

FURTHER STUDY OF COMPATIBILITY PATHS OF MECHANISMS

Contents

In Section 3.1 a number of examples were given to find the missing parts in the analogy. Bifurcations were determined by a close visual inspection of the compatibility paths. In this chapter further study on the compatibility paths of mechanisms is presented with two major objectives. Firstly, we verify various tools available in order to analyse bifurcation points of both equilibrium and compatibility paths mathematically. Secondly, we develop analogous forms of the methods used in structures for mechanisms.

The analytical method based on the Jacobian and Hessian matrices of the compatibility conditions has been reviewed in Section 2.4.3 and now it is applied to the examples introduced in Section 3.1. We also examine the influence of having different sets of state variables. Although the method was proposed for analysis of compatibility paths, we find that it can be applied to structures. The three examples of equilibrium bifurcations in Section 2.2 are used to demonstrate that. We also examine another feature of elastic structures, the stiffness matrix, and use it to target singularities, which leads to a formulation of an analogous concept for mechanisms.

With the aid of these methods, a detailed analysis is conducted in Sections 4.1 and 4.2. Based on the observations made in Chapter 3 and the results of the analytical methods, the classification proposed in Section 3.2 is extended to the analysis of points of compatibility paths. The relationship between categories of the classification and the analytical behaviour of points is established in Section 4.3.

In addition to these methods, a numerical examination of mechanisms is also presented in Section 4.4. It is intended to provide further understanding of the singularities of compatibility paths. An algorithm is also shown for the generation of the graphs of the compatibility paths.

4.1 Matrix analysis: the Jacobian and the Hessian

In Section 2.4.3 we reviewed the use of the Jacobian and the Hessian matrices to examine points on compatibility paths. If the rank of the Jacobian at a compatible

position is equal to the number of compatibility conditions, the system is a finite mechanism. However, if the rank decreases, the compatibility conditions become linearly dependent and the Hessian matrix needs to be calculated. If it is definite, the system is an infinitesimal mechanism, if it is indefinite and the mechanism preserves its mobility, a bifurcation point is obtained, while if it is semidefinite, further examinations are required (Tarnai, 1990).

4.1.1 Mechanisms

Consider first the kite-shaped mechanism, reproduced here in Figure 4.1(a). A Cartesian coordinate system is chosen so that bar O_AO_B is aligned with axis x and O_A is the origin. If the four Cartesian coordinates of the mobile nodes are used, three compatibility conditions are written as follows:

$$\begin{aligned} F_1 &= \frac{1}{2}\left[x_1^2 + y_1^2 - a^2\right] = 0, \\ F_2 &= \frac{1}{2}\left[(x_2 - x_1)^2 + (y_2 - y_1)^2 - b^2\right] = 0, \\ F_3 &= \frac{1}{2}\left[(x_2 - a)^2 + y_2^2 - b^2\right] = 0. \end{aligned} \tag{4.1}$$

The Jacobian matrix of the system is

$$\mathbf{J} = \left[\frac{\partial \mathbf{F}}{\partial \mathbf{Q}}\right] = \begin{bmatrix} x_1 & y_1 & 0 & 0 \\ x_1 - x_2 & y_1 - y_2 & x_2 - x_1 & y_2 - y_1 \\ 0 & 0 & x_2 - a & y_2 \end{bmatrix} \tag{4.2}$$

where $\mathbf{F} = [F_1 \; F_2 \; F_3]^{\mathrm{T}}$ and $\mathbf{Q} = [\, x_1 \; y_1 \; x_2 \; y_2 \,]^{\mathrm{T}}$. The rank is 3 except at the critical points $\mathbf{Q}_1 = [\, a \quad 0 \quad a+b \quad 0 \,]^{\mathrm{T}}$ and $\mathbf{Q}_2 = [\, a \quad 0 \quad a-b \quad 0 \,]^{\mathrm{T}}$. Consider the first point, which corresponds to the configuration shown in Figure 4.1(b). The Hessian is

$$\mathbf{H} = c\begin{bmatrix} 1+a/b & 0 & -a/b & 0 \\ 0 & 1+a/b & 0 & -a/b \\ -a/b & 0 & 0 & 0 \\ 0 & -a/b & 0 & 0 \end{bmatrix} \tag{4.3}$$

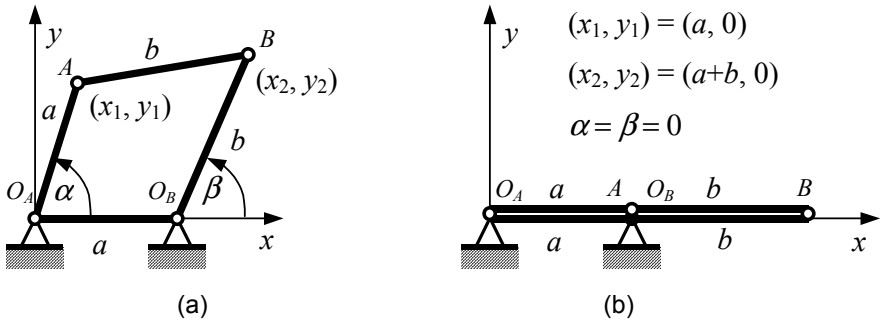

Figure 4.1: Kite-shaped four-bar mechanism. (a) General configuration and notations. (b) Configuration at one of the bifurcation points.

where c is a non-zero constant. It is easy to show that two of the eigenvalues are positive and the other two are negative:

$$e_1 = e_2 = \frac{1}{2}\left(1 + a/b + \sqrt{(1+a/b)^2 + 4(a/b)^2}\right),$$
$$e_3 = e_4 = \frac{1}{2}\left(1 + a/b - \sqrt{(1+a/b)^2 + 4(a/b)^2}\right). \tag{4.4}$$

Hence **H** is indefinite and the mechanism is at a bifurcation point.

Now if the two angles α and β are chosen as state variables instead of x and y, the single compatibility condition, formulated for bar AB, becomes

$$F = \frac{1}{2}\left[(a + b\cos\beta - a\cos\alpha)^2 + (b\sin\beta - a\sin\alpha)^2 - b^2\right] = 0. \tag{4.5}$$

The Jacobian now is a 1-by-2 matrix:

$$\mathbf{J} = \left[a^2\sin\alpha + ab\sin(\alpha-\beta) \quad -ab\sin\beta - ab\sin(\alpha-\beta)\right]. \tag{4.6}$$

The rank decreases at $(\alpha = 0, \beta = 0)$ and $(\alpha = 0, \beta = \pi)$, identical to the critical points obtained using the Cartesian coordinates. Consider again the first one and calculate the Hessian matrix, which comprises of the second derivatives of (4.5).

$$\mathbf{H} = \begin{bmatrix} ab + a^2 & -ab \\ -ab & 0 \end{bmatrix}. \tag{4.7}$$

It is easy to calculate the two eigenvalues:

$$\mathbf{e} = \frac{a}{2}\left[a+b+\sqrt{(a+b)^2+4b^2} \quad a+b-\sqrt{(a+b)^2+4b^2} \right]^{\mathrm{T}}. \tag{4.8}$$

The first one is positive while the other is negative thus **H** is indefinite. Again the configuration is a bifurcation point.

Both sets of state variables led to the same conclusion. Note that in this example only the square form of the compatibility conditions has been used in order to deal with simple formulas. It has been found that applying the square-root form in (3.8) or (3.10) yields the same results.

We can apply the same matrix analysis to the parallelogram-shaped four-bar linkage shown in Figure 2.10(a). It has an asymmetric bifurcation similar to that of the kite-shaped linkage. The matrix analysis shows the same behaviour at the bifurcation point $(\alpha = 0,\ \beta = 0)$ obtained in Section 2.4.2.

The third mechanism to analyse is the square-shaped one shown in Figure 4.2(a) with the same notations as previously. This mechanism can be obtained as a special case of the kite-shape mechanism if $b = a$. The compatibility equations are:

$$\begin{aligned} F_1 &= \frac{1}{2}\left[x_1^2 + y_1^2 - a^2\right] = 0, \\ F_2 &= \frac{1}{2}\left[(x_2 - x_1)^2 + (y_2 - y_1)^2 - a^2\right] = 0, \\ F_3 &= \frac{1}{2}\left[(x_2 - a)^2 + y_2^2 - a^2\right] = 0. \end{aligned} \tag{4.9}$$

The Jacobian matrix of the system is again

$$\mathbf{J} = \left[\frac{\partial \mathbf{F}}{\partial \mathbf{Q}}\right] = \begin{bmatrix} x_1 & y_1 & 0 & 0 \\ x_1 - x_2 & y_1 - y_2 & x_2 - x_1 & y_2 - y_1 \\ 0 & 0 & x_2 - a & y_2 \end{bmatrix}. \tag{4.10}$$

The rank decreases at three critical points: $\mathbf{Q}_1 = [\,-a \quad 0 \quad 0 \quad 0\,]^{\mathrm{T}}$, $\mathbf{Q}_2 = [\,a \quad 0 \quad 2a \quad 0\,]^{\mathrm{T}}$, $\mathbf{Q}_3 = [\,a \quad 0 \quad 0 \quad 0\,]^{\mathrm{T}}$. Our interest is in the third one, which

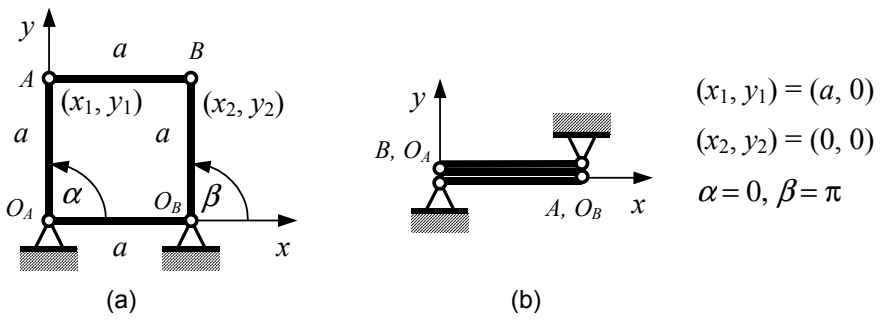

Figure 4.2: Square-shaped four-bar mechanism. (a) General configuration and notations. (b) Configuration at one of the bifurcation points.

has not been analysed before. It corresponds to the 'doubly-folded' configuration shown in Figure 4.2(b). At this point the Hessian yields

$$\mathbf{H} = c\begin{bmatrix} 0 & 0 & 1 & 0 \\ 0 & 0 & 0 & 1 \\ 1 & 0 & 0 & 0 \\ 0 & 1 & 0 & 0 \end{bmatrix}. \tag{4.11}$$

where c is a non-zero constant. The eigenvalues are $\mathbf{e} = c\begin{bmatrix} -1 & 1 & -1 & 1 \end{bmatrix}^{\mathrm{T}}$. Since there are both positive and negative elements, **H** is indefinite and the mechanism is at a bifurcation point.

Again we consider a single compatibility condition in terms of the angles as

$$F = \frac{1}{2}\left[(a + a\cos\beta - a\cos\alpha)^2 + (a\sin\beta - a\sin\alpha)^2 - a^2\right] = 0. \tag{4.12}$$

The Jacobian is a 1-by-2 matrix:

$$\mathbf{J} = a^2\begin{bmatrix} \sin\alpha + \sin(\alpha - \beta) & -\sin\beta - \sin(\alpha - \beta) \end{bmatrix}. \tag{4.13}$$

The rank decreases at $(\alpha = 0, \beta = 0)$, $(\alpha = \pi, \beta = \pi)$ and $(\alpha = 0, \beta = \pi)$. They are identical to those obtained earlier. Again we consider only the third point at which the Hessian matrix is

$$\mathbf{H} = a^2\begin{bmatrix} 0 & 1 \\ 1 & 0 \end{bmatrix}. \tag{4.14}$$

The two eigenvalues are easy to obtain: $\mathbf{e} = \begin{bmatrix} a^2 & -a^2 \end{bmatrix}^{\mathrm{T}}$ showing that **H** is again indefinite. Hence the configuration is a bifurcation point.

The last example is the six-bar mechanism presented in Section 3.1.2, see Figure 4.3(a). First the Cartesian coordinates are used and the formulation is simplified by considering the symmetry of the $O_A ADBO_B$ linkage. Thus there are four compatibility conditions and five state variables as shown in Figure 4.3(a).

$$\begin{aligned} F_1 &= \frac{1}{2}\left[(x_1 - 1)^2 + y_1^2 - 1\right] = 0, \\ F_2 &= \frac{1}{2}\left[x_1^2 + (y_1 - y_2)^2 - 2\right] = 0, \\ F_3 &= \frac{1}{2}\left[(x_3 + x_1)^2 + (y_3 - y_1)^2 - 2\right] = 0, \\ F_4 &= \frac{1}{2}\left[(x_3 - x_1)^2 + (y_3 - y_1)^2 - 2\right] = 0. \end{aligned} \tag{4.15}$$

The Jacobian matrix of the equation system is:

$$\mathbf{J} = \left[\frac{\partial \mathbf{F}}{\partial \mathbf{Q}}\right] = \begin{bmatrix} x_1 - 1 & y_1 & 0 & 0 & 0 \\ x_1 & y_1 - y_2 & y_2 - y_1 & 0 & 0 \\ x_1 + x_3 & y_1 - y_3 & 0 & x_3 + x_1 & y_3 - y_1 \\ x_1 - x_3 & y_1 - y_3 & 0 & x_3 - x_1 & y_3 - y_1 \end{bmatrix} \tag{4.16}$$

where the state variables are $\mathbf{Q} = \begin{bmatrix} x_1 & y_1 & y_2 & x_3 & y_3 \end{bmatrix}^{\mathrm{T}}$. The rank of **J** decreases in two sets of configurations. The first one occurs when $(x_1, y_1, y_2) = (0, 0, -\sqrt{2})$ regardless the other variables. It corresponds to a configuration shown in Figure 4.3(b). Nodes *A* and *B* are at the origin of the coordinate system and the angle α of bars *AC* is arbitrary.

We obtain the Hessian in terms of x_3 at $\mathbf{Q}_0 = \begin{bmatrix} 0 & 0 & -\sqrt{2} & x_3 & y_3 \end{bmatrix}^{\mathrm{T}}$:

$$\mathbf{H} = \left[\frac{\partial^2 \mathbf{F}}{\partial \mathbf{Q}^2}\right]_{\mathbf{Q}=\mathbf{Q}_0} = c \begin{bmatrix} 2x_3 & 0 & 0 & 2 & 0 \\ 0 & 2x_3 & 0 & 0 & 0 \\ 0 & 0 & 0 & 0 & 0 \\ 2 & 0 & 0 & 0 & 0 \\ 0 & 0 & 0 & 0 & 0 \end{bmatrix} \tag{4.17}$$

where *c* is a non-zero constant. The eigenvalues are:

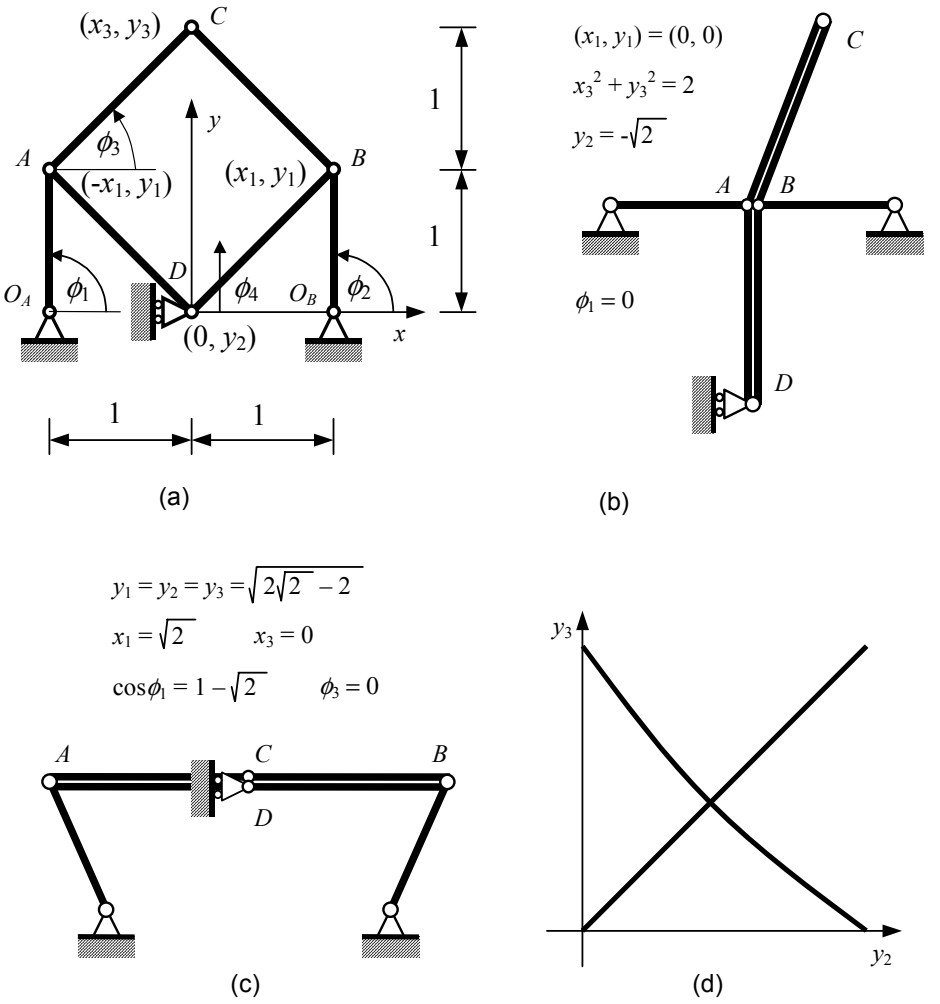

Figure 4.3: Six-bar mechanism. (a) General configuration and notations. (b)-(c) The first and the second singular configuration. (d) Compatibility paths near the second bifurcation point.

$$\mathbf{e} = c\begin{bmatrix} 0 \\ 0 \\ 2x_3 \\ x_3 + \sqrt{x_3^2 + 4} \\ x_3 - \sqrt{x_3^2 + 4} \end{bmatrix}. \tag{4.18}$$

The last two elements have opposite signs thus **H** is indefinite for any values of x_3 corresponding to any position of bar AC. As we have seen in Section 3.1.2, only two positions, $(x_3, y_3) = (0, \sqrt{2})$ and $(x_3, y_3) = (0, -\sqrt{2})$ are bifurcation points and bifurcation does not occur at all of the other positions. Obviously the use of **H** leads to

an incorrect conclusion in this example. The method erroneously detects bifurcation points at the singular configuration shown in Figure 4.3(b). This is due to the additional *infinitesimal* degree-of-freedom that causes the decrease of rank but does not correspond to new compatibility path. This infinitesimal mechanism is associated with an infinitesimal motion of the linkage in the *y* direction, see Figure 4.3(b).

The other position at which the rank of the Jacobian decreases is an extreme position mentioned in Section 3.1.2 and shown in Figure 4.3(c):

$$\mathbf{Q}_0 = \left[\sqrt{2} \quad \sqrt{2\sqrt{2}-2} \quad \sqrt{2\sqrt{2}-2} \quad 0 \quad \sqrt{2\sqrt{2}-2}\right]^{\mathrm{T}}. \tag{4.19}$$

The Hessian is

$$\mathbf{H} = \left[\frac{\partial^2 \mathbf{F}}{\partial \mathbf{Q}^2}\right]_{\mathbf{Q}=\mathbf{Q}_0} = c\begin{bmatrix} 0 & 0 & 0 & 0 & 0 \\ 0 & 0 & 2 & 0 & -2 \\ 0 & 2 & -2 & 0 & 0 \\ 0 & 0 & 0 & 2 & 0 \\ 0 & -2 & 0 & 0 & 2 \end{bmatrix} \tag{4.20}$$

whose eigenvalues are $\mathbf{e} = c\left[0 \quad 0 \quad 2 \quad 2\sqrt{3} \quad -2\sqrt{3}\right]^{\mathrm{T}}$ where *c* is a non-zero constant. It shows that **H** is indefinite and the position is a bifurcation point. The compatibility path is plotted in the coordinate system of y_2 and y_3 in Figure 4.3(d).

We can also formulate the problem using two angles shown in Figure 4.3(a): $\mathbf{Q} = \left[\phi_1 \quad \phi_3\right]^{\mathrm{T}}$. The compatibility condition now is

$$F = \frac{1}{2}\left[\left(2 - 2\cos\phi_1 - \sqrt{2}\cos\phi_3\right)^2 + \left(\sqrt{2}\sin\phi_3\right)^2 - 2\right] = 0 \tag{4.21}$$

whose Jacobian is

$$\mathbf{J} = \left[\frac{\partial F}{\partial \mathbf{Q}}\right] = \left[4\sin\phi_1\left(1 - \cos\phi_1 - \sqrt{2}\cos\phi_3\right) \quad 4\sqrt{2}\sin\phi_3\left(1 - \cos\phi_1\right)\right]. \tag{4.22}$$

Again the rank decreases in two sets of configurations.

Firstly, $\phi_1 = 0$ and ϕ_3 is arbitrary which is identical to the previous result. Now the Hessian is

$$\mathbf{H} = \begin{bmatrix} 4\sqrt{2}\cos\phi_3 & 0 \\ 0 & 0 \end{bmatrix}. \tag{4.23}$$

It is semidefinite in general and becomes zero-matrix when $\phi_3 = \pm\pi/2$, i.e. at the two bifurcation points shown in Figure 3.9(b). That means that further analysis is required to determine mobility.

The other position at which the rank of the Jacobian decreases is also identical to the previous result: $\mathbf{Q}_0 = \begin{bmatrix} \arccos\left(1-\sqrt{2}\right) & 0 \end{bmatrix}^{\mathrm{T}}$. The Hessian now is

$$\mathbf{H} = \begin{bmatrix} 8\sqrt{2}-8 & 0 \\ 0 & 8 \end{bmatrix} \tag{4.24}$$

which is positive definite, hence the mechanism is an infinitesimal mechanism.

Two sets of different results have been obtained, which can be summarized in Table 4.1.

A few conclusions can be drawn. Firstly, both formulations fail to distinguish the two real bifurcation points from the other points. This example clearly shows that the

Table 4.1: Results of the matrix analysis for the six-bar linkage

	Points of interest	
Variables	Figure 4.3(b)	Figure 4.3(c)
Cartesian coordinates x_1, y_1, y_2, x_3, y_3	Jacobian has rank deficiency Hessian is indefinite Conclusion: bifurcation	Jacobian has rank deficiency Hessian is indefinite Conclusion: bifurcation
Angles ϕ_1, ϕ_3	Jacobian has rank deficiency Hessian is semidefinite Inconclusive	Jacobian has rank deficiency Hessian is definite Conclusion: infinitesimal mechanism
Correct answers	Bifurcation points at $\phi_3 = \pi/2$ and $\phi_3 = -\pi/2$, an infinitesimal mechanism in addition to the finite one at all other positions	Bifurcation point

identification of bifurcations based on Hessian matrices does not always work, even with a coordinate system which is able to fully describe the motion of the mechanism. The method does not distinguish infinitesimal mechanisms from finite ones. As long as two exist at a point, it regards the point as a bifurcation point. Secondly, the two angles chosen do not provide enough information about the whole system. At one of the singular positions, $(\phi_1, \phi_3) = \left(\arccos\left(1-\sqrt{2}\right), 0\right)$, an incorrect result has been obtained. It is due to the incapability of the two angles ϕ_1 and ϕ_3 to describe behaviour of that point because node *D* cannot be given uniquely. Hence a suitable pair should be chosen, e.g. ϕ_3 and ϕ_4 as shown in Figure 4.3(a) or y_2 and y_3 as shown in Figure 4.3(d).

4.1.2 Structures

Although the matrix analysis using the Jacobian and the Hessians was first proposed for the analysis of compatibility paths, it can also be applied to equilibrium paths of structures. Denote F_k as equilibrium equations and the state variables are both the displacements and the loads. Both the Jacobian and Hessian matrices can be calculated following the procedure described in the previous section. The decrease of rank of the Jacobian determines the critical points. If the Hessian matrix is indefinite, then bifurcation occurs and if it is semidefinite, further examinations are required.

Let us now examine a few examples. The first example is the structure shown in Figure 2.2(a). The equilibrium equation is

$$E = PL\sin\phi - k\phi = 0 \tag{4.25}$$

where the notations are as in Section 2.2.1 and the state variables are $\mathbf{Q} = \begin{bmatrix}\phi & P\end{bmatrix}^{\mathrm{T}}$. The Jacobian matrix of the equilibrium equation is

$$\mathbf{J} = \left[\frac{\partial E}{\partial \mathbf{Q}}\right] = \begin{bmatrix}PL\cos\phi - k & L\sin\phi\end{bmatrix}. \tag{4.26}$$

The critical point where the rank decreases is easy to obtain: $\mathbf{Q}_0 = [0 \quad k/L]^{\mathrm{T}}$ which is the same as the known critical force and position. At this point the Hessian yields

$$\mathbf{H} = \left[\frac{\partial^2 E}{\partial \mathbf{Q}^2}\right]_{\mathbf{Q}=\mathbf{Q}_0} = \begin{bmatrix} 0 & L \\ L & 0 \end{bmatrix} \tag{4.27}$$

whose eigenvalues are $\mathbf{e} = [-L \quad L]^{\mathrm{T}}$ showing that $\mathbf{H}$ is indefinite hence the critical point is a bifurcation point.

It is possible to use a more complicated system of equations if the moment M of the spring is added to the state variables. Now the new variables are $\mathbf{Q} = [\phi \quad P \quad M]^{\mathrm{T}}$ and there are two equilibrium equations, one for the bar and one for the spring:

$$\begin{aligned} E_1 &= PL\sin\phi - M = 0, \\ E_2 &= k\phi - M = 0. \end{aligned} \tag{4.28}$$

The Jacobian now is a 2-by-3 matrix:

$$\mathbf{J} = \left[\frac{\partial \mathbf{E}}{\partial \mathbf{Q}}\right] = \begin{bmatrix} PL\cos\phi & L\sin\phi & -1 \\ k & 0 & -1 \end{bmatrix}. \tag{4.29}$$

The rank decreases at the critical point $\mathbf{Q}_0 = [0 \quad k/L \quad 0]^{\mathrm{T}}$ which is the same as the other one calculated before. The Hessian yields

$$\mathbf{H} = \left[\frac{\partial^2 E}{\partial \mathbf{Q}^2}\right]_{\mathbf{Q}=\mathbf{Q}_0} = \begin{bmatrix} 0 & L & 0 \\ L & 0 & 0 \\ 0 & 0 & 0 \end{bmatrix} \tag{4.30}$$

and the eigenvalues are $\mathbf{e} = [-L \quad L \quad 0]^{\mathrm{T}}$. This shows again that $\mathbf{Q}_0$ is a bifurcation point.

The second structure is shown in Figure 2.3(a). First, the single equilibrium equation is analysed:

$$E = PL\sin\phi - kL\sin\phi\, L\cos\phi = 0 \tag{4.31}$$

where the notations are again the same as in Section 2.2.2 and the state variables are $\mathbf{Q} = [\phi \quad P]^{\mathrm{T}}$. The Jacobian matrix of the equilibrium equation is

$$\mathbf{J} = \left[\frac{\partial E}{\partial \mathbf{Q}}\right] = \left[PL\cos\phi - kL^2 + 2kL^2\sin^2\phi \quad L\sin\phi\right]. \tag{4.32}$$

The critical point where the rank decreases is: $\mathbf{Q}_0 = [0 \quad kL]^{\mathrm{T}}$ which is the same as the known critical force and position. At this point the Hessian again yields

$$\mathbf{H} = \left[\frac{\partial^2 E}{\partial \mathbf{Q}^2}\right]_{\mathbf{Q}=\mathbf{Q}_0} = \begin{bmatrix} 0 & L \\ L & 0 \end{bmatrix} \tag{4.33}$$

which is indefinite as the eigenvalues are $\mathbf{e} = [-L \quad L]^{\mathrm{T}}$. Hence the critical point is a bifurcation point as expected.

Again it is possible to use a more complicated system of equations. The new state variable now is the force F in the horizontal spring and the state variable vector is $\mathbf{Q} = [\phi \quad P \quad F]^{\mathrm{T}}$. We have two equilibrium equations:

$$\begin{aligned} E_1 &= PL\sin\phi - FL\cos\phi = 0, \\ E_2 &= F - kL\sin\phi = 0. \end{aligned} \tag{4.34}$$

The Jacobian of the equation system is:

$$\mathbf{J} = \left[\frac{\partial \mathbf{E}}{\partial \mathbf{Q}}\right] = \begin{bmatrix} PL\cos\phi + FL\sin\phi & L\sin\phi & -L\cos\phi \\ -kL\cos\phi & 0 & 1 \end{bmatrix}. \tag{4.35}$$

The rank decreases at the critical point $\mathbf{Q}_0 = [0 \quad kL \quad 0]^{\mathrm{T}}$ which is the same as the other one calculated before. The Hessian yields

$$\mathbf{H} = \left[\frac{\partial^2 E}{\partial \mathbf{Q}^2}\right]_{\mathbf{Q}=\mathbf{Q}_0} = \begin{bmatrix} 0 & L & 0 \\ L & 0 & 0 \\ 0 & 0 & 0 \end{bmatrix} \tag{4.36}$$

which is again indefinite because the eigenvalues are $\mathbf{e} = [-L \quad L \quad 0]^{\mathrm{T}}$. This shows that $\mathbf{Q}_0$ is a bifurcation point.

The third structure is the asymmetric case shown in Figure 2.4(a). Due to the asymmetry, the equilibrium equation is now a more complicated formula:

$$E = PL\sin\phi - kL^2\cos\phi\left(1-\frac{d_0}{d}\right) = 0 \tag{4.37}$$

where the notations are the same as in Section 2.2.3, the state variables are again $\mathbf{Q} = \begin{bmatrix}\phi & P\end{bmatrix}^{\mathrm{T}}$ and d_0 and d are the original and deformed lengths of the spring, respectively:

$$d_0 = L\sqrt{2}, \quad d = L\sqrt{2+2\sin\phi}\,. \tag{4.38}$$

The Jacobian of the equilibrium equation is:

$$\mathbf{J} = \left[\frac{\partial E}{\partial \mathbf{Q}}\right] = \left[PL\cos\phi + kL^2\sin\phi\left(1-\frac{d_0}{d}\right) - kL^4\cos^2\phi\frac{d_0}{d^3} \quad L\sin\phi\right]. \tag{4.39}$$

The critical point is obtained at $\mathbf{Q}_0 = \begin{bmatrix}0 & kL^3/d_0^2\end{bmatrix}^{\mathrm{T}}$ which is identical to the known critical force and position of the structure. At this point the Hessian is

$$\mathbf{H} = \left[\frac{\partial^2 E}{\partial \mathbf{Q}^2}\right]_{\mathbf{Q}=\mathbf{Q}_0} = \begin{bmatrix}0 & L\\ L & 0\end{bmatrix} \tag{4.40}$$

which is indefinite as the eigenvalues are $\mathbf{e} = \begin{bmatrix}-L & L\end{bmatrix}^{\mathrm{T}}$. Hence the critical point is a bifurcation point as expected.

The extended formulation again include two equations and an additional state variable which now is the force F in the spring. The equations are:

$$\begin{aligned} E_1 &= PL\sin\phi - F\frac{L^2\cos\phi}{d} = 0,\\ E_2 &= F - k(d-d_0) = 0 \end{aligned} \tag{4.41}$$

whose Jacobian is

$$\mathbf{J}=\left[\frac{\partial \mathbf{E}}{\partial \mathbf{Q}}\right]=\begin{bmatrix} PL\cos\phi+\dfrac{FL^2\sin\phi}{d}+\dfrac{FL^4\cos\phi}{d^3} & L\sin\phi & -\dfrac{L^2\cos\phi}{d} \\ -\dfrac{kL^2\cos\phi}{d} & 0 & 1 \end{bmatrix}. \tag{4.42}$$

The rank decreases at the critical point $\mathbf{Q}_0=\begin{bmatrix}0 & kL^3/d_0^2 & 0\end{bmatrix}^{\mathrm{T}}$ which is the same as before. The Hessian yields

$$\mathbf{H}=\left[\frac{\partial^2 E}{\partial \mathbf{Q}^2}\right]_{\mathbf{Q}=\mathbf{Q}_0}=\begin{bmatrix} kL/2\sqrt{2} & \sqrt{2} & 1/2 \\ \sqrt{2} & 0 & 0 \\ 1/2 & 0 & 0 \end{bmatrix} \tag{4.43}$$

whose eigenvalues are

$$\mathbf{e}=\frac{c}{2}\begin{bmatrix} 0 \\ \mathrm{H}_{11}+\sqrt{\mathrm{H}_{11}^2+4\left(\mathrm{H}_{12}^2+\mathrm{H}_{13}^2\right)} \\ \mathrm{H}_{11}-\sqrt{\mathrm{H}_{11}^2+4\left(\mathrm{H}_{12}^2+\mathrm{H}_{13}^2\right)} \end{bmatrix}. \tag{4.44}$$

The last two elements have opposite signs, consequently the Hessian is indefinite and the critical point is a bifurcation point.

4.2 Stiffness matrix method

One of the methods to deal with singularities of equilibrium paths of structures is the concept of the stiffness matrix. The stiffness matrix of a linearly elastic structure is a matrix defining the relationship between the forces and the related displacements. If geometric or material nonlinearity is considered, the system cannot be characterized by a single matrix because the stiffness is different at different displacements. The actual stiffness at certain equilibrium positions is the tangent stiffness matrix, which establishes the relationship between infinitesimal unit increment of displacements and the increment of forces required to maintain equilibrium. In systems where one state variable can describe the displacements of the structure, the stiffness matrix is reduced to a scalar value. In the following we deal with only such systems.

Applying a load parameter to the structure may affect the stiffness of the structure. If the load parameter has a critical value, the stiffness becomes singular and the structure loses its stability either with a limit point or with a bifurcation. In many cases the primary equilibrium path of the structure is straight referring to the original undeformed shape of the structure. At a particular value of the load parameter the stiffness becomes zero and the equilibrium path bifurcates, e.g. in the case of the three examples discussed previously. However, if the critical deformation is not known, the equilibrium equation needs to be formulated in addition to the condition of the vanishing of the stiffness. The two conditions together yield the critical deformation and load. This is the typical case for limit points.

4.2.1 Structures

Consider the three structures introduced in Section 2.2. Now we attempt to use the stiffness to find the critical value of the load.

The first structure is a hinged cantilever with a rotational spring shown in Figure 2.2(a). At the undeformed shape the equilibrium is satisfied as the vertical force is in the axis of the bar. If a small displacement is applied with the load unchanged the moment of the external load is not balanced by the moment of the spring, therefore an extra dM moment should be added to the spring. The sign of dM is set so that positive dM corresponds to positive deformation of the spring. The equilibrium equation at this disturbed position is:

$$PL \sin d\phi = k\, d\phi - dM\,. \tag{4.45}$$

Since the displacement is infinitesimal, the trigonometric function is replaced by its linear approximation, i.e. the first term in its Taylor series:

$$dM = k\, d\phi - PL\, d\phi\,. \tag{4.46}$$

The stiffness is now easy to obtain as:

$$\mathrm{K} = \frac{dM}{d\phi} = k - PL\,. \tag{4.47}$$

The structure loses its stability when the stiffness becomes zero providing the critical load

$$P_{cr} = \frac{k}{L}\,. \tag{4.48}$$

which is identical to the well-known value.

The second structure is shown in Figure 2.3(a). Now a horizontal dQ force is added to the disturbed system to maintain equilibrium:

$$PL\sin d\phi = kL\sin d\phi\, L\cos d\phi - dQ\, L\cos d\phi\,. \tag{4.49}$$

The linear approximation of the trigonometric terms yield

$$PL\, d\phi - kL^2\, d\phi = -L\, dQ \tag{4.50}$$

which provides the stiffness of the structure:

$$K = \frac{dQ}{d\phi} = kL - P\ . \tag{4.51}$$

The critical load parameter is obtained as

$$P_{cr} = kL\,. \tag{4.52}$$

The third example is the structure shown in Figure 2.4(a). The equilibrium equation of the disturbed structure is

$$PL\sin d\phi = k\left(1 - \frac{d_0}{d}\right)L^2\cos d\phi - dQ\, L\cos d\phi \tag{4.53}$$

where dQ is a horizontal force at the top of the bar and d and d_0 are defined in (4.38). The linear approximation now includes d, which a nonlinear term of $d\phi$. Rearranging (4.53) we obtain the stiffness

$$K = \frac{dQ}{d\phi} = \frac{kL}{2} - P \tag{4.54}$$

which becomes zero at the critical load:

$$P_{cr} = \frac{kL}{2}. \tag{4.55}$$

It coincides with the known critical load shown in Section 2.2.3.

4.2.2 Mechanisms

A similar formulation is possible for mechanisms as well. Consider a compatibility condition written in the form

$$X(\alpha,\beta)^2 + Y(\alpha,\beta)^2 = l^2 \tag{4.56}$$

where α and β are the kinematic state variables at a compatible configuration, X and Y are the Cartesian projections of the distance between the two nodes for which the compatibility condition is formulated, and l is the length of the bar between the nodes. If a small $d\alpha$ increment of displacement is applied, the length of the bar needs to be modified by an appropriate de increment. At the new compatible configuration the following equation holds:

$$\left[X(\alpha,\beta) + \frac{\partial X}{\partial \alpha} d\alpha \right]^2 + \left[Y(\alpha,\beta) + \frac{\partial Y}{\partial \alpha} d\alpha \right]^2 = (l + de)^2 . \tag{4.57}$$

Combining the two equations and ignoring the higher-order terms of the infinitesimal quantities we obtain

$$\frac{de}{d\alpha} = X \frac{\partial X}{\partial \alpha} + Y \frac{\partial Y}{\partial \alpha} \tag{4.58}$$

which we define as the analogue of the scalar stiffness property. When

$$\frac{de}{d\alpha} = 0, \tag{4.59}$$

the mechanism has a singular configuration because (4.59) indicates an (at least) infinitesimal motion while the parameter is constant.

It is important to mention that this stiffness property is mathematically related to the Jacobian matrix of the system. If the Jacobian of the single compatibility condition is derived, the singularity of the stiffness property is essentially identical to the singularity of the corresponding element of the Jacobian. At singular positions this element becomes zero. It is also possible to select β as a variable so that (4.59) becomes $\partial e/\partial\beta = 0$. This is related to the second element of the Jacobian.

This method can be applied in two ways. In the first case a compatibility path is explicitly known in terms of one of the state variables and the other state variable is determined so that singularity occurs. This can be used to find bifurcation points. It is similar to the structural approach where the straight path is known. On the other hand, limit points can also be identified. In this case compatibility paths are usually not known explicitly and the singular configuration is obtained by solving the stiffness condition and the compatibility condition simultaneously.

Consider the kite-shaped mechanism in Figure 2.9(a). At $\alpha = 0$ the mechanism is compatible for an arbitrary β thus the compatibility equation yields equality. Applying a small $d\alpha$ disturbance would requiry a small de increment of the bar length. The following equation holds:

$$[a + b\cos\beta - a\cos(\alpha + d\alpha)]^2 + [b\sin\beta - a\sin(\alpha + d\alpha)]^2 = (b + de)^2 . \qquad (4.60)$$

Substituting $\alpha = 0$ into (4.60) and approximating the trigonometric functions with their linear term gives:

$$a^2\, d\alpha^2 - 2ab\, d\alpha \sin\beta = 2b\, de + de^2 . \qquad (4.61)$$

Ignoring the higher-order terms we easily derive the stiffness

$$K = \frac{de}{d\alpha} = -a\sin\beta . \qquad (4.62)$$

This quantity becomes zero at $\beta = 0$ and $\beta = \pi$ which correctly indicates the bifurcation points.

If we assume that no compatibility path is known, then two conditions are to be satisfied simultaneously. One of them is the compatibility equation in terms of □ and □ and the other one states that the stiffness equals zero, which is now a more complicated expression:

$$K = \frac{de}{d\alpha} = \frac{a}{b}\left(a\sin\alpha + b\sin(\alpha - \beta)\right) = 0\,. \tag{4.63}$$

The solutions are $(\alpha = 0, \beta = 0)$ and $(\alpha = 0, \beta = \pi)$ providing the bifurcation points.

The parallelogram-shaped and the square-shaped four-bar linkages can be analysed in the same way. The method indicates the bifurcation points similarly to the kite-shaped linkage.

The last example to consider is the six-bar mechanism. Perturbing the compatibility condition of the mechanism (4.21) we obtain the equation

$$\left[2 - 2\cos(\phi_1 + \mathrm{d}\phi_1) + \sqrt{2}\cos\phi_3\right]^2 + \left[\sqrt{2}\sin\phi_3\right]^2 = \left(\sqrt{2} + de\right)^2\,. \tag{4.64}$$

The $\phi_1 = 0$ configuration is again compatible. Substituting this into (4.64) and approximating the trigonometric terms we obtain

$$0 = 2\sqrt{2}\,de + de^2 \tag{4.65}$$

which shows that the stiffness is zero at any value of ϕ_3. Since only two points are bifurcation points, we have the same problem as given by the Jacobian matrix in the previous section.

If the compatibility is not used implicitly, the stiffness condition yields:

$$K = \frac{de}{d\phi_1} = 2\sin\phi_1\left(\sqrt{2}(1 - \cos\phi_1) - \cos\phi_3\right) \tag{4.66}$$

which becomes zero if

$$\sin\phi_1 = 0\,, \tag{4.67a}$$

or

$$\cos\phi_3 = \sqrt{2}\left(1-\cos\phi_1\right). \tag{4.67b}$$

From the compatibility condition (4.21) we obtain

$$\sin\phi_1 = 0\,, \tag{4.68a}$$

or

$$\cos\phi_3 = \frac{1}{\sqrt{2}}\left(1-\cos\phi_1\right). \tag{4.68b}$$

It shows again that the $\phi_1 = 0$ branch of the compatibility path is entirely singular but there is no other singular point because equations (4.67b) and (4.68b) have no common points apart from $\phi_1 = 0$. Thus the result is the same as obtained before.

4.2.3 Limit points

Singularities occur at limit points as well. The stiffness can be used to identify limit points on both the equilibrium path and compatibility path. Consider first the structure shown in Figure 2.3(a). If a small eccentricity ε is applied to the load, the equilibrium path will have a limit point as shown in Figure 2.3(b). This point can also be determined as follows.

As the location of the load is different the equilibrium equation now is

$$P\left(L\sin\phi + \varepsilon\cos\phi\right) = kL^2\sin\phi\cos\phi\,. \tag{4.69}$$

Dividing (4.69) by $L\cos\phi$ and rearranging we obtain

$$P = \frac{kL\sin\phi}{\tan\phi + \varepsilon/L}\,. \tag{4.70}$$

Applying an infinitesimal $d\phi$ increment of the displacement, the equilibrium is perturbed and an infinitesimal dQ force acting in the direction of the spring is needed. The equilibrium of the perturbed position is:

$$P\left(L\sin(\phi+d\phi)+\varepsilon\cos(\phi+d\phi)\right)=kL^2\sin(\phi+d\phi)\cos(\phi+d\phi)-dQL\cos(\phi+d\phi)\,. \quad (4.71)$$

Again rearranging we obtain:

$$P\left(\tan(\phi+d\phi)+\frac{\varepsilon}{L}\right)=kL\sin(\phi+d\phi)-dQ\,. \quad (4.72)$$

Consider the following linear approximations:

$$\sin(\phi+d\phi)\approx\sin\phi+d\phi\cos\phi\,, \quad (4.73a)$$

$$\tan(\phi+d\phi)\approx\tan\phi+d\phi\left(1+\tan^2\phi\right). \quad (4.73b)$$

Substituting (4.73) into (4.72) and subtracting (4.70) yield

$$P\left(1+\tan^2\phi\right)d\phi=kL\,d\phi\cos\phi-dQ \quad (4.74)$$

from which the stiffness is obtained as

$$K=\frac{dQ}{d\phi}=kL\cos\phi-P\left(1+\tan^2\phi\right). \quad (4.75)$$

Applying the trigonometric equality

$$1+\tan^2\phi=\frac{1}{\cos^2\phi} \quad (4.76)$$

to (4.75) it is easy to get the load parameter in terms of ϕ where the stiffness is zero:

$$P=kL\cos^3\phi\,. \quad (4.77)$$

We combine the equilibrium condition (4.70) and the stiffness condition (4.77) to eliminate the load. A trigonometric transformation yields

$$\frac{\varepsilon}{L} = \tan^3 \phi \,. \tag{4.78}$$

For a given imperfection the limit point occurs at the displacement

$$\phi_{\text{cr}} = \arctan\left(\sqrt[3]{\frac{\varepsilon}{L}}\right). \tag{4.79}$$

Again using the trigonometric equality (4.76) we obtain the critical load parameter from (4.77):

$$P_{\text{cr}} = \frac{kL}{\left(1+\left(\frac{\varepsilon}{L}\right)^{2/3}\right)^{3/2}}. \tag{4.80}$$

A similar analysis can be done for mechanisms. Consider the paralellogram-shaped mechanism in Figure 2.9(a) with a small imperfection ε in bar $O_A A$. The compatibility equation of the mechanism is

$$\left[a + b\cos\beta - (b+\varepsilon)\cos\alpha\right]^2 + \left[b\sin\beta - (b+\varepsilon)\sin\alpha\right]^2 = a^2 . \tag{4.81}$$

Expanding the square terms (4.81) is simplified to

$$b^2 + (b+\varepsilon)^2 + 2ab\cos\beta - 2a(b+\varepsilon)\cos\alpha - 2b(b+\varepsilon)\cos(\alpha-\beta) = 0 . \tag{4.82}$$

Applying a small increment $d\alpha$ to the angle α will require a small increment *de* of the length of bar *AB*. A new equation is formulated to maintain compatibility in the modified position:

$$\left[a + b\cos\beta - (b+\varepsilon)\cos(\alpha+d\alpha)\right]^2 + \left[b\sin\beta - (b+\varepsilon)\sin(\alpha+d\alpha)\right]^2 = (a+de)^2 . \tag{4.83}$$

Again expanding (4.83) and subtracting (4.81) the stiffness condition is obtained:

$$K = \frac{de}{d\alpha} = \frac{b+\varepsilon}{a}\left(a\sin\alpha + b\sin(\alpha-\beta)\right) = 0 . \tag{4.84}$$

The solution of (4.81) and (4.84) yields the limit point(s) of the mechanism though it can be calculated only numerically. However, the problem can be reduced to a one-varibale equation by expressing β from (4.84) and substituting it to (4.81).

4.3 Extension of classification

In Chpater 3 we have introduced a classification system which groups the points of compatibility paths into five categories according to their behaviour. With the aid of the matrix method discussed in Section 4.1, singularities of compatibility paths are further analysed.

In order to obtain the planar plot of the compatibility paths of a mechanism, a single compatibility condition needs to be formulated in terms of two kinematic state variables. Such a compatibility function is written for a particular bar of the linkage and can be plotted over the coordinate plane (ξ,η):

$$F(\xi,\eta)=0\,. \tag{4.85}$$

The compatibility function defines a surface $z=F(\xi,\eta)$ in the three-dimensional space (ξ,η,z) over the coordinate plane (ξ,η). Now the Jacobian matrix is the gradient of the compatibility function (4.85), which is related to the tangent plane. The Hessian matrix consists of the second derivatives hence is related to the curvature of the surface.

At common points of the coordinate plane $z=0$ and the surface, (4.85) is satisfied referring to compatible configurations. The intersections can be of various forms resulting in different types of mobility that a mechanism may have:

(a) The compatibility function has one common point with the coordinate plane in the neighbourhood of the point: the variation of surface is of higher-order (at least second-order), and an infinitesimal mechanism is obtained.

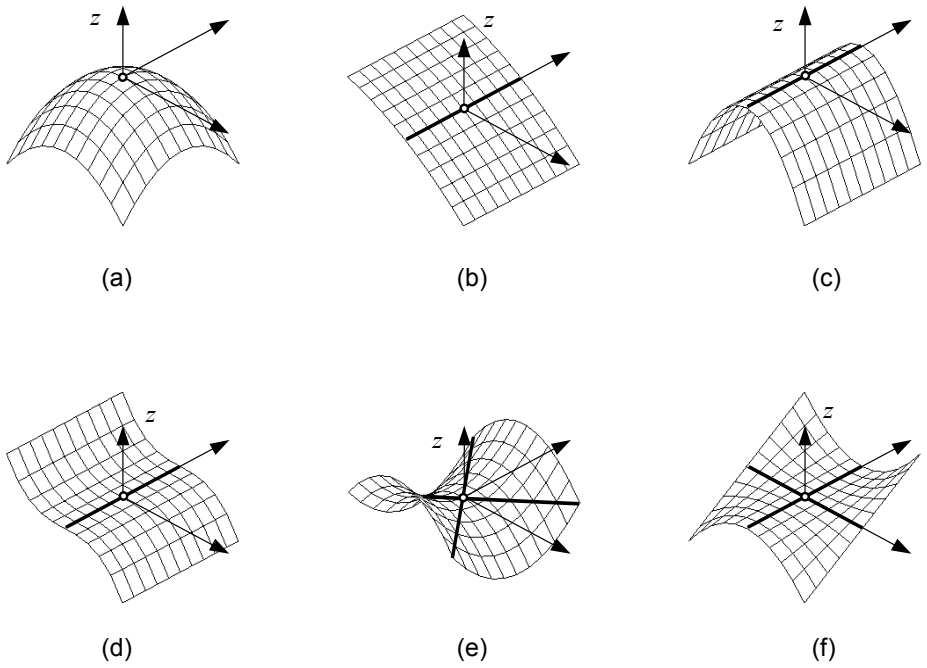

Figure 4.4: Local shapes of the compatibility paths. (a) Infinitesimal mechanism. (b) Finite mechanism. (c)-(d) A finite and an infinitesimal mechanism. (e)-(f) Two finite mechanisms.

(b) The compatibility function intersects the coordinate plane with a non-zero tangent: a compatibility path is formed and the compatibility condition has a first-order variation (and higher) in any direction not parallel to the path.

(c) The compatibility function intersects the coordinate plane with a zero tangent: a compatibility path is formed and the compatibility condition has an odd-order variation (and higher) in any direction not parallel to the path.

(d) The compatibility function touches the coordinate plane: a compatibility path is formed, tangent is zero and the compatibility condition has an even-order variation (and higher) in any direction not parallel to the path.

A set of corresponding schematic plots are given in Figures 4.4(a)-(d), respectively. In the vicinity of a given compatible position the above cases can either occur separately, or some of them can form various different combinations, which are listed below. The corresponding local forms of the compatibility function around that

particular point are schematically plotted in Figure 4.4(e)-(f), respectively. The vertical axis of the coordinate system is associated with z. The other two indicate the plane $z = 0$ where the orientation of the axes with respect to the surface is indifferent. The notations of Figure 4.4 match those of the list:

(a) The value of the compatibility function has the same sign except at the point in question where it is zero. The surface has a tangent plane identical to plane $z = 0$. The bar-assembly is an infinitesimal mechanism at that point. In the simplest case the Hessian matrix of the compatibility conditions is definite. If the compatibility condition fits to the coordinate plane with higher-order, then the mechanism is infinitesimal to a higher-order and the Hessian becomes semidefinite or zero matrix. The two-bar linkage shown in Figure 2.8(b) is an infinitesimal mechanism of the first-order.

(b) The compatibility function intersects plane $z = 0$ at one line with a non-zero tangent. The Jacobian has no rank deficiency and the bar-assembly is a finite mechanism. The point is either a regular point or a limit point of a compatibility path. A regular point can occur in two cases: either both elements of the Jacobian are non-zero or the compatibility path is straight and parallel to a coordinate axis. In this latter case one state variable is constant and the first derivative is zero. If the point is a limit point, one of the elements of the Jacobian becomes zero but the state variable is not constant. Examples for regular points and limit points are provided by the parallelogram-shaped linkage in Figure 2.10, etc. The straight regular compatibility path is demonstrated by the kite-shaped linkage in Figure 2.9.

(c) The compatibility function touches the coordinate plane at a line that passes through the point. The tangent plane is identical to the coordinate plane. The surface is even-order at the point in directions other than that of the line. The bar-assembly has a finite mechanism and infinitesimal one the order of which depends on the order of the surface. The point exhibits a split-vanish phenomenon. The Jacobian is zero and

the Hessian is either semidefinite or zero. An example of this case is given where the six-bar linkage is in a singular position but not at the bifurcation points, see Figure 3.6(b). The Hessian is semidefinite here indicating that an additional infinitesimal mechanism of the first-order exists further to the finite mechanism represented by the straight compatibility path. If the Hessian is zero, then the infinitesimal mechanism is of higher-order. No example has been found for this case.

(d) The compatibility function intersects the coordinate plane at a line that passes through the point. The tangent plane overlaps plane $z = 0$. The surface is odd-order at the point. Again the bar-assembly has a finite mechanism and infinitesimal one that is at least second-order. The order depends on the order of the surface. Examples have yet to be found for this case.

(e) The compatibility function intersects plane $z = 0$ at two lines with non-zero tangent. The lines intersect each other at the point, which is a saddle point. The bar-assembly has two finite mechanisms. The Jacobian matrix is zero and the Hessian matrix is indefinite at this point. The bifurcation points of the kite-shaped four-bar linkage, see Figure 2.9(a) or the parallelogram-shaped four-bar linkage, see Figure 2.9(a) are simple examples of this case.

(f) The compatibility function intersects plane $z = 0$ at a line with a non-zero tangent and touches it at a line with a zero tangent. The lines intersect each other at the point. Again the bar-assembly has a bifurcation point with two finite mechanisms. The point is a split-vanish bifurcation point. Both the Jacobian and the Hessian is zero. This case occurs at the symmetric bifurcation points of the six-bar linkage shown in Figure 3.6(a).

(g) The compatibility function intersects or touches plane $z = 0$ at two lines with higher-order. The lines intersect each other at the point. Again the bar-assembly has

a bifurcation point with two finite mechanisms. There are several combinations depending on the order though no mechanism examples are given yet.

Irregular compatibility paths contain split-vanish points. At split-vanish points the Jacobian has a rank deficiency and the Hessian becomes semidefinite or zero. Points in (c) and (f) indicate that the Hessian may be insufficient to distinguish between general split-vanish points and split-vanish bifurcation points.

The split-vanish phenomenon demonstrated by the six-bar mechanism exhibits some useful mathematical insights. Firstly, the split-vanish compatibility path is vertically straight and parallel to the coordinate axis of a control parameter. Hence the derivatives of the compatibility condition with respect to the variable in form of the Hessian matrix provide further information. The Hessian is semidefinite except at the bifurcation points where it becomes zero. This condition may serve as a distinction between a general and a bifurcation point.

Though it has not been demonstrated by examples in all cases, a few hypothetical cases need to be considered which the Jacobian and the Hessian are insufficient to distinguish.

Firstly, if the Hessian is definite, the point of the surface is a local maximum or minimum and the mechanism is first-order infinitesimal. However, there are higher-order hilltop points where the Hessian becomes zero. Such points correspond to infinitesimal mechanisms of higher-order.

Secondly, if the Hessian is indefinite, the surface is a saddle and the mechanism has a bifurcation point. The compatibility paths emanate from the point along the asymptotic lines (infinitesimally). Again, it is possible to have higher-order saddle points where the surface fits the zero plane to a higher-order. The Hessian may become zero at the bifurcation point.

It is also possible to have a surface with various higher-order behaviour that are neither of the cases above. In all these cases the Hessian becomes zero and hence not suitable for any classification.

Thirdly, the surface may be higher-order near a straight compatibility path even though there is no bifurcation. If the surface is first-order, a regular compatibility path is obtained, such as in case of the kite-shaped mechanism. If it is second-order, a split-vanish phenomenon occurs as seen for the six-bar mechanism. It may also be possible to find surfaces that produce compatibility paths at higher-order. If it is odd-order, the path cannot vanish. On the other hand, if it is even-order, it is possible to perturb the system so that the split-vanish phenomenon occurs. Again, the Hessian is zero in these cases.

Finally, we may consider the case when the compatibility path is not straight though the surface exhibits higher-order behaviour. Numerical methods may be needed for further examination.

It is important to emphasize again that most of the several kinds of higher-order behaviour listed above are hypothetical in a sense that no mechanism representations have been given yet. Whether such physical cases exist is yet to be justified or falsified. An exception of the above list is made by the higher-order infinitesimal mechanisms whose existence is well-known. It seems also likely to be possible to find mechanisms that can produce higher-order split-vanish phenomenon. Further research is needed along this line.

To determine the properties of a critical point according to what has been discussed here, a procedure is proposed as follows:

(a) Formulate the compatibility condition in terms of the two state variables as $F(\xi, \eta) = 0$ and consider the point $P(\xi_0, \eta_0)$. If P satisfies the compatibility condition, the state variables correspond to an existing (feasible) configuration of the mechanism.

(b) Calculate the Jacobian matrix $\mathbf{J} = [\partial F/\partial \xi \quad \partial F/\partial \eta]$ and determine whether the rank decreases at P. The condition for rank deficiency is $\mathbf{J}_1 = 0$ and $\mathbf{J}_2 = 0$.

(c) If there is no rank deficiency, the point is either a regular point or a limit point. A limit point occurs if one of $\mathbf{J}_1$ and $\mathbf{J}_2$ is zero but the compatibility path is not

straight (i.e. there is local extremum in the path). A general regular point occurs if either both elements of **J** are non-zero or *P* is on a straight path parallel to one of the coordinate axes.

(d) If the rank of **J** reduces, the Hessian matrix $\mathbf{H} = \left[\partial^2 F / \partial\xi \partial\eta\right]$ is to be calculated at *P*.

(e) If the Hessian is definite, *P* is a distinct point of compatibility and the mechanism is infinitesimal of the first-order. If the Hessian is indefinite, *P* is a saddle point of the surface $z = F(\xi, \eta)$ and a regular bifurcation point is obtained. If the Hessian is semidefinite or zero, the mechanism has a higher-order singularity and further viewpoints should be considered.

(f) If *P* is not a point of a straight compatibility path $\xi = \xi_0$, numerical methods are required for further analysis. If it is, the order of the surface in state variable ξ can distinguish between split-vanish points (even-order) and not split-vanish points (odd-order). Further distinction between general split-vanish points and split-vanish bifurcation points may be made using numerical methods.

4.4 Computation of graphs of compatibility paths

Various plots of compatibility paths have been shown so far in this dissertation. Due to the nonlinearity of the compatibility conditions, it is not always possible to obtain one kinematic state variable in terms of the other analytically.

A numerical method is presented here to provide an approximate graphical representation of the compatibility condition. The steps of this numerical approach are as follows:

(a) Select a region in state variable space (ξ, η) within which the calculation is carried out. Divide the region by placing an orthogonal grid on the coordinate plane, see Figure 4.5(a).

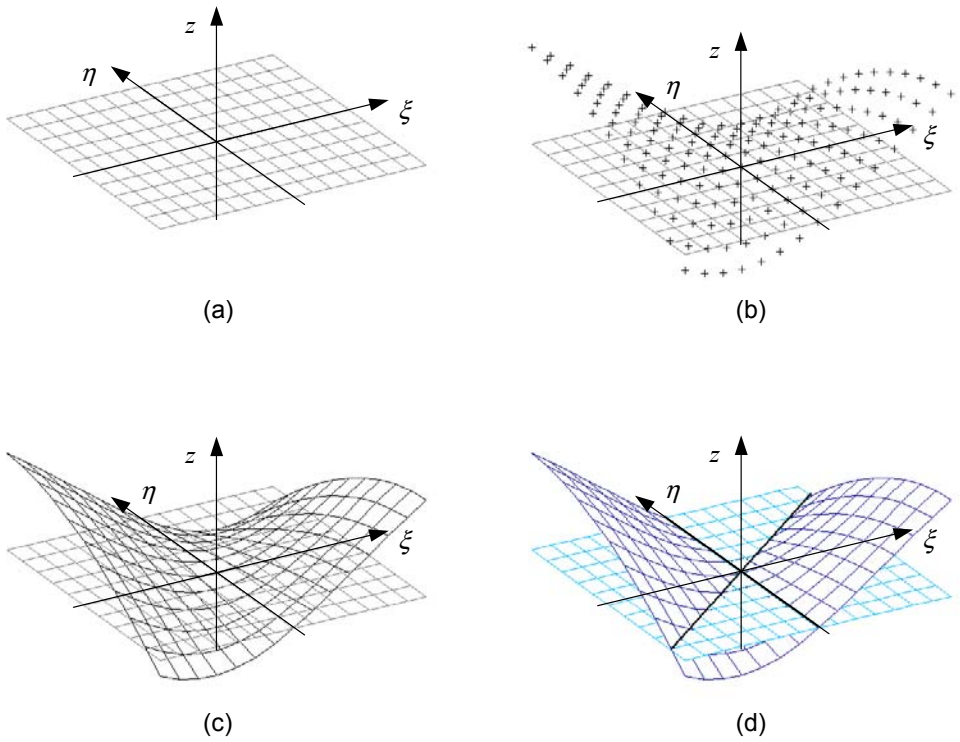

Figure 4.5: Numerical approximation of compatibility paths. (a) A rectangular grid is created on the state variable plane. (b) The compatibility condition is evaluated at the discrete grid points. (c) An approximate (linear) function is fitted to the values. (d) Zero positions are calculated.

(b) Calculate the value of the compatibility function $F(\xi,\eta)$ at the nodes of the grid. The results form a set of discrete points in the three-dimensional space (ξ,η,z) where $z = F(\xi,\eta)$, see Figure 4.5(b).

(c) Fit an approximating two-variable function to the calculated values. It is most practical to apply linear approximation, that is to use linear interpolation in the grid elements between the nodes, see Figure 4.5(c).

(d) Equilibrium or compatibility positions are represented by zero points and lines of the equilibrium or the compatibility function, that is by the intersections of the surface with plane $z = 0$. The zero lines are approximated by the intersections of the approximation multi-linear surface and the coordinate plane, see Figure 4.5(d).

The steps of this method can easily carried out by most programming languages, e.g. MATLAB, Version 6.1 (The Mathworks, Inc., 2001).

The method applies to mechanisms with both perfect and imperfect geometry. In case of imperfect geometry the constraint condition is formulated and fed into the algorithm accordingly. In fact, the compatibility paths shown in Figures 2.9(a), 2.10(b), 3.2, 3.4(b), 3.7(a), 3.8(b), 3.11(b) and (c) were obtained by this method.

Though it provides a good overview on the behaviour of the mechanism, the method is an approximate one. While it is expected to give satisfactory results at general positions, such as in Figure 4.4(b), it might fail to give good approximation in the neighbourhood of bifurcation points where more lines are present. Some particular types of singularities may require a special approach, e.g. in the presence of infinitesimal mechanisms as seen in the six-bar linkage.

At singular positions the general approximation method could fail for a few reasons. One case can be that the approximation could not distinguish between two crossing lines and two non-intersecting lines passing close to each other. An example is given in Figure 4.6 showing two different approximations for the same set of points. In the first case the discrete points are approximated by two crossing curves while in the other case the neighbouring branches are connected forming two separate curves.

Another case where the approximate method may fail to find a path occurs when the compatibility surface touches the coordinate plane without intersections, i.e. a maximum or minimum is reached at $z = 0$. A cross-section of the compatibility surface is shown in Figure 4.7. If the zero point is inside a grid element, as shown in

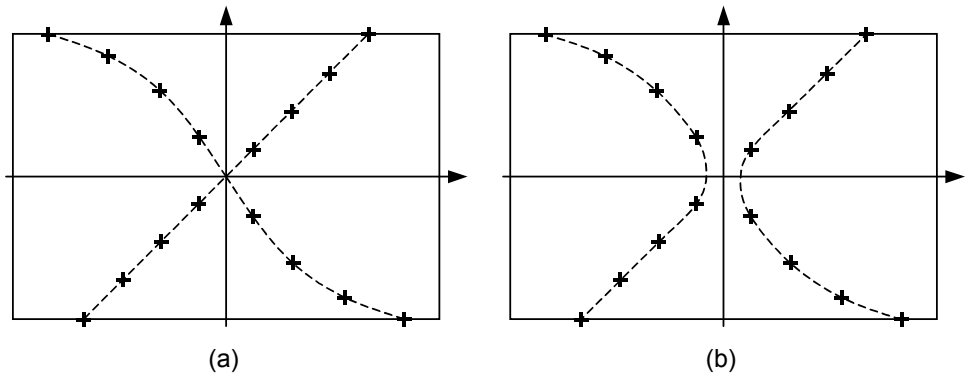

Figure 4.6: Approximations of paths at bifurcation points with the same set of points. (a) The two curves intersect. (b) The curves pass by near each other.

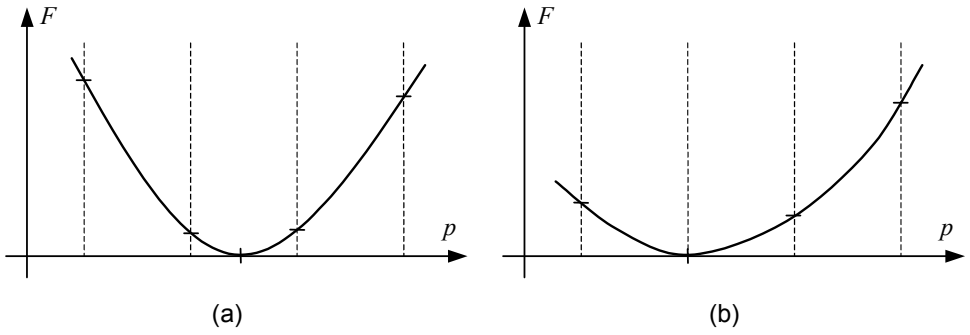

Figure 4.7: (a) Zero point inside a grid element. (b) Zero point at a grid point.

Figure 4.7(a), the evaluated values at the grid points are the same sign, hence the linear approximation fails. In the special case of having a compatibility path fitting to a grid point or a grid line exactly, the compatibility surface will have an extremum $z = 0$ at that grid point, as shown in Figure 4.7(b). Now the method could also fail to find it due to the limited floating point accuracy of the computation.

Further to this, one might need to calculate the compatibility paths in a selected region of the state variable space more precisely. In order to do that the numerical method introduced earlier can be enhanced in a number of ways.

The simplest way of increasing the accuracy of the computation of the paths is to refine the grid. It increases the computational cost at a square rate, therefore the recommendation is to use it only for the close neighbourhood of the singular point. The practical limit of the refining is set by the floating point accuracy of the programming language applied. It is usually in the range of 10 to 20 digits though there exist packages for significantly higher precision.

Another way is to replace the linear approximation with a higher-order one. In the case where a compatibility path crosses a grid line, the intersection point can be calculated with higher precision by evaluating more values of the compatibility condition along the line and fitting a higher-order polynomial curve. Moreover, the Newton-Raphson procedure can also be used to iterate the zero point as the derivatives of the compatibility condition are often available.

If the compatibility path touches the coordinate plane without intersection, this approach will fail. It is a degenerate case where the approximate curve may have more zero points or none at all. The exact solution is a limit situation between the two. To find it we have to exploit the fact that the zero point is an extremum at the same time. This extremum point can be approximated to any precision within the range of the floating point accuracy. If the difference between the extremum and zero is larger than the computational limit in magnitude, then there is no solution. If the extremum approaches zero within this range, the point can be called a solution. However, to find an 'exact' solution, infinite precision would be required, which is numerically impossible. Therefore we have to bear in mind that not only the position but the existence of the zero point is also subject to numerical error. In this case a sensible approach is to examine the mechanism configuration to determine whether it is feasible or not. This behaviour can be demonstrated by the six-bar linkage whose straight path is generated where the compatibility surface touches the plane $z = 0$.

The existence of compatibility paths around a singular point can be studied by examining the shape of the compatibility surface. At a regular bifurcation point the surface is an ordinary saddle and in the neighbourhood of the point the quadrants of the surface are positive and negative alternately. A cross-section of the surface through the bifurcation point in any given direction can be expanded into Taylor series. The first non-zero term of the series defines the sign of the surface in the small vicinity of the point.

For any smooth surface, if the surface is positive and negative in two chosen directions, then there is a compatibility path (or more) in the section between the two directions. It is due to Bolzano's intermediate value theorem (Bolzano, 1817; James, 1992). The exact direction of the path is the limit position between the positive and negative sections of the surface. It can be located by the sign change of the first non-zero term in the Taylor series.

Other paths are obtained where the compatibility surface touches the tangent plane without intersection. This case is observed at the straight compatibility path of the six-

bar linkage. The path separates sections with the same sign thus the first non-zero term does not change sign. However, all terms disappear in the Taylor series in the direction of the line because the compatibility is fulfilled in that particular direction. Though no mechanism example has demonstrated different behaviour, we still need to consider the hypothetical case when the path is not straight. Now the compatibility is not fulfilled in the direction of the tangent of the path at that point hence the Taylor series has higher-order non-zero terms and this condition does not hold.

Finally, if the rank deficiency of the Jacobian occurs but only one compatibility path exists, then an infinitesimal mechanism must appear, see Figure 4.4(c) and (d). Again create a section of the surface in any direction other than the compatibility path and expand the function into Taylor series. If the first non-zero term is the nth, the mechanism is infinitesimal of the order n-1.

5

APPLICATION OF THE ELEMENTARY CATASTROPHE THEORY

Contents

In this chapter a new approach to the compatibility of mechanisms is presented. Firstly, it is summarized why the analysis previously shown might not always be sufficient. Secondly, elementary catastrophe theory is introduced followed by its applications in kinematics of mechanisms.

5.1 Problem statement

Chapters 2 and 3 contain compatibility paths of various mechanisms. These paths depend on kinematic state variables chosen to describe the motion. They can be Cartesian coordinates of nodes, or angles. Hence, when the number of state variables is greater than two, a multi-dimensional space is required to plot the compatibility paths.

It has also been pointed out in Section 4.1 that different sets of state variables may not always serve equally. Consider the six-bar mechanism introduced in Section 3.1.2, shown here again in Figure 5.1(a). As we have seen, angles ϕ_1 and ϕ_3 are sufficient to describe the motion of the linkage around one of the symmetric bifurcations shown in Figure 5.1(b). If angle ϕ_1 is replaced with y_1, which is the y coordinate of node A, the resulting compatibility paths are essentially the same as the original ones, see Figure 5.1(c). On the other hand, if x_1, the x coordinate of node A, is chosen, the graph becomes different, see Figure 5.1(d). The symmetric bifurcation is not visible because x_1 is not suitable to show the behaviour.

Simple examples like this demonstrate that different parameter sets have different validity and no obvious choice can be obtained automatically.

Similar problems appear in the stability theory. Different sets of state variables provide different equilibrium paths, which may even become fundamentally different. For example, in buckling of a cylindrical shell, if the vertical force and the longitudinal compression are chosen as state variables, the planar plot of the compatibility paths is characteristically different from the three-dimensional one obtained by including a third state variable, the radial displacement, see Figure 5.2 (von Kármán and Tsien, 1941).

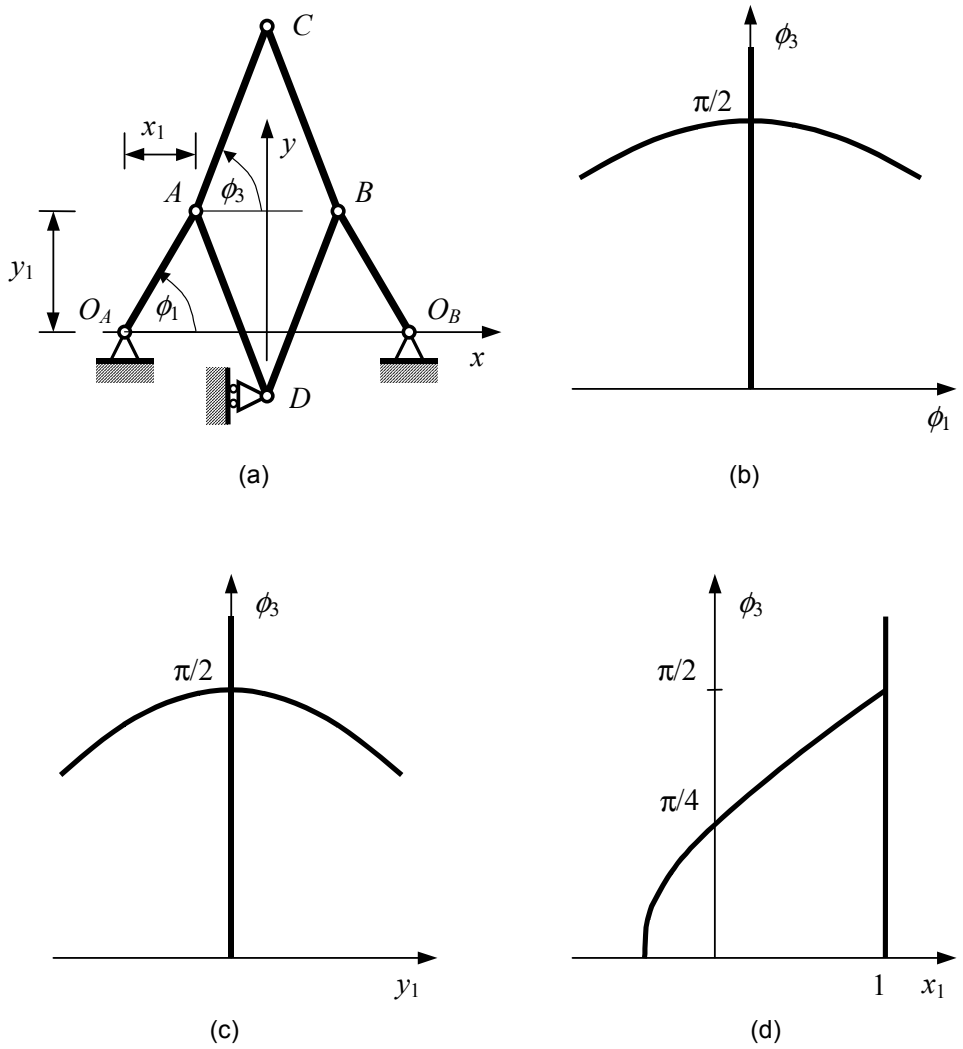

Figure 5.1: A six-bar mechanism. (a) Basic structure. (b)-(d) Compatibility paths obtained using three different parameter sets.

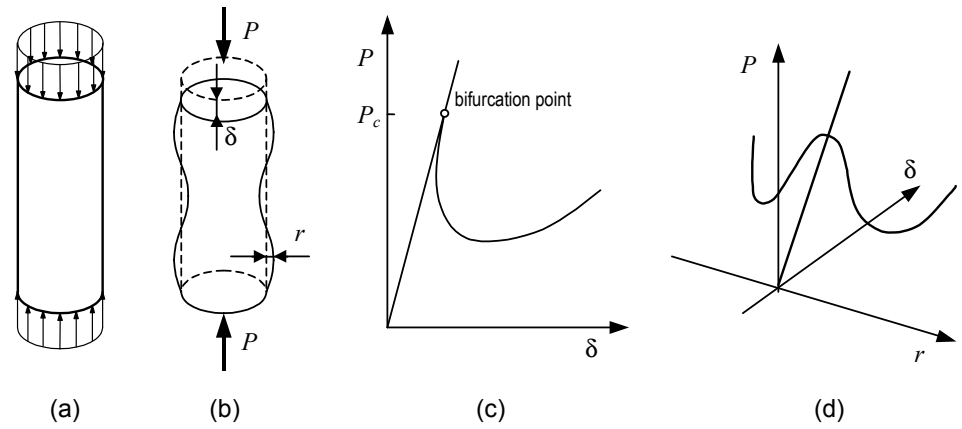

Figure 5.2: Buckling of cylindrical shell under axial load. (a) Structure. (b) Axial and radial deformations. (c)-(d) Equilibrium paths.

The question arises what the relationship between the various compatibility paths is and how to chose state variables so that the plot represents the essential behaviour of the mechanism. By reducing the number of state variables the graph obtained is a projection (or a transformation) of a more general case. The state variables should be chosen to describe the position of all nodes of the mechanism uniquely so that the projections preserve all characteristics of the compatibility path. For example, in the parallelogram-shaped mechanism the angle is more suitable to define a node than the Cartesian coordinate because other coordinates and distances derived from the latter are multi-value functions.

Another concern is the behaviour of structures and mechanisms with imperfections. The imperfect equilibrium paths of the three structure examples are given in Section 2.2, see Figures 2.2(b), 2.3(b) and 2.4(b). We have addressed this issue in Section 2.4.1 where similar problems occur for mechanisms.

Due to these problems, the graphs of equilibrium or compatibility paths may not be sufficient to reveal the true nature of the behaviour of the object we study. A new approach is required, which, in the stability theory of structures, is provided by the application of the elementary catastrophe theory. A brief introduction of it has been given in Section 2.3. Hence in this chapter we apply the catastrophe theory to the bifurcations of compatibility paths of mechanisms. Two concepts are proposed: the first is based on the analogy between compatibility and equilibrium, the second one utilizes a potential function introduced in Section 3.4.3 for the classification of singularities.

5.2 The analogy concept

5.2.1 Basic technique

In the stability theory, the equilibrium of elastic structures is the gradient of the total potential energy function. Critical points of the equilibrium paths are classified by the local form of the potential energy (Thom's theorem).

Table 5.1: Canonical and equilibrium forms for the cuspoid catastrophe types listed in Thom's theorem.

Type	**Canonical form** (f)	**Equilibrium form** (f_{u_1})
A_2	$u_1^3 + t_1 u_1$	$3u_1^2 + t_1$
A_3	$\pm\left(u_1^4 + t_2 u_1^2 + t_1 u_1\right)$	$\pm\left(4u_1^3 + 2t_2 u_1 + t_1\right)$
A_4	$u_1^5 + t_3 u_1^3 + t_2 u_1^2 + t_1 u_1$	$5u_1^4 + 3t_3 u_1^2 + 2t_2 u_1 + t_1$
A_5	$\pm\left(u_1^6 + t_4 u_1^4 + t_3 u_1^3 + t_2 u_1^2 + t_1 u_1\right)$	$\pm\left(6u_1^5 + 4t_4 u_1^3 + 3t_3 u_1^2 + 2t_2 u_1 + t_1\right)$
A_6	$u_1^7 + t_5 u_1^5 + t_4 u_1^4 + t_3 u_1^3 + t_2 u_1^2 + t_1 u_1$	$7u_1^6 + 5t_5 u_1^4 + 4t_4 u_1^3 + 3t_3 u_1^2 + 2t_2 u_1 + t_1$

We propose to classify compatibility conditions on the basis of the analogy between equilibrium and compatibility. As the equilibrium equation is derived from the potential energy function, equilibrium forms can be derived from the canonical forms listed in Thom's theorem. That is, if the structure exhibits a certain catastrophe type, the equilibrium equation is locally equivalent to a corresponding form, see Tables 5.1 and 5.2.

Therefore we shall call a singular position of a mechanism equivalent to a catastrophe type if the compatibility condition is locally equivalent to the equilibrium forms of that particular catastrophe. For example, consider any of the mechanisms with two kinematic state variables and one compatibility condition shown in the previous chapters. If the compatibility condition at a bifurcation point can be transformed to the first, second, etc. equilibrium form in Table 5.1, then the mechanism is equivalent to the fold, the cusp, etc., respectively.

Although we presented the equivalent energy formulation for mechanisms in Section 3.4, the forms are difficult to handle mathematically. This is the reason why we opt to use the equilibrium forms of Thom's theorem rather than the canonical forms.

In the following analysis, for problems with a single compatibility condition and two state variables, we also designate one as a variable while the other as a control

parameter because they are related by the compatibility condition. At a bifurcation point the compatibility condition is expanded into Taylor series. After a suitable linear transformation, forms similar to one of the equilibrium forms in Table 5.1 can be obtained. The designation of the variable and the control parameter will be discussed in detail in Section 5.5.

If two compatibility conditions and three state variables are needed at a bifurcation point, then two equilibrium forms are derived. Now they are compared to those in Table 5.2.

This method is in accordance with the wider concept of the catastrophe theory. Gilmore (1981) states that "Catastrophe Theory attempts to study how the qualitative nature of the solutions of equations depends on the parameters that appear in the

Table 5.2: Canonical and equilibrium forms for the umbilic catastrophe types listed in Thom's theorem

Type	**Canonical form** (f)	**Equilibrium forms** (f_{u_1}, f_{u_2})
D_4^-	$u_1^2 u_2 - u_2^3 + t_3 u_1^2 + t_2 u_2 + t_1 u_1$	$2u_1 u_2 + 2t_3 u_1 + t_1$ $u_1^2 - 3u_2^2 + t_2$
D_4^+	$u_1^2 u_2 + u_2^3 + t_3 u_1^2 + t_2 u_2 + t_1 u_1$	$2u_1 u_2 + 2t_3 u_1 + t_1$ $u_1^2 + 3u_2^2 + t_2$
D_5	$\pm\left(u_1^2 u_2 + u_2^4 + t_4 u_2^2 + \ldots\right.$ $\left.\ldots + t_3 u_1^2 + t_2 u_2 + t_1 u_1\right)$	$\pm\left(2u_1 u_2 + 2t_3 u_1 + t_1\right)$ $\pm\left(u_1^2 + 4u_2^3 + 2t_4 u_2 + t_2\right)$
D_6^-	$u_1^2 u_2 - u_2^5 + t_5 u_2^3 + t_4 u_2^2 + \ldots$ $\ldots + t_3 u_1^2 + t_2 u_2 + t_1 u_1$	$2u_1 u_2 + 2t_3 u_1 + t_1$ $u_1^2 - 5u_2^4 + 3t_5 u_2^2 + 2t_4 u_2 + t_2$
D_6^+	$u_1^2 u_2 + u_2^5 + t_5 u_2^3 + t_4 u_2^2 + \ldots$ $\ldots + t_3 u_1^2 + t_2 u_2 + t_1 u_1$	$2u_1 u_2 + 2t_3 u_1 + t_1$ $u_1^2 + 5u_2^4 + 3t_5 u_2^2 + 2t_4 u_2 + t_2$
E_6	$\pm\left(u_1^3 + u_2^4 + t_5 u_1 u_2^2 + t_4 u_2^2 + \ldots\right.$ $\left.\ldots + t_3 u_1 u_2 + t_2 u_2 + t_1 u_1\right)$	$\pm\left(3u_1^2 + 2t_5 u_1 u_2 + t_3 u_2 + t_1\right)$ $\pm\left(4u_2^3 + 2t_5 u_1 u_2 + 2t_4 u_2 + t_3 u_1 + t_2\right)$

equations". In stability theory the number and type of equilibrium positions are investigated subject to given parameters (load, imperfections, etc.). Mathematically the problem reads as how many solutions the equilibrium equations may have in terms of the parameters in the equations. If a structure exhibits a cuspoid catastrophe of type A_k at the critical value of the load parameter, the equilibrium equation is kth order. It implies that with a suitable small perturbation the equation can yield k solutions in the small vicinity of the critical point. For example, the asymmetric structure in Figure 2.4(a) exhibits a fold catastrophe point at the critical load. If a small $\varepsilon < 0$ offset is applied to the position of the load, the equilibrium paths are obtained, which are drawn by dashed thin lines in Figure 2.4(b). In the vicinity of the critical point two equilibrium positions exist.

A similar interpretation is possible for compatibility paths of mechanisms. If the compatibility equation is kth order in its variable for a given value of the parameter, the system can be modified by a suitable small perturbation so that the compatibility equation yields k solutions, i.e. k feasible configurations exist. Based on the analogous mathematical and physical behaviour of the two systems, we define such a kinematic system equivalent to catastrophe type A_k.

The compatibility conditions in this analysis can be written in various forms. We opt to use both (3.9) and (3.10) given in Section 3.3. In the following both are investigated.

5.2.2 The kite-shaped four-bar linkage

Consider first the kite-shaped four-bar linkage shown in Figure 2.9(a). The state variables are α and β; the compatibility condition is written for the coupler bar AB. The square root form is

$$F(\alpha;\beta) = \sqrt{(a + b\cos\beta - a\cos\alpha)^2 + (b\sin\beta - a\sin\alpha)^2} - b = 0\,. \qquad (5.1)$$

The bifurcation occurs at $\alpha = \beta = 0$ where (5.1) is expanded into its Taylor series:

$$F(\alpha;\,\beta)\approx\frac{1}{2}\frac{a}{b}(a+b)\,\alpha^2-a\alpha\beta+\ldots \tag{5.2}$$

where the ellipsis refers to higher-order terms, which are ignored. Furthermore, a semicolon is used in (5.1) and (5.2) to separate the variable and the control parameter. These notations are used in similar formulas in the following. Taking α as a variable, a linear transformation is applied to eliminate the mixed term:

$$\alpha=\sqrt{\frac{2b}{a(a+b)}}\,\overline{\alpha}+\frac{b}{a+b}\,\beta\,. \tag{5.3}$$

The new form now is

$$F(\alpha;\,\beta)\approx\overline{\alpha}^2-\frac{ab}{2(a+b)}\beta^2+\ldots \tag{5.4}$$

The second term is regarded as a new parameter t_1 in order to match the equilibrium form in the first row in Table 5.1. Hence the bifurcation point is equivalent to the fold catastrophe. Note that the actual magnitude of the coefficient of the characteristic term is irrelevant, the linear transformations in this analysis are chosen to obtain unity.

Let us extend the investigation to the imperfect system perturbed by geometric imperfections. Let ε_1, ε_2, ε_3 and ε_4 denote the length errors for bars O_AO_B, O_BB, AB and O_AA, respectively. The compatibility condition now is

$$F(\alpha;\,\beta)=\sqrt{(a_1+b_2\cos\beta-a_4\cos\alpha)^2+(b_2\sin\beta-a_4\sin\alpha)^2}-b_3=0 \tag{5.5}$$

where $a_1=a+\varepsilon_1$, $a_4=a+\varepsilon_4$, $b_2=b+\varepsilon_2$ and $b_3=b+\varepsilon_3$. The Taylor series expansion gives

$$F(\alpha;\,\beta)\approx\frac{1}{2}\frac{a}{b}(a+b)\,\alpha^2-a\alpha\beta+\varepsilon_1+\varepsilon_2-\varepsilon_3-\varepsilon_4+\ldots \tag{5.6}$$

We apply the same linear transformation as above. The compatibility condition has now the form

$$F(\alpha;\,\beta)\approx\overline{\alpha}^2-\frac{ab}{2(a+b)}\beta^2+\varepsilon_1+\varepsilon_2-\varepsilon_3-\varepsilon_4+\ldots \tag{5.7}$$

and the new parameter to be introduced is

$$t_1 = -\frac{ab}{2(a+b)}\beta^2 + \varepsilon_1 + \varepsilon_2 - \varepsilon_3 - \varepsilon_4 . \tag{5.8}$$

Note that in (5.4) the parameter can take only non-positive values due to β^2. By introducing the geometric imperfections, t_1 may become positive in (5.8).

It clearly shows that the bifurcation point is related to the *fold catastrophe*.

Now let us investigate the implication of using a different form of compatibility condition. Consider the square form of the compatibility condition with imperfections included:

$$F = \frac{1}{2}\left[(a_1 + b_2\cos\beta - a_4\cos\alpha)^2 + (b_2\sin\beta - a_4\sin\alpha)^2 - b_3^2\right] = 0 . \tag{5.9}$$

The Taylor series expansion at the bifurcation point gives

$$F(\alpha;\beta) \approx \frac{1}{2}a(a+b)\alpha^2 - ab\alpha\beta + b\varepsilon_1 + b\varepsilon_2 - b\varepsilon_3 - b\varepsilon_4 + \ldots \tag{5.10}$$

Again a linear transformation is needed:

$$\alpha = \sqrt{\frac{2}{a(a+b)}}\,\overline{\alpha} + \frac{b}{a+b}\beta . \tag{5.11}$$

resulting in the compatibility condition

$$F(\alpha;\beta) \approx \overline{\alpha}^2 - \frac{ab^2}{2(a+b)}\beta^2 + b\varepsilon_1 + b\varepsilon_2 - b\varepsilon_3 - b\varepsilon_4 + \ldots \tag{5.12}$$

Assigning the sum of all but the first term in (5.12) a new parameter t_1, the equilibrium form related to the fold catastrophe is obtained again. Hence both formulations of the compatibility condition show the same behaviour.

A similar analysis can be carried out for the parallelogram-shaped linkage shown in Figure 2.10(a). It shows that the asymmetric bifurcation point is associated with the *fold catastrophe*. These two mechanisms are the kinematic counterparts of the asymmetric structure shown in Figure 2.4(a), which exhibits the *fold catastrophe* as well.

5.2.3 The square-shaped four-bar linkage

Consider now the square-shaped four-bar linkage shown in Figure 3.8(a). It comes as a special case of the previous examples with all bars being identical. The state variables are α and β again and the compatibility condition is written for the coupler bar *AB*:

$$F(\alpha;\beta)=\sqrt{(a+a\cos\beta-a\cos\alpha)^2+(a\sin\beta-a\sin\alpha)^2}-a=0\,. \qquad (5.13)$$

The bifurcation point we are interested in is at $(\alpha=0,\beta=\pi)$ where two straight compatibility paths intersect. The Taylor series expansion gives:

$$F(\alpha;\beta)\approx a\alpha\tilde{\beta}-\frac{1}{6}a\alpha^3\tilde{\beta}-\frac{1}{4}a\alpha^2\tilde{\beta}^2-\frac{1}{6}a\alpha\tilde{\beta}^3+\ldots \qquad (5.14)$$

where $\tilde{\beta}$ denotes the local state variable: $\tilde{\beta}=\beta-\pi$. The Taylor series has no pure terms because (5.13) is satisfied along the coordinate axes, i.e. it is an infinitely degenerate case. Now consider imperfections similar to the previous example:

$$F(\alpha;\beta)=\sqrt{(a_1+a_2\cos\beta-a_4\cos\alpha)^2+(a_2\sin\beta-a_4\sin\alpha)^2}-a_3=0 \qquad (5.15)$$

where $a_i=a+\varepsilon_i$, $i=1,2,3,4$. Omitting the higher-order terms beyond the third, the Taylor series expansion gives

$$F(\alpha;\beta)\approx\frac{1}{2}(\varepsilon_1-\varepsilon_2)\alpha^2+(a+\varepsilon_1)\alpha\tilde{\beta}+\frac{1}{2}(\varepsilon_1-\varepsilon_4)\tilde{\beta}^2-\varepsilon_1+\varepsilon_2-\varepsilon_3+\varepsilon_4+\ldots \qquad (5.16)$$

A second-order term of the variable appears, resulting in the fold catastrophe. The imperfections reduce the infinite degenerateness of the mechanism.

Consider now the square form of the compatibility condition with imperfections included:

$$F=\frac{1}{2}\left[(a_1+a_2\cos\beta-a_4\cos\alpha)^2+(a_2\sin\beta-a_4\sin\alpha)^2-a_3^2\right]=0\,. \qquad (5.17)$$

The Taylor series expansion at the bifurcation point is calculated again. Omitting the higher-order and also the mixed terms of the state variables one obtains:

$$F(\alpha;\beta)\approx\frac{1}{2}a(\varepsilon_1-\varepsilon_2)\alpha^2+a(a+\varepsilon_2+\varepsilon_4)\alpha\tilde{\beta}+\frac{1}{2}a(\varepsilon_1-\varepsilon_4)\tilde{\beta}^2-$$

$$-a\varepsilon_1+a\varepsilon_2-a\varepsilon_3+a\varepsilon_4+\ldots \tag{5.18}$$

Again the second-order term of the variable appeared. It is a fold catastrophe. Both formulations of the compatibility condition show the same behaviour as they have the same characteristic terms with different coefficients.

5.2.4 The six-bar linkage

Consider the six-bar linkage shown in Figure 3.1(a). We use two angles with a compatibility equation written for bar *BC*:

$$F(\phi_1;\phi_3)=\sqrt{\left(2-2\cos\phi_1-\sqrt{2}\cos\phi_3\right)^2+\left(\sqrt{2}\sin\phi_3\right)^2}-\sqrt{2}=0\,. \tag{5.19}$$

Expanding (5.19) into Taylor series at the bifurcation point $(\phi_1=0,\phi_3=\pi/2)$ and introducing the local variable $\tilde{\phi}_3=\phi_3-\pi/2$ gives

$$F(\phi_1;\phi_3)\approx\frac{\sqrt{2}}{4}\phi_1^4+\tilde{\phi}_3\phi_1^2+\ldots \tag{5.20}$$

Taking ϕ_1 the variable, (5.20) is a fourth-order expression. It corresponds to the third equilibrium form in Table 5.1, i.e. it is equivalent to the *swallowtail catastrophe*. In order to get all terms in this formula, we introduce geometric imperfections again. It is easy to modify (5.19) with the imperfections of bars *AC* and *BC*. On the other hand, all of the other perturbations ruin the symmetry of linkage O_AADBO_B and thus the expression becomes complicated. Therefore here only the Taylor series expansion is shown with imperfections ε_1, ε_2 and ε_3 for bars O_AA, *AC* and *BC*, respectively.

$$F(\phi_1;\phi_3)\approx\frac{\sqrt{2}}{4}\phi_1^4+\left(\tilde{\phi}_3-\frac{\sqrt{2}}{4}\varepsilon_1\right)\phi_1^2+\left(-\frac{1}{4}\varepsilon_1^3\right)\phi_1+(\varepsilon_2-\varepsilon_3)+\ldots \tag{5.21}$$

Due to these imperfections the linear and the constant terms appear in (5.21) in addition to those in (5.20). Let us introduce new parameters t_1, t_2 and t_3:

$$t_1 = \varepsilon_2 - \varepsilon_3, \quad t_2 = -\frac{1}{4}\varepsilon_1^3, \quad t_3 = \tilde{\phi}_3 - \frac{\sqrt{2}}{4}\varepsilon_1 \tag{5.22}$$

so that the equilibrium form of the of the *swallowtail catastrophe* is obtained.

Consider now the alternative compatibility condition in square form

$$F = \frac{1}{2}\left[\left(2 - 2\cos\phi_1 - \sqrt{2}\cos\phi_3\right)^2 + \left(\sqrt{2}\sin\phi_3\right)^2 - 2\right] = 0\,. \tag{5.23}$$

Again, the imperfections make (5.23) complicated hence only the Taylor series is given here:

$$F(\phi_1;\phi_3) \approx \frac{1}{2}\phi_1^4 + \left(\sqrt{2}\,\tilde{\phi}_3 - \frac{1}{2}\varepsilon_1\right)\phi_1^2 + \left(-\frac{\sqrt{2}}{4}\varepsilon_1^3\right)\phi_1 + \left(\sqrt{2}\varepsilon_2 - \sqrt{2}\varepsilon_3\right) + \ldots \tag{5.24}$$

Note that the same terms are obtained with slightly different coefficients. The new parameters are introduced in a similar way.

In Chapter 3 and 4 we have seen the differences between the symmetric bifurcations of equilibrium and compatibility. It has also been shown in Section 2.2 that the two structures with the two types of symmetric equilibrium bifurcations correspond to the cusp catastrophe. Our analysis demonstrates that the six-bar linkage is equivalent to a higher-order catastrophe, the *swallowtail*.

The higher-order term in the compatibility condition is the result of the symmetry of the perfect configuration at the bifurcation point, see Figure 5.3(a). Nodes *A* and *B* have the same *y* coordinate and the distance contains a second-order term of ϕ_1. Taking ϕ_3 constant, the compatibility condition for *BC* is obtained from the right-angled triangle *ABC* hence the term ϕ_1^4, see Figure 5.3(b).

The approach based on catastrophe theory presented here helps to analyse and understand the singular behaviour experienced at the straight compatibility path $\phi_1 = 0$ shown in Figure 3.7(a). The singularity demonstrated by the Jacobian matrix, see

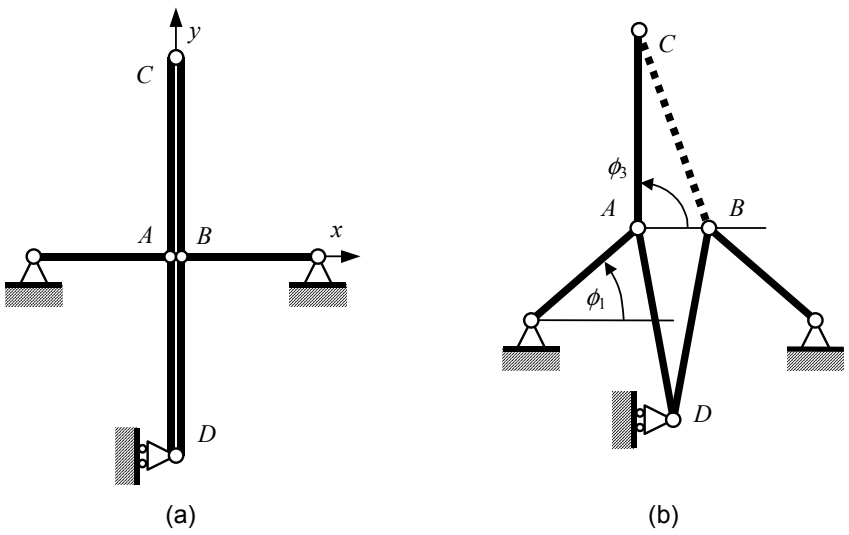

Figure 5.3: (a) Bifurcation point 2' of the six-bar mechanism. (b) Configuration near the bifurcation point at unchanged ϕ_3.

Section 4.1.1, suggests that a catastrophe of a certain type may occur along that path. Let us carry out the analysis at a point: ($\phi_1 = 0$, $\phi_3 = \phi_{3,0}$). $\phi_3 \neq \pm\pi/2$ so that the point in consideration is not one of the bifurcation points. The Taylor series obtained will be the same as (5.20) except that $\tilde{\phi}_3 = \phi_3 - \pi/2$, which is now a non-zero constant. Hence the characteristic term of the series is a second-order one, which indicates the fold catastrophe. In other words, the points along the straight compatibility path are not regular points as defined in Section 3.2 but correspond to a catastrophe type which is lower-order than that at the bifurcation points.

To understand how this occurs let us examine the mathematics of the swallowtail in detail (Gáspár, 1999). The canonical form can be written as

$$f(u_1, t_1, t_2, t_3) = u_1^5 + t_3 u_1^3 + t_2 u_1^2 + t_1 u_1 \tag{5.25}$$

where the variable is denoted by u_1 and the parameters by t_1, t_2 and t_3. The equilibrium form is derived from (5.25):

$$\frac{df}{du_1} = 5u_1^4 + 3t_3 u_1^2 + 2t_2 u_1 + t_1 = 0\,. \tag{5.26}$$

It requires a four-dimensional space to plot, and therefore it cannot be visualized. Critical points are obtained where the second derivative becomes zero:

$$\frac{d^2 f}{du_1^2} = 20u_1^3 + 6t_3 u_1 + 2t_2 = 0\,. \tag{5.27}$$

Eliminating the variable from the equation system of (5.26) and (5.27), the bifurcation set is obtained in the three-dimensional space of the parameters. It is a set of points (t_1, t_2, t_3) where singularity of a certain type occurs.

The bifurcation set is a manifold in the parameter space that divides the space into regions within which the properties of the stationary positions are the same. For example, the bifurcation set of the one-parameter catastrophe type, the fold, is a single point in the one-dimensional space.

The swallowtail catastrophe requires three parameters hence the bifurcation set consists of surfaces in the three-dimensional space (t_1, t_2, t_3). The schematic graph of the bifurcation set is plotted in Figure 5.4. The surfaces correspond to the fold (A_2) while their intersections produce more complicated singularities. On the intersection line in the symmetry plane (t_1, t_3) two fold catastrophes occur, and the cusp (A_3) can be found on the other lines. The point $(t_1, t_2, t_3) = (0, 0, 0)$ is the swallowtail catastrophe point (A_4) itself.

Let us now compare the Taylor series in (5.20) with the equilibrium form in (5.26). The variable is ϕ_1 and parameter t_3 is represented by $\tilde{\phi}_3$. In (5.20) all other parameters (imperfections, etc.) are zero, i.e. no linear term of ϕ_1 and constant term are present. Hence this system corresponds to $t_1 = t_2 = 0$ in the parameter space and the straight compatibility path $\phi_1 = 0$ coincides with axis t_3. Note that axis t_3 is part of the bifurcation set: its points represent the fold catastrophe (except the origin, which is the swallowtail). Consequently, the reason why the straight compatibility path is singular is that the entire path has a special location in the parameter space, as it is part of the bifurcation set.

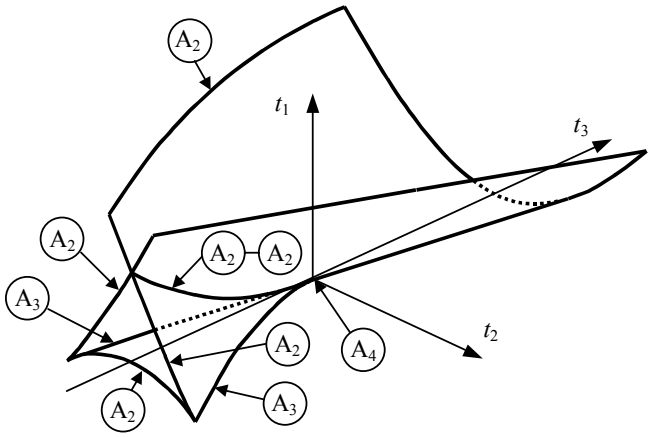

Figure 5.4: The bifurcation set of the swallowtail catastrophe in the parameter space (t_1, t_2, t_3). Regular stationary points are not labelled in the graph.

Let us now pay attention to another special position on the bifurcation set. Figure 3.7(a) also shows the compatibility paths of the imperfect mechanism if the length of bar AC is perturbed by a small ε. Note that if $\varepsilon > 0$, two curves are obtained in symmetric positions. Each has a limit point in the vicinity of the original bifurcation point. The extrema occur simultaneously and they are functions of the imperfection. The corresponding values of the imperfection and the extrema define the line in the parameter space where two fold catastrophes are present, see Figure 5.4.

A more complicated relationship among the parameters is required to obtain the line of the cusp catastrophe (A_3) shown in Figure 5.4. In stability theory the cusp catastrophe is usually demonstrated by the symmetric bifurcation of the Euler problem, though it represents only a section of the bifurcation set. The schematic plot of the bifurcation set of the cusp catastrophe is shown in Figure 5.5(a) (Gáspár, 1999).

The two lines correspond to the fold catastrophe points and divide the parameter plane into two regions: there is only one equilibrium position in the upper one while there are three of them between the branches of the cusp. There are various possibilities to pass from one region to the other, two relevant cases are discussed here.

If the cusp point is passed by tangentially to the direction of the peak as shown in Figure 5.5(b), the number of equilibrium positions suddenly changes producing a

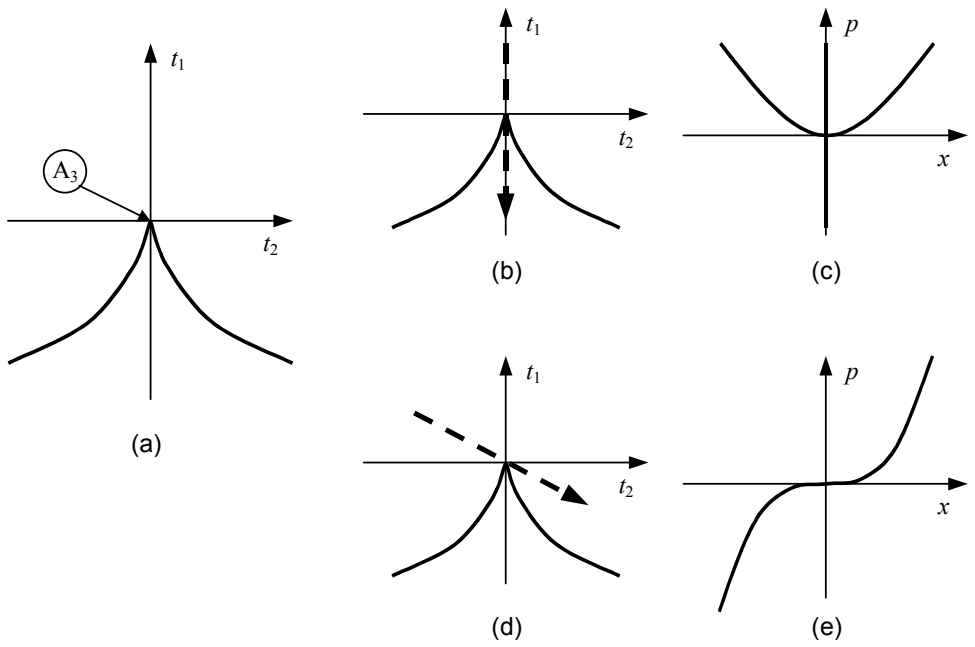

Figure 5.5: (a) The bifurcation set of the cusp catastrophe in the parameter space (t_1, t_2). The origin corresponds to the cusp catastrophe point, the lines to positions where the fold catastrophe occurs (regular stationary points are not labelled in the graph). (b) A direction in the parameter plane, tangentially to the peak, and (c) the corresponding equilibrium paths. (d) Any other direction, and (e) the corresponding equilibrium paths.

symmetric bifurcation in the equilibrium path in the coordinate system of the variable (x) and the load parameter (p), see Figure 5.5(c). However, if the cusp point is passed by in any other direction as shown in Figure 5.5(d), then the corresponding equilibrium path has no bifurcation though the curve is locally third-order at the critical point, see Figure 5.5(e). Consequently, the symmetric bifurcation can be visualised only in a particular direction in the parameter space.

The difficulty the choice of the parameter can cause is apparent in the analysis of the bifurcation set of the swallowtail catastrophe. The cusp points form two lines in the bifurcation set as shown in Figure 5.4. If a cross section is taken through a cusp point, the cusp is tilted, i.e. the peak is not symmetric to any of the parameter axes. Hence it requires a special combination of the parameters to produce the symmetric bifurcation.

At the cusp points, in addition to Equations (5.26) and (5.27), the following equation also holds:

$$\frac{d^3 f}{du_1^3} = 60u_1^2 + 6t_3 = 0\,. \tag{5.28}$$

From equations (5.26), (5.27) and (5.28), the critical point can be found in terms of the parameters:

$$t_1 = -15u_{1,0}^4, \quad t_2 = 20u_{1,0}^3, \quad t_3 = -10u_{1,0}^2\,. \tag{5.29}$$

Let us now find the Taylor series of the equilibrium equation (5.26) around the critical point $u_{1,0}$. Introducing the substitution $u_1 = u_{1,0} + v$ gives

$$\begin{aligned}\frac{df}{dv} = 5v^4 + \left(20u_{1,0}\right)v^3 + \left(30u_{1,0}^2 + 3t_3\right)v^2 + \left(20u_{1,0}^3 + 6t_3u_{1,0} + 2t_2\right)v + \ldots \\ \ldots + \left(5u_{1,0}^4 + 3t_3u_{1,0}^2 + 2t_2u_{1,0} + t_1\right) = 0\end{aligned}\,. \tag{5.30}$$

To obtain the equilibrium form of the cusp catastrophe, the second-order term needs to be eliminated. Substituting $u_{1,0}$ in terms of parameter t_3 in (5.29) yields the coefficients in the polynomial (5.30) as follows:

$$\begin{gathered}s_4 = 5, \quad s_3 = 20 \cdot 10^{-1/2}\left(-t_3\right)^{1/2}, \quad s_2 = 0 \\ s_1 = t_2 - 40 \cdot 10^{-3/2}\left(-t_3\right)^{3/2}, \quad s_0 = -1/4 \cdot t_3^2 + 2 \cdot 10^{-1/2}\left(-t_3\right)^{1/2} t_2 + t_1\end{gathered} \tag{5.31}$$

If the third coefficient s_3 is constant, all the higher terms (namely the fourth) can be omitted. Now equation (5.30) will produce a symmetric bifurcation if the first coefficient is regarded a control parameter. The constant term, which is independent of the variable *v*, must be zero. Thus in the infinitesimal vicinity of the critical point, a symmetric bifurcation is obtained in terms of the variable *v* and the newly defined control parameter.

Now comparing the compatibility equation (5.24) of the six-bar mechanism with the equilibrium equation (5.26) the following equalities hold:

$$t_3 = \phi_3 - \frac{\sqrt{2}}{4}\varepsilon_1, \tag{5.32}$$

$$t_2 = -\frac{1}{4}\varepsilon_1^3, \tag{5.33}$$

$$t_1 = \varepsilon_2 - \varepsilon_3. \tag{5.34}$$

Equation (5.31) shows that s_3 becomes a constant if t_3 is a constant, which leads to a particular relationship between ϕ_3 and ε_1. Furthermore, s_1 will vary with t_2 only. Let us define s_1 as a control parameter. Finally, t_1 is to be defined so that s_0 in (5.31) remains zero, and thus the equilibrium form of the cusp is obtained.

5.2.5 The A-shaped linkage

We have shown in Section 5.2.4 that the fourth-order term in the Taylor series in (5.20) is the result of the geometry of the triangle formed by the moving nodes *A*, *B* and *C*, see Figure 5.3(b). This leads us to believe that, if the relative motion between nodes *A* and *B* in the coordinate directions is suitably chosen, the compatibility condition can be modified accordingly. We can therefore define a motion so that the order of the pure term in the Taylor series is different from the fourth. For example, we may obtain a third-order term by this approach, resulting in the equilibrium form of the cusp catastrophe.

Consider a part of a mechanism shown in Figure 5.6(a). For simplicity both bar *AC* and *BC* have unit length. The compatibility condition can be written as

$$F(\phi; s) = \sqrt{(\Delta x - \sin s)^2 + (\Delta y - \cos s)^2} - 1 = 0 \tag{5.35}$$

where Δx and Δy are the coordinates of *B* and *s* is the kinematic state variable representing the angle between bar *AC* and the vertical axis. In order to obtain an approximation of $F(\phi; s)$ in the form of

$$F(\phi; s) \approx -c_y \phi^3 - c_x s \phi^2 + \ldots, \tag{5.36}$$

obviously the following must hold.

$$\Delta x(\phi) = c_x \phi^2 + \ldots, \quad \Delta y(\phi) = c_y \phi^3 + \ldots. \tag{5.37}$$

Is it possible?

Consider now a linkage shown in Figure 5.6(b). All bars have unit length and arranged on an equilateral triangle. The base of the mechanism is a simple four-bar linkage *DEFG* to which a coupler point is attached rigidly.

The important feature of the linkage is that node *E* is aligned with *H* and *D* as well as *F* is aligned with *H* and *G*. It implies that the motion of the coupler point *H* in terms of the variable ϕ has no linear term. In fact, it can be shown that the motion is approximately:

$$x_H = \frac{2\sqrt{3}}{3}\phi^2 + \frac{4}{3}\phi^3 + \frac{11\sqrt{3}}{6}\phi^4 + \ldots, \quad y_H = \frac{2\sqrt{3}}{3}\phi^3 + 2\phi^4 + \ldots \tag{5.38}$$

This is precisely what we want.

Now join the linkage shown in Figure 5.6(b) with the parts in Figure 5.6(a) by attaching *B* with *H* by a hinge. A linkage is obtained as shown in Figure 5.6(c). Due to the peculiar geometry we refer to this mechanism as the A-shaped linkage in the following.

When (5.38) is substituted into (5.36) for Δx and Δy, the compatibility condition for bar *BC* is obtained. The higher-order terms in (5.38) do not affect the characteristics of the Taylor series:

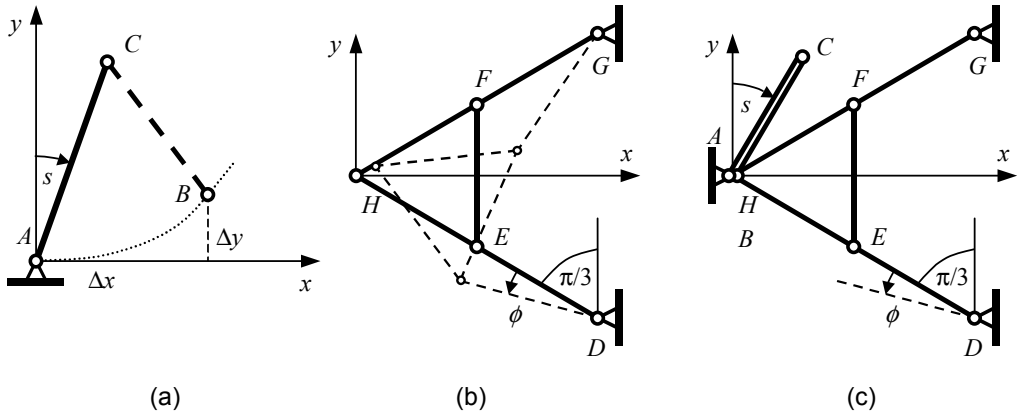

Figure 5.6: Mechanism for the generation of third-order variation of the compatibility condition. (a) Relative motion between nodes *A* and *B*. (b) A-shaped linkage. (c) The whole bar-assembly.

$$F(\phi; s) \approx -\frac{2}{3}\sqrt{3}\,\phi^3 - \frac{2}{3}\sqrt{3}\,s\,\phi^2 + \ldots \tag{5.39}$$

The second term is second-order in ϕ, therefore a linear transformation is applied:

$$\phi = \left(-\frac{2}{3}\sqrt{3}\right)^{-1/3}\bar{\phi} - \frac{1}{3}s\,. \tag{5.40}$$

The Taylor-series has now the form:

$$F(\phi; s) \approx \bar{\phi}^3 - \frac{1}{3}\left(-\frac{2}{3}\sqrt{3}\right)^{2/3} s^2\,\bar{\phi} - \frac{4}{81}\sqrt{3}\,s^3 + \ldots \tag{5.41}$$

In a similar way to the previous examples, imperfections are also considered. It is easy to formulate the perturbations of bars *AC* and *BC* while those of the other bars make the motion of node *H* even more complicated. Let us introduce three parameters, ε_1, ε_2 and ε_3 for bars *DE*, *AC* and *BC*, respectively. The compatibility condition now can be expanded into its Taylor series as:

$$F(\phi; s) \approx -\frac{2}{3}\sqrt{3}\,\phi^3 + \left(-\frac{2}{3}\sqrt{3}\,s - \frac{5}{6}\varepsilon_1\right)\phi^2 + \left(\frac{1}{3}\sqrt{3}\,\varepsilon_1\right)\phi + \left(-\varepsilon_1 + \varepsilon_2 - \varepsilon_3\right) + \ldots \tag{5.42}$$

Again a linear transformation is needed to eliminate the second-order term:

$$\phi = \left(-\frac{2}{3}\sqrt{3}\right)^{-1/3}\bar{\phi} - \frac{1}{3}s - \frac{5}{36}\sqrt{3}\,\varepsilon_1\,. \tag{5.43}$$

The new Taylor series now is:

$$F(\phi; s) \approx \bar{\phi}^3 + \left(\frac{2}{9}\sqrt{3}\left(-\frac{2}{3}\sqrt{3}\right)^{-1/3} s^2 + \frac{1}{3}\sqrt{3}\left(-\frac{2}{3}\sqrt{3}\right)^{-1/3}\varepsilon_1\right)\bar{\phi} + \left(-\varepsilon_1 + \varepsilon_2 - \varepsilon_3\right) + \ldots \tag{5.44}$$

Introduce new parameters as the terms in brackets in (8.44):

$$t_1 = -\varepsilon_1 + \varepsilon_2 - \varepsilon_3, \quad t_2 = \frac{2}{9}\sqrt{3}\left(-\frac{2}{3}\sqrt{3}\right)^{-1/3} s^2 + \frac{1}{3}\sqrt{3}\left(-\frac{2}{3}\sqrt{3}\right)^{-1/3}\varepsilon_1\,. \tag{5.45}$$

The compatibility condition is now equivalent to the second equilibrium form in Table 5.1 and hence to the *cusp catastrophe*.

The alternative form of the compatibility condition can also be used:

$$F(\phi; s) = \frac{1}{2}\left[(\Delta x - \sin s)^2 + (\Delta y - \cos s)^2 - 1\right] = 0 \tag{5.46}$$

A detailed analysis carried out in the same way gives the identical equilibrium form.

5.3 Higher-order catastrophes

In the previous section mechanisms have been shown presenting the first three cuspoid catastrophe types, the fold, the cusp and the swallowtail. In this section we propose a method in order to create higher catastrophe types.

A way of creating higher-order catastrophes is to exploit the higher-order movements of the points of the mechanism. For example, the A-shaped mechanism has been created from a two-bar chain so that the appropriate node of the linkage follows a pre-described trajectory by means of a carefully designed linkage, see Figure 5.6. The modified compatibility condition produces the expected catastrophe type.

The same technique can be used to create higher-order catastrophes.

For example, if nodes A and B in Figure 5.6(a) are made to move simultaneously, having the same y coordinate, the elongation of bar BC has a special relationship with Δx. Consider the triangle ABC in Figure 5.7 where A and B have the same y coordinate. If Δx changes with the nth power of ϕ, the elongation of BC can be given by the $(2n)$th

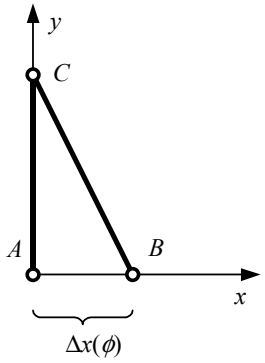

Figure 5.7: Compatibility of bar BC due to the relative movement of A and B.

power, as a consequence of Pythagoras' theorem. If Δx has third-order term of the variable ϕ, the distance *BC*, for which the compatibility condition is set up, has sixth-order term. It is related to the cuspoid catastrophe A_6 (the wigwam). The basic elements to produce such a movement in *A* and *B* are given by two identical A-shaped mechanisms, see Figure 5.8(a). This is a compound linkage with two identical A-shaped mechanisms *DEFGH* and *D'E'F'G'H'* with their symmetry axis aligned with coordinate axis *y*. Let them overlap each other so that the fixed nodes coalesce: *D* = *D'* and *G* = *G'*. At the starting position all other nodes coalesce as well. Two identical links, *HC* and *H'C*, are attached in a similar way to the previous cases. In order to synchronize the motion of the two linkages, a reverser mechanism, bars *EJ* and *JF'* are also added. The small offset between the two A-shaped linkages in the schematic diagram is only for better visualization.

The A-shaped mechanisms produce third-order motions of nodes *H* and *H'* in *x* direction in terms of the variables which control the motion. The reverser mechanism ensures that the two mechanism are mirror images to the symmetry axis, hence one variable (ϕ) is sufficient for the entire linkage and the two coupler points, *H* and *H'*, have the same *y* coordinate, see Figure 5.8(b). Consequently, the compatibility condition is a sixth-order one.

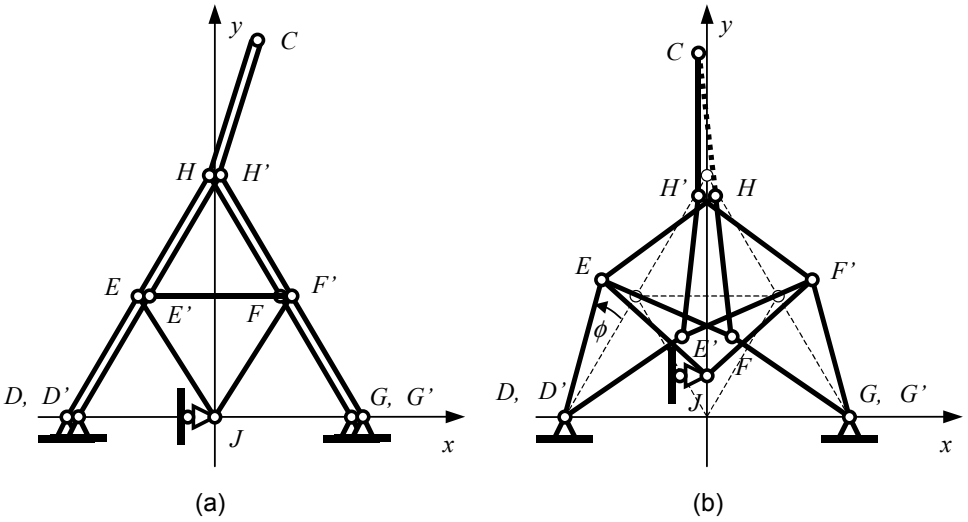

Figure 5.8: Compound A-shaped mechanism. (a) Configuration at the bifurcation point. (b) Actuation of the mechanism.

It is clear from this example that complicated linkages are needed for higher-order catastrophes. The proposed approach can easily produce even-order terms from lower-order ones, while odd-orders, e.g. the fifth or the seventh are likely to be more difficult to obtain.

5.4 Degenerate mechanism

The perturbation terms in the Taylor series of a given catastrophe constitute the unfolding of the catastrophe (see Thom's theorem in Section 2.3.1). This phenomenon enables the creation of all lower-order catastrophe types in the neighbourhood of a higher-order one. In Section 5.2.4 we have shown an example where lower catastrophe types occur in the vicinity of the point. As we have seen, the swallowtail catastrophe can be perturbed by suitably chosen imperfections in order to obtain the fold or the cusp types.

The idea is utilized through the square-shaped four-bar linkage presented in Section 3.1.4, see Figure 3.8(a). In this degenerate case, all terms of the variable in the Taylor series vanish simultaneously. Hence the compatibility condition at the bifurcation point is regarded infinitely degenerate, and can be taken as an A_∞ cuspoid catastrophe. The idea of unfolding suggests that lower-order variations and hence lower-order catastrophe types can be obtained. For the point is infinitely degenerate, it follows that cuspoid catastrophes of any order can be produced by a suitable perturbation of the system.

In fact, this phenomenon also exists in stability theory. Gáspár (1984, 1999) presented an infinitely degenerate elastic structure, which has been reviewed in Section 2.2.4, see Figure 2.5. Gáspár has considered the higher-order perturbation to the force in the horizontal spring in terms of the elongation, i.e. the spring behaves nonlinearly. He showed that the total potential energy function has a $(j+1)$th term in

the Taylor series expansion if only the *j*th imperfection factor is considered. Hence a cuspoid catastrophe A_j occurs.

Imperfections with a similar effect can be designed for the degenerate four-bar linkage. If the compatibility condition is *k*th order in the variable α at the bifurcation point, it is possible to perturb the polynomial mathematically to get *k* solutions for α in the vicinity of the singularity for a given β. The physical representation of a perturbation is an imperfect system which can have *k* feasible positions for α. Hence the bifurcation point is regarded as a cuspoid catastrophe A_{k+1}. In short, the aim is to perturb the degenerate bifurcation point by an imperfection so that it becomes *k*th order. As the point is infinitely degenerate, a suitable imperfection may, in principle, produce any given *k*.

Small *constant* imperfections have been introduced in Section 5.2. The Taylor series contains the second-order term of the variable. This imperfect system can have only two compatible positions for a given parameter near the bifurcation point, hence only the fold catastrophe can occur. In order to get higher-order terms, the system needs to be perturbed in a more complicated way. To understand the necessity of this, the mathematics of transversality is to be briefly introduced (Poston and Stewart, 1978).

Consider the *n*-dimensional space $\mathbb{R}^n$ with two affine subspaces *X* and *Y* of dimensions *s* and *t*, respectively. They meet transversely if either their intersection $X \bigcap Y$ is empty or its dimension is $s+t-n$ (if this number is non-negative). This definition leads to the definition of the transversality of manifolds. Two submanifolds of $\mathbb{R}^n$ meet transversely at a given point provided either the point is not a common point, or their tangent affine hyperplanes (affine subspaces of $\mathbb{R}^n$) meet transversely. A simple example is given in Figure 5.10. The touching circles denoted by heavy lines in Figure 5.10(a) meet non-transversely because their tangents coincide. On the other hand, the intersecting circles in Figure 5.10(b) meet transversely as their tangents intersect at an angle.

This can be applied to the degenerate four-bar linkage as follows. The parameter β defines the position of node *B* on the plane. To have a compatible configuration node *A*

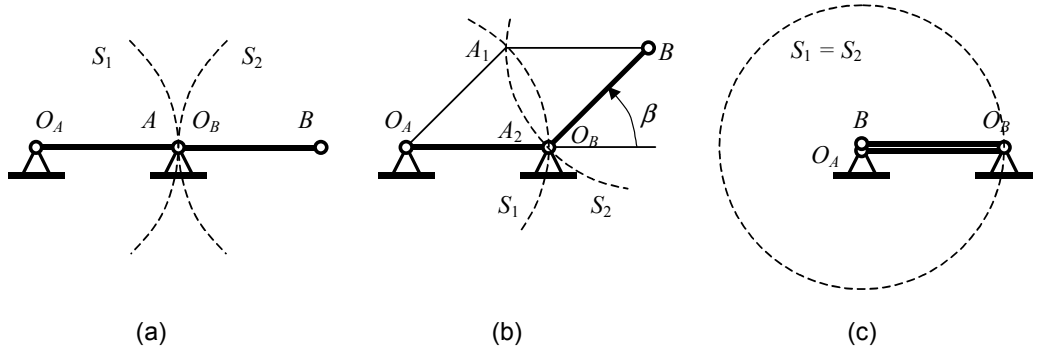

Figure 5.9: Transversality of sets S_1 and S_2. (a) Non-transverse intersection at one point. (b) Transverse intersections at two points. (c) Non-transverse intersection at all points.

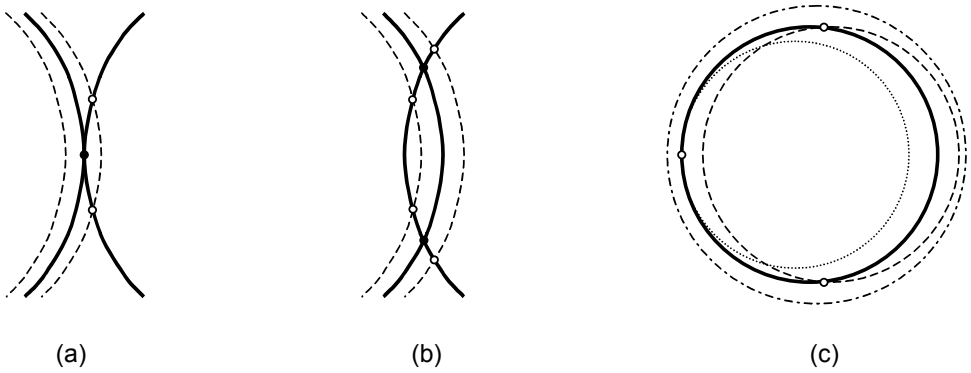

Figure 5.10: Perturbation of intersections of two sets. (a) Non-transverse intersection at one point. (b) Transversal intersections at two points. (c) Non-transverse intersections at all points.

has to be both on the circle with radius a centred at O_A (set S_1) and on the circle with radius a centred at B (set S_2). Where the two sets meet transversely, a non-singular configuration is obtained. If they meet non-transversely, singularity occurs.

Figure 5.9 shows three typical cases. In the first case where $\beta = 0$, i.e. O_BB remains horizontal, there is only one possible position for A. This is a non-transverse intersection and the compatibility path has a bifurcation point, see Figure 5.9(a). In case of $\beta \neq 0$ the sets meet transversely and two compatible configurations are obtained, see Figure 5.9(b). Finally, at the degenerate bifurcation point the two sets are identical, which is a non-transverse intersection again, see Figure 5.9(c). If constant imperfections are applied to the bar lengths, the perturbed system is obtained as shown in Figure 5.10, in which only the intersections of the sets are shown; continuous lines show the original circles, and dashed, dotted and dashdot lines correspond to various imperfections.

In the first case the non-transverse intersection disappears if one of the circles is perturbed, see Figure 5.10(a). Either two transverse intersections are obtained or none, depending on the imperfection. In the second case the number and type of intersections remain unchanged, see Figure 5.10(b). In the last case, shown in Figure 5.10(c), several possibilities arise: one non-transverse intersection (dotted line), two transverse intersections (dashed line) or none (dashdot line).

Note that in either case the maximum number of intersections is two, i.e. only the fold catastrophe is possible. Compare this with the earlier results in this chapter showing second-order terms of the variable in the imperfect systems. In order to produce higher-order catastrophe types, a more sophisticated imperfection system should be applied, which will be discussed next. In fact, the degenerate case has a potential for any cuspoid catastrophe.

5.4.1 Imperfections of the nodal distances

The first approach to obtain higher-order catastrophes is based on imperfections of the bar lengths as before, but now higher-order variations are also considered. Consider again the square-shaped four-bar linkage shown in Figure 3.8(a). When an imperfection ε_4 exists for bar O_AA, the compatibility condition, written for bar AB, becomes

$$F(\alpha;\beta)=\sqrt{\left(a+a\cos\beta-\left(a+\varepsilon_4\right)\cos\alpha\right)^2+\left(a\sin\beta-\left(a+\varepsilon_4\right)\sin\alpha\right)^2}-a=0\,. \quad (5.47)$$

Assume

$$\varepsilon_4=\sum_{i=1}^{r}c_i\alpha^i \quad (5.48)$$

where c_i $(i=1,2,\ldots)$ denote constants. Substitute it into (5.47). The Taylor series expansion is calculated at the critical value of the parameter: $\beta=\pi$. At this value $\cos\beta=-1$ and $\sin\beta=0$ hold, thus it is easy to show that the compatibility can be reduced to

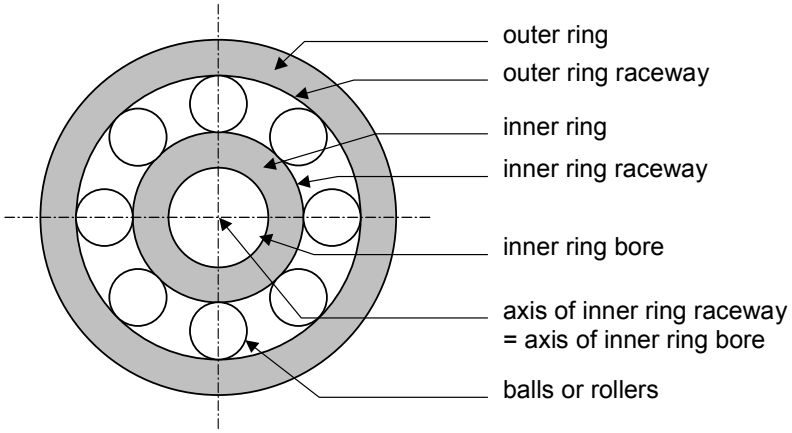

Figure 5.11: Schematic diagram of a ball or roller bearing. In case of perfect geometry the elements are circular and the axis of inner ring raceway coincides with the axis of inner ring bore.

$$F(\alpha;\beta)=\sqrt{((a+\varepsilon_4)\cos\alpha)^2+((a+\varepsilon_4)\sin\alpha)^2}-a=\sqrt{(a+\varepsilon_4)^2}-a=\varepsilon_4 \qquad (5.49)$$

which is identical to the form (5.48). Consequently, if only the *j*th order variation is present in (5.48), the bifurcation point is equivalent to the A_j catastrophe. The geometrical explanation to this is that the imperfection given in (5.48) distorts the circle defined by positions of *A*, see Figure 5.9(c). Sets S_1 and S_2 now have only one non-transverse intersection at the bifurcation point.

The imperfection given in (5.48) does exist in reality. A typical example can be found in linkages containing ball or roller bearings.

The main structure of a bearing consists of an inner and an outer ring with a series of rolling elements (balls or rollers) in between (Eschmann, et al., 1985). A schematic diagram is shown in Figure 5.11.

The axis of the inner ring raceway defines the axis of rotation of the inner ring. The axis of the inner ring bore is the axis of the spindle attached to the inner ring. In the square-shaped linkage the outer and inner rings are attached to bar O_AO_B and O_AA, respectively, and the nominal length of the bars is measured from the appropriate axis. If the geometry is perfect, the two axes coincide and a mechanism with perfect configuration (exact bar lengths) is obtained.

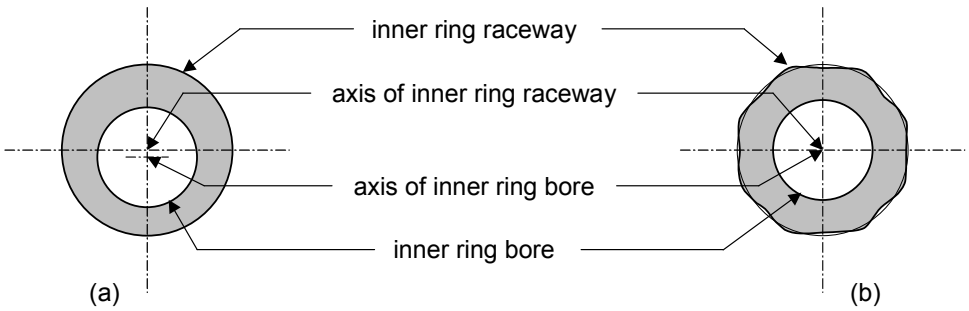

Figure 5.12: Imperfections of the inner ring of a ball or roller bearing. (a) Round raceway eccentric to round bore. (b) Irregular wave-shaped raceway concentric with round bore.

However, due to various manufacturing errors or extensive use, imperfections set in. One type of imperfection is because the inner ring bore is eccentric to the inner ring raceway, see Figure 5.12(a). Bar O_AA still rotates around the axis of the inner ring raceway though the nominal length is measured from the axis of the inner ring bore. Hence the physical length of bar O_AA is modified by the eccentricity.

The second type of imperfection is due to an irregular wave-shaped raceway, see Figure 5.12(b), which may be caused by wear. As the inner ring is rotating inside the outer ring, the axis of the bore is shifting because the radius of the raceway is not a constant but perturbed by an irregular wave with small amplitude. The shape of the wave defines the shift of the axis. The perfectly round shape (constant radius) is infinitely degenerate hence a suitable perturbation results in a variation of any order. The end node of bar O_AA is centred at the axis of the bore therefore the nominal length of the bar is modified by the shift.

5.4.2 Imperfections in three-dimensional space

The second approach to get higher-order catastrophes is to modify the configuration of the square-shaped mechanism but to keep the bar length *unchanged*. This is realized in three-dimensional space because such singularities cannot be obtained in the plane as we have seen above.

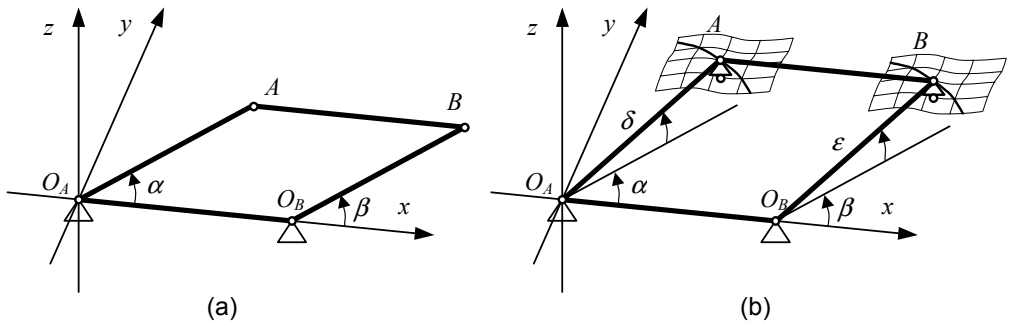

Figure 5.13: Square-shaped four-bar linkage. (a) Planar configuration. (b) Spatial configuration.

The objective is to reproduce the identical circles shown in Figure 5.9(c) in three-dimensional space. Thus non-transverse intersections are obtained at all points again. Unlike the planar configuration, the linkage can be perturbed in the space around the bifurcation point so that the distorted circles meet non-transversely to any given degree.

Let the linkage fit to the coordinate plane (x, y) in the three-dimensional space (x, y, z) where the nodes are given as $O_A(0, 0, 0)$, $O_B(a, 0, 0)$, $A(a\cos\alpha, a\sin\alpha, 0)$ and $B(a + a\cos\beta, a\sin\beta, 0)$, see Figure 5.13(a). Let us modify the configuration by making the moving nodes A and B supported by rollers. They move on predefined surfaces, as shown in Figure 5.13(b).

These surfaces are small perturbations of the original plane (x, y), and are given by the elevation angles δ and ε, in terms of α and β, respectively:

$$\delta = \delta(\alpha), \quad \varepsilon = \varepsilon(\beta). \tag{5.50}$$

Nodes A and B now track the three-dimensional curves in the coordinate system (x, y, z):

$$A(a\cos\delta\cos\alpha, a\cos\delta\sin\alpha, a\sin\delta), \quad B(a + a\cos\varepsilon\cos\beta, a\cos\varepsilon\sin\beta, a\sin\varepsilon). \tag{5.51}$$

The compatibility condition is again written for bar AB as

$$F(\alpha; \beta) = \sqrt{X^2 + Y^2 + Z^2} - a = 0. \tag{5.52}$$

where X, Y and Z are the projections of the distance AB to the coordinate axes:

$$X = a + a\cos\varepsilon(\beta)\cos\beta - a\cos\delta(\alpha)\cos\alpha,$$

$$Y = a\cos\varepsilon(\beta)\sin\beta - a\cos\delta(\alpha)\sin\alpha, \tag{5.53}$$

$$Z = a\sin\varepsilon(\beta) - a\sin\delta(\alpha).$$

If the surfaces are suitably chosen in the neighbourhood of the bifurcation point $(\alpha = 0,\ \beta = \pi)$, the objective given above is achieved. First, node *B* has to be moved out of the plane (x, y) otherwise it would coalesce with O_A at the bifurcation point and hence arbitrary α would satisfy the compatibility condition. It is sufficient to suppose that *B* is lifted off the plane by a small constant ε_0:

$$\varepsilon(\beta) = \varepsilon_0. \tag{5.54}$$

Now let function $\delta = \delta(\alpha)$ be approximated by the Taylor series:

$$\delta = \delta(\alpha) = \delta_1\alpha + \delta_2\alpha^2 + \delta_3\alpha^3 + \ldots \tag{5.55}$$

where $\delta_i\ (i = 1, 2, \ldots)$ are the coefficients. Substituting (5.55) into the compatibility condition (5.52) the Taylor series are obtained in the form:

$$F = f_1(\varepsilon_0, \delta_1)\alpha + f_2(\varepsilon_0, \delta_1, \delta_2)\alpha^2 + f_3(\varepsilon_0, \delta_1, \delta_2, \delta_3)\alpha^3 + \ldots$$
$$\ldots + \text{higher} - \text{order and mixed terms} \tag{5.56}$$

where f_k denotes the coefficient of the *k*th order term of α. We have found that each function f_k depends on the coefficients $\delta_i\ (i = 1, 2, \ldots, k)$ because further $\delta_i\ (i > k)$ factors have no effect on the *k*th power of α.

In order to obtain the cuspoid catastrophe A_k, all terms up to the $(k-1)$th in (5.56) have to be eliminated, i.e. their coefficients be made equal to zero. The first coefficient can be eliminated by a suitable definition of δ_1 in terms of ε_0. When substituted to the next one, this can be repeated for δ_2, etc.

5.5 Discussion

In this chapter we have introduced a classification method for mechanisms with the aid of catastrophe theory. The mathematical formulation of the system may pose a few questions which we address here.

5.5.1 Control parameter

In Section 5.2.1 we have proposed a classification method for mechanisms based on the analogy between equilibrium and compatibility. It requires that one of the two kinematic state variables be designated as a variable while the other as control parameter in order to obtain the forms in Table 5.1. As there is no *a priori* distinction between the two state variables, the choice seems arbitrary. However, the assignment of the control parameter needs to be done so that the behaviour of the mechanism at the singular point is best revealed. On practical grounds, the state variable having the higher term in the Taylor series is to be regarded as the variable because it exhibits a more sophisticated behaviour.

However, the mobilization of a linkage may define the choice of the control parameter. If a machine is driven by an actuator attached to one of the elements, it is a sensible supposition to associate a control parameter with the position of that particular element.

5.5.2 Single compatibility condition

Two types of compatibility conditions have been introduced in Section 3.3. The square form (3.9) incorporates the square of both the distance between two nodes and the length of the corresponding bar, while the square root form (3.10) expresses the equality of the distance and the length. The latter one bears a direct geometrical meaning.

Both forms have been examined in Section 5.2 and found to yield the same results concerning the significant terms in the Taylor series of the compatibility function.

5.5.3 Combination of compatibility conditions

This behaviour suggests that the mathematical behaviour of the system may be independent from the formulation of the compatibility.

Most of the mechanisms shown in Section 5.2 are described by a reasonably simple single compatibility conditions in the form (3.10) due to the symmetry or the simplicity of the bar assembly. The A-shaped mechanism is an exception because the position of node H in terms of ϕ is quite complicated. When geometric imperfections are considered, the single compatibility condition becomes more complex, mainly because the imperfections ruin the symmetry that many of the mechanisms have.

Hence the need arises to find a simpler formulation with an equivalent effect. A formulation may be based on a different set of state variables and compatibility conditions. It has been demonstrated in Section 4.1 that the problem can be described by the Cartesian coordinates of the nodes and a sufficient number of compatibility conditions, which are significantly simpler. In order to carry out the classification proposed in Section 5.2.1, a single function has to be created incorporating the individual conditions.

Such a combination is given by a simplified form of the energy function (3.27) introduced in Section 3.4.3. It is defined as the sum of the squares of the individual conditions equals zero:

$$U = \sum_i F_i^2 = 0 \tag{5.57}$$

This condition is satisfied if and only if all the individual ones are satisfied, therefore it expresses the compatibility of the system and may be used for the classification of the singular positions.

It has been shown in Section 4.1 that different state variables can be chosen in some cases, from the most compact set with two state variables and one compatibility condition to the most general approach based on all Cartesian coordinates and conditions for all bars.

If the single compatibility condition is applied, the function U in (5.57) becomes the square of the condition. The problem is essentially the same as before with an important difference that the order of the characteristic term in the Taylor series is now exactly the double of that of the compatibility condition.

In the case of any other formulation of compatibility, (5.57) is a sum of square terms and the behaviour is to be analysed in detail. This formulation is referred to as the *combined formulation* in the following and will be compared to the *single condition formulation*. As the single compatibility condition describes the motion uniquely in terms of two kinematic variables, it forms a basis for the analysis conducted earlier in this chapter. Assuming the proposed function (5.57) to be useful, the combined formulation is expected to provide terms of the same order as the single condition formulation. The individual conditions can be either in square form (3.7) or square root form (3.8) in terms of the Cartesian coordinates. In the case of the square form, function (5.57) becomes a polynomial having terms up to the fourth-order in its Taylor series, which cannot provide sufficient information on the behaviour in certain cases. Hence only the square root form will be applied in the following.

Consider again the kite-shaped four-bar linkage. The single compatibility condition (5.1) has a second-order term of α, as shown in Section 5.2.2. Consequently, function U, created as the square of (5.1), has the fourth power of the variable. If the Cartesian coordinates are used, the compatibility is written as

$$\begin{aligned} F_1 &= \sqrt{x_1^2 + y_1^2} - a = 0\,, \\ F_2 &= \sqrt{(x_2 - x_1)^2 + (y_2 - y_1)^2} - b = 0\,, \\ F_3 &= \sqrt{(x_2 - a)^2 + y_2^2} - b = 0\,. \end{aligned} \tag{5.58}$$

The function (5.57) becomes

$$U = F_1^2 + F_2^2 + F_3^2 . \tag{5.59}$$

It is easy to show that the pure terms with the lowest-order are: x_1^2, y_1^4, x_2^2 and y_2^4. Either (5.59) or the square of (5.1) is used, the characteristic term is fourth-order.

The behaviour of the parallelogram-shaped four-bar linkage is similar. Again, if the single compatibility condition is used, function U has fourth-order terms in α. If the Cartesian coordinates are used, in a similar way to the previous case, one can find that U is second-order in the x coordinates and fourth-order in the y coordinates.

In case of the degenerate square-shaped four-bar linkage, the single condition (5.13) has no pure terms, hence function U has none either. However, the most general formulation results in second and fourth-order terms, in a similar way to the previous two cases. Now there is clearly a discrepancy between the two formulations.

The six-bar linkage provides more choices of conditions. The single condition formulation obviously results in the eighth-order term. If the four angles are used, as introduced in Section 3.1.2, only second-order terms are obtained. Finally, if the most general formulation is applied, second and fourth-order terms are produced.

The discussion of the A-shaped linkage goes in a way similar to that of the six-bar mechanism. The single condition approach results in a sixth-order term of the variable. Again two other formulations can be considered. It can be shown that the results are similar to those of the six-bar mechanism.

The examples demonstrate that the Taylor series of the function defined in (5.57) widely varies with the choice of the state variables and the compatibility conditions. We conclude that the simplification of the formulation of the problem is done on the expense of the loss of important behaviour. The combination of simple conditions cannot reflect the higher-order variation of the state variables that is found with the single compatibility condition. Consequently, the single compatibility condition has to be used in preference to the combined formulation even if it makes the mathematical formulation more complex.

5.5.4 State variables

Another problem to be addressed is related to the state variables that describe the motion of a linkage. It has been shown in Section 5.1 that different sets of state variables result in different compatibility paths. The state variables have to be chosen to define the position of the entire linkage uniquely. The general formulation based on the Cartesian coordinates is a unique description of the system while the single condition with two state variables may offer more choices. It becomes clear in the case of the more complicated examples, e.g. the A-shaped linkage. It is essentially a four-bar linkage with a rigid triangle attached to the coupler bar. It is easy to see that either the rotation of the sidebars or of the rigid body can define the shape uniquely. The analysis in Section 5.2.5 uses one of them: the angle of bar *DE*.

The question arises whether or not the three choices are equivalent concerning the classification of the mechanism. In the base configuration the four-bar linkage is not in a singular form hence the angles defining the positions of the bars are linearly related during the motion of the bar-assembly. Therefore either of them provides the same characteristic term in the Taylor series.

We conclude then that the third-order term in the compatibility condition is not the result of a special choice of the variable but the only possible outcome provided the variable is chosen to describe the motion uniquely. A similar reasoning is applied to the compound A-shaped linkage where the reverser linkage provides a non-singular transmission of motion between the two parts of the linkage. In this case even the position of the reverser linkage can be used as a variable with the same effect as the other choices.

However, if a linkage is in a singular form, the unique description of the system is more complicated, as demonstrated by the two-bar linkage shown in Figure 5.14(a). If the rotation of bar *AB* is given by the angle ϕ, it is easy to show that the displacement of node *C* is approximately proportional to ϕ^2. A compound of two of these mechanisms is shown in Figure 5.14(b). Now the rotation of bar *DE* is approximately

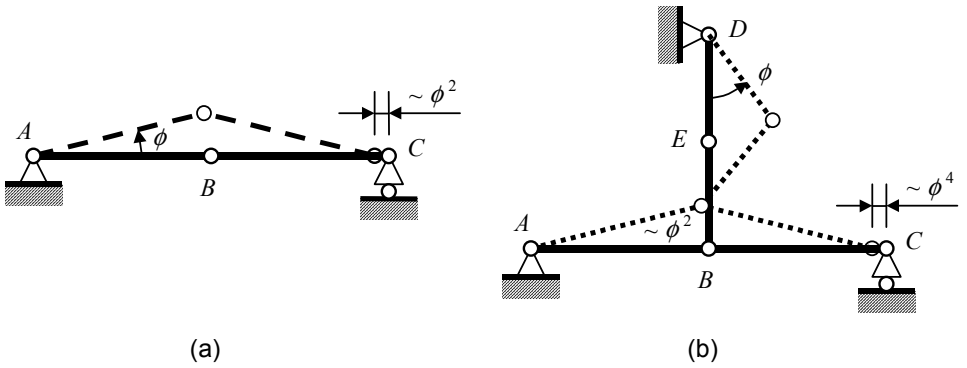

Figure 5.14: (a) Three-hinged two-bar mechanism. (b) Combination of two two-bar mechanisms.

proportional to $\phi^{1/2}$. If ϕ is associated with bar *DE* instead, the rotation of bar *AB* is second-order in ϕ and hence the displacement of *C* is fourth-order.

The cause of this is that two choices of the variable are not equivalent in representing the motion of the mechanism. If ϕ is given as in Figure 5.14(b), *AB* and the rest of the mechanism are determined uniquely. On the other hand, if the position of *AB* is defined by angle ϕ, *DE* will have two possible positions. Clearly more state variables and compatibility conditions are needed to overcome the problem.

6

CONCLUSIONS

Contents

6.1 New results

In this dissertation we have explored the relationship between the equilibrium of elastic structures and compatibility of mechanisms. The theory of elastic stability has a long history and a substantial amount of literature. Various instability phenomena have been studied in depth in the past. On the other hand, singularities of compatibility paths of mechanisms have attracted relatively little attention. We try to bridge this gap by establishing an analogy between the two subjects so that mathematical tools, used in structural stability, can be used in the analysis of compatibility of mechanisms.

In our study we have considered bar-linkages consisting of straight rigid bars and frictionless pin joints. We have restricted our examination to planar linkages with only one degree-of-freedom. We have also assumed quasi-static behaviour ignoring all time-related effects, inertial forces, etc. Within this framework, various aspects of the behaviour of the two subjects have been compared and studied. Our achievements are summarized as follows.

(a) The compatibility conditions of a mechanism have been mathematically formulated as implicit nonlinear functions of the state variables and parameters, in a similar way to equilibrium equations in structural stability. One of the state variables is designated a kinematic variable while the other a control parameter as analogues of the generalized coordinate and the load parameter, respectively. Further parameters are considered by introducing imperfections to the system resulting in a compatibility condition and a plot of the compatibility paths. The compatibility paths can be analysed the same way as equilibrium paths of a structure.

(b) New bifurcation modes have been found in addition to the asymmetric one, reported in the past by other researchers. A six-bar linkage is shown which produces two symmetric bifurcations, one referring to an increasing control parameter while the other to a decreasing one. A complete analogy with three fundamental modes of equilibrium bifurcation has been established. A special four-bar linkage is also

studied which has a degenerate symmetric bifurcation point, analogous to the degenerate equilibrium bifurcation.

(c) Various formulations are studied with the aim to create the kinematic counterpart of the potential energy of elastic structures. We have found that a formulation involving external nodal forces is not suitable to function as its equilibrium analogue. A formulation based on the strain energy of the bar-assembly yields the compatibility conditions by a differentiation with respect to the bar forces. A third function is created from which the compatibility condition is derived by differentiation with respect to its variable. It is a formal analogue of the equilibrium case though its complexity prevents any practical analysis. It also lacks the physical meaning of energy.

(d) A classification system is proposed for the compatibility paths of mechanisms. It groups points into five categories according to their behaviour. Unlike elastic structures, the concept of stability cannot be applied to compatibility due to the lack of an exact match of the potential energy of structures. The axis of the classification is the distinction between regular and split-vanish behaviour.

(e) We have applied existing methods to the analysis of compatibility of mechanisms. We found that the matrix method worked well with most cases except when the compatibility paths exhibit split-vanish behaviour. We have also shown that this method can be adopted to the analysis of equilibrium. Furthermore, an analogue of the stiffness of structures is also created for mechanisms. Though these methods do not always prove to be the most efficient, a formal analogy is nonetheless proven to exist.

(f) The application of elementary catastrophe theory to the kinematics of mechanisms is proposed. The analogy between compatibility and equilibrium validates the classification of singularities of compatibility paths according to the classification system given in Thom's theorem. Mechanism examples have demonstrated a few cuspoid catastrophe types. A proposal has been made to generate higher-order

catastrophes. The analysis of the degenerate bifurcation justified the generation of arbitrary cuspoid catastrophe types analogously to the behaviour of the degenerate structure in structural stability.

6.2 Future research

A few questions may define the directions of future research in the subject as follows. This dissertation is primarily concerned with the existence and behaviour of singularities of compatibility paths of mechanisms. However, practical engineering design aims to avoid singularities which have an undesired effect on the design objectives. Examples demonstrated that the simple way of disturbing the system by small imperfections usually makes the bifurcation disappear. Though a sensible demand may arise to address the problem with a systematic approach and to develop appropriate design rules.

Furthermore, we have found the analytical formulation of the compatibility conditions became complicated as complex linkages were considered. Further study could be done on a more systematic way of writing the conditions. Numerical methods could be taken into consideration in order to develop an automated approach for the calculation of the system.

We have also encountered the more complicated situation where the increase of the instantaneous degrees-of-freedom at a singular point is more than one. In case of an increase of two, the corresponding equilibrium cases are the umbilic catastrophes whose equilibrium equations are derived from the potential function as a gradient vector. Consequently, the equations are related in a certain way that may not be valid for the compatibility conditions. It is to be the subject of further research whether compatibility can be formulated as a gradient system and how any classification can be carried out.

We have restricted our investigation to mechanisms with a single degree-of-freedom, which form a significant part of mechanical engineering research and design. However,

linkages can also be constructed with two or more degrees-of-freedom. The compatibility paths now are replaced by higher-dimensional manifolds. It is yet unexplored what relationship such systems may have with equilibrium of structures. The extension of the analogy into this direction requires a substantial amount of study.

REFERENCES

Arnol'd, V. I., 1972, *Normal forms for functions near degenerate critical points, the Weyl groups of A_k, D_k, and E_k, and Lagrangian singularities.* Funkcional Anal. i Priložen 6, 3-25. Functional Analysis and its Applications 6, 254-272.

Bolzano, B. P. J. N., 1817, *Rein analytischer Beweis...* (*Pure Analytical Proof*).

Calladine, C. R., 1978, *Buckminster Fuller's "tensegrity" structures and Clerk Maxwell's rules for the construction of stiff frames*. International Journal of Solids and Structures, *14*, 161-172.

Donelan, P. S., Gibson, C. G. and Hawes, W., 1999, *Trajectory singularities of general planar motions*. Proceedings of the Royal Society of Edinburgh, 129A, 37-55.

Eschmann, P., Hasbargen, L. and Weigand, 1985, *Ball and roller bearings: theory, design, and application*. Wiley, Chichester.

Euler, L., 1744, *Methodus Inveniendi Lineas Curvas Maximi Minimive Proprietate Gaudentes* (Appendix, De curvis elasticis). Marcum Michaelem Bousquet, Lausanne and Geneva.

Gáspár, Zs., 1977, *Buckling models for higher catastrophes*. Journal of Structural Mechanics, vol. 5, no. 4, p. 357-368.

Gáspár, Zs., 1984, *Buckling model for a degenerated case*. News letter of the Technical University of Budapest, vol. 2, no. 4, pp. 5-8. Published by the Technical University of Budapest, Section of Scientific Relations.

Gáspár, Zs., 1999, *Stability of elastic structures with the aid of catastrophe theory.* In: *Structural stability in engineering practice.* Edited by L. Kollár, E & FN Spon, London.

Géradin, M., 1999, *Finite element simulation of deployable structures.* In *Deployable Structures*, CISM Courses and Lectures, No. 412, Udine, Italy, July 5-9, 1999; Springer: Wien, New York, 2001, 239-360.

Gibson, C. G. and Hobbs, C. A., 1993, *Simple singularities of space curves*. Math. Proc. Camb. Phil. Soc., vol. 113, pp. 297-310.

Gibson, C. G. and Hobbs, C. A., 1995, *Singularities of general one-dimensional motions of the plane and space*. Proceedings of the Royal Society of Edinburgh, 125A, 639-656.

Gibson, C. G. and Hobbs, C. A., 1996, *Singularity and bifurcation for general two-dimensional planar motions*. New Zealand Journal of Mathematics, vol. 25, 141-163.

Gibson, C. G., Hawes, W. and Hobbs, C. A., 1994, *Local pictures for general two-parameter planar motions*. Advances in Robot Kinematics and Computationed Geometry, 49-58.

Gibson, C. G., Marsh, D. and Xiang, Y., 1996, *An algorithm to generate the transition curve of the planar four-bar mechanism*. Mechanism and Machine Theory, vol. 31, no. 4, pp. 381-395.

Gibson, C. G., Marsh, D. and Xiang, Y., 1998, *Singular aspects of general planar motions with two degrees of freedom*. International Journal of Robotics Research, vol. 17, no. 10, Oct 1998, pp. 1068-1080.

Gilmore, R., 1981, *Catastrophe theory for scientists and engineers*. Dover Publications, New York.

Gromoll, D. and Meyer, W., 1969, *On differentiable functions with isolated critical points*. Topology 8, 361-370.

Hansen, J. S. and Hui, D., 1977, *Application of the parabolic umbilic catastrophe in the theory of elastic stability*. Proceedings of the Sixth Canadian Congress of Applied Mechanics, Vancouver, 441-442.

Hui, D. and Hansen, J. S., 1980, *The swallowtail and butterfly cuspoids and their application in the initial postbuckling of single-mode structural systems.* Quarterly of Applied Mathematics *38*, 17-36.

Hunt, G. W. and Williams, K. A. J., 1984, *Closed-form and asymptotic solutions for an interactive buckling model*. Journal of the Mechanics and Physics of Solids, vol. 32, no. 2, p. 101-118.

Hunt, G. W. and Williams, K. A. J., 1984, *On truncation of the structural potential function*. Mathematical Proceedings of the Cambridge Philosophical Society, vol. 95, pt. 3, Nov 1984, p. 495-510.

Hunt, G. W., 1981, *An algorithm for the nonlinear analysis of compound bifurcation*. Philosophical Transactions of the Royal Society of London, Ser. A. *300*, 443-471.

Hunt, K. H., 1978, *Kinematic geometry of mechanisms*. Oxford University Press.

Ikeda, K. and Murota, K., 2002, *Imperfect bifurcation in structures and materials.* Applied Mathematical Sciences (149), Springer.

James, G., 1992, *Modern engineering mathematics*. Addison Wesley.

Kaliszky, S., 1990, *Mechanika II. Szilárdságtan*. (University textbook) Tankönyvkiadó, Budapest.

Koiter, W. T., 1945, *On the stability of elastic equilibrium*. Dissertation, Delft, Holland.

Kumar, P. and Pellegrino, S., 2000, *Kinematic bifurcations in the simulation of deployable structures*. Fourth International Colloquium on Computation of Shell & Spatial Structures, IASS-IACM, Chania, Greece, June 4-7, 2000.

Kuznetsov, E. N., 1989, *On immobile kinematic chains and a fallacious matrix analysis.* Trans. ASME, J. Appl. Mech., *56*: 222-224.

Litvin, F. L., 1980, *Application of theorem of implicit function system existence for analysis and synthesis of linkages*. Mechanism and Machine Theory, 15, pp. 115-125.

The MathWorks, Inc., 2001, MATLAB, Version 6.1.

Maxwell, J. C., 1890, *On the calculation of the equilibrium and stiffness of frames*. The Scientific Papers of James Clerk Maxwell, vol. 1, pp. 598-604, University Press, Cambridge.

Morse, M., 1931, *The critical points of a function of* n *variables*. Transactions of the American Mathematical Society 33, 72-91.

Oxford Advanced Learner's Dictionary, 2000, 6th edition, Oxford University Press.

Pellegrino, S. and Calladine, C. R., 1986, *Matrix analysis of statically and kinematically indeterminate frameworks.* International Journal of Solids and Structures, *22*: 409-428.

Poston, T. and Stewart, I., 1978, *Catastrophe theory and its applications*. Pitman, London.

Szabó, J. and Roller, B., 1978, *Anwendung der Matrizenrechnung auf Stabwerke*; Akadémiai Kiadó: Budapest, Hungary.

Tarnai, T., 1984, *Bifurcation of equilibrium and bifurcation of compatibility*. *Abstracts of Lectures*, 16th IUTAM Congress, Lyngby, Denmark, lecture 652.

Tarnai, T., 1990, *Kinematically indeterminate structures and structural topology*. (in Hungarian), DSc thesis, Hungarian Academy of Sciences, Budapest.

Tarnai, T., 1999, *Rigidity and kinematic bifurcation of structures*. 40th Anniversary Congress of the International Association for Shell and Spatial Structures (IASS), CEDEX, Madrid, Spain, Sep 20-24 ,1999; 1: B 2.81-B 2.90.

Tarnai, T., 2002, *Elastic structures with zero stiffness*. In *Lightweight Structures in Civil Engineering*, Proc. Int. IASS Symp. (ed.: J. Obrebski), Warsaw.

Tarnai, T. and Szabó, J., 2002, *Rigidity and stability of prestressed infinitesimal mechanisms.* Calladine Festschrift (ed.: S. Pellegrino), Kluwer, Dordrecht (in press)

Thom, R., 1972, *Stabilité Structurelle et Morphogénèse*. Benjamin, New York.

Thom, R., 1975, *Structural Stability and Morphogenesis*. Benjamin–Addison Wesley, New York.

Thompson, J. M. T., 1963, *Basic principles in the general theory of elastic stability.* Journal of Mechanics and Physics of Solids, *11*, 13.

Thompson, J. M. T., 1969, *A general theory for the equilibrium and stability of discrete conservative systems.* Zeitschrift für Angewandte Mathematik und Physik, *20*, 797.

Thompson, J. M. T. and Gáspár, Zs., 1977, *A buckling model for the set of umbilic catastrophes*. Mathematical Proceedings of the Cambridge Philosophical Society, vol. 82, pt. 3, Nov 1977, p. 497-507.

Thompson, J. M. T. and Hunt, G. W., 1973, *A general theory of elastic stability*. (Section 1.2) Wiley-Interscience, London.

Thompson, J. M. T. and Hunt, G. W., 1984, *Elastic instability phenomena*. Wiley, Chichester.

Thompson, J. M. T. and Supple, W. J., 1973, *Erosion of optimum designs by compound branching phenomena*. Journal of the Mechanics and Physics of Solids, vol. 21, no. 3, May 1973, p. 135-144.

Trotman, D. J. A. and Zeeman, E. C., 1976, *The classification of elementary catastrophes of codimension less than or equal to 5.* Structural stability, the theory of catastrophes and applications in the sciences (Proceedings of the Conference held at Battelle Seattle Research Center, April 21-25, 1975. Edited by P. Hilton.) 263-327, Lecture Notes in Math. 525, Springer-Verlag.

von Kármán, T. and Tsien, H-S., 1941, *The buckling of thin cylindrical shells under axial compression.* Journal of the Aeronautical Sciences, 8, 303-12.

Xiang, Y., 1995, *Bifurcations of singularities of planar mechanisms with one- and two-degrees of freedom*. PhD thesis, Napier University, Edinburgh.

Zeeman, E. C., 1977, *Catastrophe theory. Selected papers, 1972-1977*. Addison-Wesley.